THESIS FOR THE DEGREE OF DOCTOR OF PHILOSOPHY

Precipitation of Kraft Lignin from Aqueous Solutions

Tor Sewring

Department of Chemistry and Chemical Engineering
CHALMERS UNIVERSITY OF TECHNOLOGY
Gothenburg, Sweden
2019

Precipitation of Kraft Lignin from Aqueous Solutions

TOR SEWRING
ISBN 978-91-7597-885-7

Doktorsavhandlingar vid Chalmers tekniska högskola
Ny serie nr 4566
ISSN 0346-718X

CHALMERS UNIVERSITY OF TECHNOLOGY
Department of Chemistry and Chemical Engineering
SE-412 96 Gothenburg
Sweden
Phone: +46 (0)31-772 10 00

Cover: A Sample of softwood kraft lignin taken from the source of lignin used in this study. Photo in the background: woods.

Printed by Chalmers Reproservice
CHALMERS UNIVERSITY OF TECHNOLOGY
Gothenburg, Sweden
2019

Precipitation of Kraft Lignin from Aqueous Solutions

TOR SEWRING
Forest Products and Chemical Engineering
Department of Chemistry and Chemical Engineering
Chalmers University of Technology

ABSTRACT

One way of improving the materials yield of a kraft paper pulp process, and simultaneously providing the industry with aromatic macromolecular structures, is to extract lignin from the black liquor. This can be done by lowering the pH of the black liquor, which will result in the precipitation of the lignin. The suspension of particles is then filtered and washed to retrieve a purified lignin in solid form. For these operations to be conducted efficiently, the solubility of kraft lignin and the course of the particle formation process needs to be understood. This thesis investigates experimentally the particle formation process on the micron-scale. Furthermore, a model describing kraft lignin particle-particle interactions on the nano-scale has been developed.

During acid-induced precipitation in model systems, the particle formation process was studied as a function of relevant process parameters such as pH, salt concentration level, temperature, presence of xylan and anionic specificity. The precipitation experiments were carried out in a precipitation vessel, where the (particle-size related) chord length distribution, in the range 1-1000 µm, was measured *in situ* as the kraft lignin particles were formed. The technique used (FBRM®) enabled the precipitation to be monitored as the pH was lowed. This allowed the particle concentration of various size classes to be analysed as a function of the precipitation conditions in a range relevant to industrial use.

The onset of particle formation (≥ 1 µm) was found to depend on the process conditions. Moreover, beyond the onset condition, the sizes of the particles increased as the pH decreased or the salt concentration increased; the total volume of the particles formed (≥ 1 µm) followed the same trend. The results indicate that electrostatics influence the particle formation significantly due to the ionisable phenolic and carboxylic groups on kraft lignin, in a wide range of conditions: 1-4 mol Na^+ kg^{-1} water and pH 13-4. The temperature dependency was also significant (45-77 °C): the particles were largest at 77 °C whilst at 45 °C, the system even underwent gelation at some conditions (pH 9, 1 M Na^+). Additionally, the presence of xylan during co-precipitation with kraft lignin (5 g / 95 g lignin) retarded the build-up of agglomerates, with a larger effect being observed at 77 °C than at 65 °C. The xylan was found to be distributed evenly in the precipitated lignin.

Numerical predictions of the dispersion stability of kraft lignin nanoparticles (10-1000 nm) were made using a modified Poisson-Boltzmann model within the DLVO framework. For NaCl solutions, the predictions agreed reasonably well with the onsets of particle formation (> 1 µm) found experimentally. They were, however, less accurate for Na_2SO_4 based aqueous solutions, although they predicted the same anionic relative salting-out ability observed in the experiments (*i.e.* $Cl > SO_4^{2-}$) at high salt concentrations (2-4 M Na^+).

Keywords: kraft lignin, acid precipitation, *in situ* measurements, particle size distribution, pair interactions, modified Poisson-Boltzmann model.

List of Publications

This thesis is based on the work contained in the following papers:

I. **Filtration properties of kraft lignin:**
The influence of xylan and precipitation conditions
Durruty, Julie; Sewring, Tor; Schneider, Helen; Schneider, Lynn; Mattsson, Tuve; Theliander, Hans
Nordic Pulp & Paper Research Journal, Special issue on lignin, 32: 508-526 (2017).

II. **A study of kraft lignin acid precipitation in aqueous solutions using focused beam reflectance measurement (FBRM®)**
Sewring, Tor; Theliander, Hans
Journal of Science & Technology for Forest Products and Processes, 6: 46-53 (2018).

III. **Acid precipitation of kraft lignin from aqueous solutions:**
The influence of pH, temperature and xylan
Sewring, Tor; Durruty, Julie; Schneider, Lynn; Schneider, Helen; Mattsson, Tuve; Theliander, Hans
Journal of Wood Chemistry & Technology, *39: 1-13 (2019)*.

IV. **Predictions of pair interaction potentials between kraft lignin macromolecules in black liquors by utilization of a modified Poisson-Boltzmann approach**
Sewring, Tor; Zhu, Weizhen; Sedin, Maria; Theliander, Hans
Industrial & Engineering Chemistry Research, published online (2019).
DOI: 10.1021/acs.iecr.8b05929

V. **Acid precipitation of kraft lignin from aqueous solutions:**
The influence of anionic specificity and salt concentration level
Sewring, Tor; Theliander, Hans
Submitted.

Contribution Report

The author of this thesis has made the following contributions to the papers included:

I. Co-author. The study was based on a preliminary experimental study performed by Helen Schneider and Lynn Schneider under the supervision of both the author and Julie Durruty. Supervision of the synthesis of attaching dye to xylan was a joint effort made with Julie Durruty, as was planning and performing confocal laser scanning florescence microscopy. The author interpreted the results together with co-authors.

II. Main author. Planned and performed the experiments. Analysed and evaluated the results and wrote the paper with the support of the co-author.

III. Main author. The study was based on a preliminary experimental study performed by Helen Schneider and Lynn Schneider under the joint supervision of the author and Julie Durruty. The main part of the experiments was planned and performed by the author and Julie Durruty. The author performed the analysis and the results were interpreted together with the co-authors.

IV. Main author. Conducted the mathematical modelling, wrote the computer program and performed the numerical simulations as well as the analysis. Wrote the manuscript with the support of the co-authors.

V. Main author. Planned the experiments with the co-author. Conducted the experiments and the analysis. Evaluated the results and wrote the manuscript with the support of the co-author.

Related work

Some of the work has also been presented at conferences:

A study of kraft lignin acid precipitation in aqueous solutions using focused beam reflectance measurement (FBRM®)

Sewring, Tor; Theliander, Hans
International Chemical Recovery Conference 2017
May 24-26, 2017, Halifax, Canada.

The Influence of anion specificity on kraft lignin acid precipitation from aqueous solutions

Sewring, Tor; Theliander, Hans
15th European Workshop on Lignocellulosics and Pulp
June 26-29, 2018, Aveiro, Portugal.

Table of Contents

1 Introduction

This chapter presents the background to this thesis, along with the objectives of the study. The first part of the background places this study in a wider perspective. Thereafter, the macromolecules kraft lignin and xylan are introduced, along with previous findings found in the literature regarding the precipitation of kraft lignin from aqueous solutions.

1.1 The forest-based materials biorefinery

Today's macro trends, such as digitalisation, increasing living standards and the transition from a society based on fossil fuels to one based on renewable sources, all influence industrial sectors, not least the forest industry. The Nordic forest industry has been successful in utilising the forest for the production of construction timber for several centuries, and cardboard and hygiene products for almost a century. Digitalisation, however, has resulted in a decreasing demand for printing paper, especially newsprint. Furthermore, the Nordic export of pulp and paper products is currently being challenged by cheap wood biomass and rapidly-expanding industries located in the southern hemisphere.

A new product portfolio, including innovative and advanced products of high value, is necessary for the Nordic forest industry from an economic perspective. Consensus on the need to transition away from a fossil-based society that makes a tangible impact on the climate is also increasing steadily worldwide, which means that both fuels and materials currently based on oil will have to be replaced. The demand for fuel and material based on renewable and sustainable resources can therefore be expected to increase.

There is thus both an economical and environmental incentive for the Nordic pulp and paper industry to transform from its conventional form into an industry that integrates the production of pulp and paper with biorefining. This is where the concept of the forest-based materials biorefinery starts, based upon a highly-developed and comprehensive industrial infrastructure that has been built up over the past 150 years or so. The long-term engineering aim of this biorefinery concept is to have a high yield of material and low energy demand, which makes it appropriate to focus on the production of materials, rather than fuel, from the biomass available. A mild disintegration of the wood is desired in order to preserve the inherent properties of its complex structure, and especially so for end-products of high value, such as functional materials. The gaol is to utilise all three of the main constituents of wood, *i.e.* cellulose, hemicelluloses and lignin, in various ways.

The dominant chemical pulping process used today is the kraft process. Its main purpose is to produce pulp by separating the lignin from the wood tissue and liberate the cellulose fibres. The kraft process has been developed into a rather efficient process for separating cellulose from lignin. However, almost all of the lignin is currently combusted to produce electricity and steam for both internal and external use once the inorganic cooking chemicals in the black liquor have been recovered. Black liquor has a high content of lignin and is thus a source of this aromatic macromolecule. Extracting lignin from black liquor is done commercially (MeadWestvaco, Indulin® kraft lignin) and lignin extraction has moreover been a subject of research for several decades. Although there is a global annual production of 50-60 million metric tonnes of black liquor containing kraft lignin, only a mere 0.1 tonnes of the lignin are utilised for purposes other than the above-mentioned production of electricity and steam. New commercialised extraction technologies, coupled with the enormous amount of lignin present in black liquor that is available annually, provide a great potential for utilising kraft lignin as a raw material for the production of materials/chemicals such as bio-oils, adhesives, carbon fibres and composite materials (Kadla *et al.* 2002, Lora and Glasser 2002, Gellerstedt *et al.* 2010, Nguyen *et al.* 2014, Thakur *et al.* 2014). Moreover, the colloidal behaviour of kraft lignin in various liquid environments may be exploited in the production of nanoparticles (Lievonen *et al.* 2016) and tuneable functional coatings (Cusola *et al.* 2018), as has been investigated in recent studies.

The LignoBoost™ technology has been installed in two pulp mills for commercial purposes to date: Domtar in Plymouth, USA, and Stora Enso in Sunila, Finland. LignoBoost™ is a lignin extraction process for the production of high purity kraft lignin in a sequence of four main operations: precipitation with CO_2, a first filtration step, suspension of the filter cake formed and a second filtration step with washing. An efficient process requires careful control of both the yield of the precipitation and the operational costs. The operational costs are related mainly to the consumption of chemicals and power. Furthermore, the purity of the lignin obtained may be of concern in some applications, where a very high level of purity is necessary.

1.2 Wallenberg Wood Science Center

The Wallenberg Wood Science Center is a joint research centre for Chalmers University of Technology and The Royal Institute of Technology (KTH). Its vision is new materials from wood, and therefore conducts both fundamental and applied research related to wood, materials originating from wood and processes to produce such materials: the chain from wood chips to new materials.

The network is multi-disciplinary and conducts research activities primarily. The centre, moreover, conducts a graduate student education programme in fields such as wood chemistry and biology, biorefining technology, biotechnology, surface and colloidal science, material science and applications based on raw materials sourced from wood.

1.3 Kraft lignin: Extraction and its properties

Most of the wood tissue, 40-50 %, consists of cellulose whilst 15-30 % is lignin and the remainder is mainly xylans and glucomannans. The structure of the wood tissue varies with species. In softwood, the microstructure of the wood tissue consists of wood fibres known as tracheids, which can be described as hollow tubes with closed ends; the lumen is in the centre (*i.e.* the hollow part), confined by the wood cell wall. The wood cell wall has several layers with a variety of structures and molecular compositions: the inner layer (S3), middle layer (S2), outer layer (S1), the primary cell wall and the middle lamella, with the latter acting as a "glue" between the wood fibres. The composition of lignin varies throughout the cell wall, being lowest in the S2/S3 layer and highest in the middle lamella. The layers S1-S3, consist of fibrils of cellulose embedded in a matrix containing mainly xylan, glucumannans and lignin in various proportions. Native lignin is a macromolecule comprised of interlinked phenylpropane-units: the most common interlinkage is β-aryl-ether (*β*-O-4'), followed by the condensed bonds dihydroxy biphenyl (5-5') and phenyl coumarane (*β*-5') (Henriksson 2008). Lignin can also be found linked to the carbohydrates xylan and glucomannan, which are referred to as Lignin Carbohydrate Complexes Complexes (LCCs) (Lawoko 2005).

Kraft lignin is extracted from wood tissue during the kraft cooking process; it is during this stage that it obtains many of its specific properties that make it differ from native lignin. The final properties of the kraft lignin extracted in a kraft pulp process depend on several parameters related to both the process and the origin of the wood. The path taken by lignin through the kraft process starts with the wood chips: these are impregnated with cooking chemicals before being heated up in the digester (the major reaction vessel in the chemical pulping process). During impregnation, the lumen of the wood fibres in the chips becomes filled with the cooking liquor containing the active ions (those for cooking being HO^- and HS^-), and the wood cell wall swells. The cooking chemicals react with the lignin in the highly alkaline environment of the impregnated wood tissue and cleave a large number of the *β*-O-4' linkages in the macromolecular structure. This results in the amount of phenolic hydroxyl groups increasing, often referred to as simply phenolic groups. The liberated lignin fragments dissolve at the highly alkaline conditions and are transported, by diffusion, out from both the cell wall and the lumen; out from the wood tissue and into the surrounding liquid. However, due to the harsh cooking conditions, moieties of degraded glucomannans are also found in the liquor, typically in the form of low molecular weight acids. Xylan, which is discussed further in 1.4 Xylan, also exists in the liquor in a polymeric form or as sugar residues.

All three steps (reaction, solvation and transport) are critical not only for the kinetics of the cooking process but also for the properties of the lignin thus obtained. The solubility and mass transport of lignin fragments, for instance, are critical and can be limiting factors; the cooking time can influence the polydispersity of the resulting lignin (Svärd *et al.* 2016). Rather recently, it was shown that solubility and/or mass transport are probably the limiting factors here (Mattsson *et al.* 2017).

After the cooking process, the mixture is sent to the pulp washing department to separate the pulp from the dissolved lignin and cooking chemicals: the results are washed pulp and black liquor. Black liquor is a complex electrolyte comprised mainly of inorganic ions (the spent cooking chemicals), dissolved lignin fragments and dissolved parts of the

carbohydrates. The concentrations of the species dissolved in the black liquor vary according to the wood species and cooking conditions (Frederick 1997).

The solubility of kraft lignin is crucial in controlling the two operations described above (cooking and washing) so that an efficient separation of pulp fibres from lignin and inorganic salts is obtained. The conditions also change drastically from one operation to the other: in the cooking liquor, the concentrations of both the hydroxide and sodium ions are relatively high whilst in the washing stage, their concentrations are reduced due to dilution.

The black liquor obtained after the washing department has to be concentrated before it can be injected into the recovery boiler so that the organic material can be combusted and the inorganic cooking chemicals recovered. The removal of water is made in a series of evaporators, also referred to as the black liquor evaporation train. Once again, the conditions change: the solid content and boiling point temperature elevation both increase as all the more water is removed during the evaporation process (Bialik *et al.* 2008). Keeping track of the solubility of kraft lignin is therefore of importance.

When the solid content in the evaporation train reaches a certain level, a stream of black liquor is removed for lignin extraction. As mentioned previously, the LignoBoost™ process can be integrated into the conventional kraft pulping process.

Research efforts have been made to understand and improve the filterability and purification of kraft lignin. A critical development was resuspension of the filter cake, after the first filtration, by dilution with acidic water. This kept the pH low, allowing the sodium to be washed out without re-dissolving the lignin before the second filtration stage and washing (Öhman *et al.* 2007). The filtrates from the process, which contain the inorganic salts and some dissolved organic material, are finally fed back into the evaporation train, whilst the lignin forms a cake with a reasonable dry content and very low content of ash.

The precipitation stage is carried out in a precipitation vessel, where the pH is lowered by sparging CO_2 into the liquid. It is particularly important to control two of the parameters, namely the final pH and the precipitation temperature. Research related to this process step has been conducted for several decades already; the focus of early work was the influence of pH on the yield, which was found to increase as the pH was decreased (Alén *et al.* 1979, Uloth and Wearing 1989). In later studies, the influence of temperature was also investigated; the yield was found to decrease as the temperature was increased for the precipitation of black liquors concentrated to around 30 wt% at temperatures of 45-70 °C) (Wallmo *et al.* 2009, Zhu and Theliander 2015). Investigations were also carried out at 80 °C: measurements of particle size showed that the agglomerates become larger at 80 °C than at 70 °C (Öhman and Theliander 2007). To the knowledge of the author, no explanation for this increase in size at increased temperatures has been put forward as yet. It has nevertheless been observed that the properties of precipitated lignin are different at temperatures around 85 °C, where it becomes “soft” and “tacky” (Uloth and Wearing 1989). The yield decreased a few percent, however, due to it being measured after filtration; no conclusions could be drawn regarding the changes in the yield of the precipitation stage alone in this range.

Kraft lignin fragments are polydisperse, which may have practical consequences, *e.g.* as the yield of precipitation increases, the average molecular weight of the precipitated lignin has been shown to decrease whilst the content of phenolic groups increases (Zhu *et al.*

2015). These groups are rather abundant, having an average content range of about 2-5 mol/kg lignin, although low contents of carboxylic groups have also been quantified, with average contents of around 0.1-0.8 mol/kg lignin (Robert *et al.* 1984, Argyropoulos 1994, Froass Peter *et al.* 1998, Norgren and Lindström 2000, Crestini *et al.* 2017, Fritz *et al.* 2017). Molecular weights may range over several orders of magnitude: from just a few hundred Da (oligomers) to over a few hundred thousand Da (Norgren and Lindström 2000, Zhu *et al.* 2015, Mattsson *et al.* 2016, Crestini *et al.* 2017). The weight-averaged molecular weight is, however, often found to be around 5-20 kDa.

Other functional groups are methoxyl and aliphatic hydroxyl groups, the contents of which are often inversely correlated to the content of phenolic groups (Argyropoulos 1994, Zhu *et al.* 2015, Crestini *et al.* 2017, Zinovyev *et al.* 2017). Comparisons between two commercially-available softwood kraft lignins, *i.e.* Indulin AT (MeadWestvaco) and BioChoice™ lignin (Domtar Plymouth, precipitated using LignoBoost™ technology), both of pinewood origin, showed only minor differences in the contents of some key functional groups (Hu *et al.* 2016). Despite the varying conditions to which they were subjected (such as the cooking process), the contents of phenolic, aliphatic hydroxyl and carboxylic groups were found to be very similar according to the results of analysis using UV-spectroscopy and P NMR: the use of the latter method, however, showed that the content of phenolic groups was 18 % higher in the BioChoice lignin. The weight-averaged molecular weight values were also rather similar: 6.5 and 6.8 kDa, with a polydispersity of 9.9 and 7.1, for Indulin and BioChoice, respectively.

The abundances of different types of intramolecular bonds and functional groups of kraft lignins have been studied for several decades and relatively much is known about them. However, detailed information of the physical properties of the macromolecules, such as size and shape, is much less conclusive in the literature. One aspect is, of course, that the three-dimensional conformation of the molecules may be solvent and condition-dependent, which may also be very important for its phase behaviour in different environments.

In early work, results from investigations of softwood lignosulphonates (obtained in sulphite pulping) indicated that, based on the analysis of viscosity measurements of lignin in different solvents, the macromolecules were compact swollen submicron-gels rather than hard spheres or linear polymers (Goring 1962). Later, electron microscopy-images of lignosulphonates in water were analysed and an alternative form was proposed: flat, disk-like structures with a thickness of about 2 nm and roughly circular in shape, with a diameter of about 10 nm (Goring *et al.* 1979). Analysis of the self-diffusion coefficients measured indicated that the kraft lignin was best described as a very compact branched macromolecule oblate, ellipsoid in shape, with an axial ratio of 18 (Garver and Callaghan 1991). Analysis of SAXS measurements of dissolved kraft lignin, at pH 12.8 (0.1 M ionic strength), indicated that the dissolved fragments were elongated structures about 1.0 nm thick and 2.0 nm wide (at a lignin concentration of 20 g/L) (Vainio *et al.* 2004). The radius of gyration was estimated to 1.6 nm at pH 12.8, which increased to around 2.2-2.6 nm (1-10 g lignin/L) as the pH was decreased to pH 7, in 0.1 NaCl solution. This indicated that no extensive association occurred when the pH was lowered at the conditions investigated. The radius of gyration increased to 3.5 nm at pH 7 and 0.025 NaCl, which was suggested as being due to the charges on the lignin structure being less screened, resulting in a more extended conformation. The hydrodynamic radius distributions for the softwood kraft lignins Indulin and Curan 100 have been measured by ^{1}H PFG NMR self-diffusion measurements and virtually resemble lognormal distributions: the mode-values were 1 and

0.6 nm, respectively (Norgren and Mackin 2009). Molecular dynamics simulations of softwood lignin model macromolecules have been conducted in an explicit-water environment (Petridis et al. 2011), which used a ~13 kDa macromolecule model (native lignin) and assigned the following interlinkage-abundances to it: 50 % *β*-O-4', 30 % 5-5', 10 % *β*-5' and 10 % *α*-O-4'. Moreover, the number of branch points were varied in the range 1-6 at 300 K. Charged groups were utilised in the modelling of the water molecules, but not for the lignin. The highly-branched structure of 6 points adopted a close to spherical shape, while those of lower numbers of branching (2-5) exhibited a larger degree of asphericity: 0.06 for the former case and ~0.1-0.2 for the latter (*cf* asphericity values, 0 = sphere, 1 = rod). Nevertheless, all branched molecules adopted a compact ellipsoid rather than an oblate shape (300-360 K). A typical average number of branch-points for spruce lignin is about 3 for a molecule with a molecular weight of the model molecules (Yan *et al.* 1984). The asphericity of the branched molecules showed no temperature dependency. However, lignin-water hydrogen bonding decreased with increased temperature as well as the density of the hydration shell of the lignin.

1.4 Xylan

Softwood contains about 5-10 % arabinoglucuronoxylan, the linear polymer backbone of which consists of xylose sub-units substituted with *α*-L-arabinofuranose and 4-O-methylglucuronic acid. The degree of substitution of *α*-L-arabinofuranose is one per 8-9 xylose units, whilst the corresponding degree for 4-O-methylglucuronic acid is 5-6 (Teleman 2008). The most common hardwood xylan is O-acetyl-(4-O-methylglucuro) xylan, also referred to as glucuronoxylan. Unlike softwood xylan, this is partially substituted with acetyl groups. The substitution degree of 4-O-methylglucuronic acid is lower than for softwood xylans, being one per 8-20 xylose units (Teleman 2008). The 4-O-methylglucuronic acid increases the solubility of xylan in an aqueous solution significantly: it is an acid sugar carrying a carboxylic group, which is ionised at neutral and alkaline conditions ($pK_a \approx 3.4$ (Laine *et al.* 1994)).

Xylans are partially degraded and dissolved during the kraft cooking process: about 40 % of the arabinoglucuronoxylan is removed from the wood tissue (Sjöström 1977). The degradation is dependent on both the temperature and concentration of hydroxide ions, and increases as these two parameters are increased (Wigell *et al.* 2007). At an alkali concentration of 1.25 mol HO^-/kg liquor, however, the loss of xylan at temperatures up to 93 °C is around or below 10 %. The loss was also shown to be proportional to the yield during cooking, which may be explained by the fact that lignin and xylan are linked to each other chemically and form LCCs (Lawoko 2005). Extracted kraft lignin has been shown to contain low amounts of xylan but, then again, it is the most abundant carbohydrate moiety present in softwood lignin (Zhu *et al.* 2015, Zinovyev *et al.* 2017). The xylan may vary in molecular weight, from polymeric to fragments of low molecular weight (*i.e.* oligomers), and its content increases as the molecular weight of the lignin increases (Zhu *et al.* 2016, Zinovyev *et al.* 2017). It possible that lignin fractions of high molecular weight containing xylan may be LCCs, because the molecular weight of lignin increases at the end of the cook (Obiaga and Wayman 1973, Gellerstedt and Lindfors 1984, Pakkanen and Alén 2012, Dang Binh *et al.* 2016), and the content xylan increases too, in the form of either free or chemically-linked xylan.

1.5 Precipitation of kraft lignin

Empirical knowledge gained from industry and several studies that have been carried out (Norgren *et al.* 2001, Norgren *et al.* 2002, Zhu and Theliander 2015) indicates that the ionisation of phenolic groups is critical for the dissolution of kraft lignin in aqueous solutions such as black liquor. In general, kraft lignin is dissolved at alkaline conditions due to the ionisation of these groups and, conversely, precipitates out from solution as the solution is acidified due to the protonation of the same groups. The pH at which kraft lignin precipitates has been shown to be around the pK_a value of the phenolic groups (Norgren *et al.* 2001, Norgren *et al.* 2002). Furthermore, the precipitation yield has been shown not only to increase with increasing concentration of ions but also to be sensitive to it over a wide range of concentrations: from relatively low concentrations of up to 1 mol Na^+ kg^{-1} water (Norgren *et al.* 2001) to concentrated black liquor conditions with a corresponding concentration of about 3-4 mol Na^+ kg^{-1} water (Zhu and Theliander 2015), which is the condition of the stream in a commercial lignin extraction unit.

The dependency of the solubility of kraft lignin on pH and ion concentration indicates that electrostatics play an important role. However, two other parameters have also been shown to influence the phase behaviour of kraft lignin, which may not necessarily influence electrostatics forces: molecular properties and temperature. High molecular weight lignin precipitates at higher pH values than low molecular weight counterparts (Norgren *et al.* 2002, Zhu *et al.* 2016). The van der Waals force between two particles increases as the sizes of the particles increase, which results in stronger attractive interactions (Israelachvili 2011). Furthermore, the more hydrophobic the particles are in aqueous solutions, the stronger the force will become, due to differences in the dielectric properties of the solvent and the lignin. Thus, it is reasonable that van der Waals forces may partially explain results showing that solubility is lower for fractions of high molecular weight. Another factor that may also decrease solubility is the correlation between the content of ionisable groups (such as phenolic and carboxylic groups) and molecular weight, as discussed in 1.3 Kraft lignin: Extraction and its properties.

The content of ionisable groups decreases as the molecular weight of the kraft lignin increases (Zhu *et al.* 2016, Zinovyev *et al.* 2017). An increase in the charge density usually increases the solubility of charged macromolecules in the type of systems investigated; one potential consequence of increased charge density is an increase in electrostatic interactions. Zeta potentials measured for softwood kraft lignin may be found in a wide range: values from about -40 mV up to about -90 mV have been reported in aqueous phases at various pH levels (Dong *et al.* 1996, Wei *et al.* 2012, Lievonen *et al.* 2016, Fritz *et al.* 2017)

The phenolic groups are weakly acidic and their degree of ionisation is strongly dependent on the pH of the surrounding aqueous solution (Norgren and Lindström 2000). This is due to the equilibrium protonation/deprotonation reaction of these groups, which is dependent on the surface activity of protons, and thus regulates the ionisation degree. This activity is, for instance, influenced by the electrostatic attraction of the charges on the surface of the lignin and, consequently, it could be lower than that in bulk (this is discussed further in 2.4 Charge regulation). The pK_a for phenolic groups of kraft lignin is rather complicated not only because of the electrostatic effects discussed above but also the inherent heterogeneity of molecular properties. The substitution pattern of lignin-like phenolic compounds has

been found to influence the acidity of the phenolic groups: one investigation found pK_a values between 6 and 11 at 25 °C (Ragnar *et al.* 2000). All the pK_a values found in that particular study were not equally likely to represent the actual lignin, but rather show the potential spread in the acidity of the different phenolic alcohols present in kraft lignin: when the structure of the extracted softwood kraft lignin proposed was examined, some types of structure were found more likely to be present than others (Crestini *et al.* 2017), in that case obtained by LignoBoost technology (Öhman *et al.* 2013). An average, or apparent, pK_a value is often used to characterise kraft lignin in terms of acidity. This value may vary from source to source, as it depends on factors such as the wood species used as the raw material and the pulping conditions. The apparent pK_a value at 21 °C for Indulin kraft lignin in dilute aqueous solutions has been found to be around 10.6 and 10.4 at 0.01 and 0.1 M NaCl, respectively (Norgren and Lindström 2000).

The phase transition of kraft lignin, from the dissolved state to stable solid particles in dilute aqueous solutions, has been shown to be qualitatively predictable by the DLVO theory (Norgren *et al.* 2001, Israelachvili 2011). The parameters shown to influence the stability of the dispersion of kraft lignin were salt concentration, pH and temperature (Norgren and Lindström 2000, Norgren *et al.* 2001).

Measurements of the critical coagulation concentration (C.C.C.) of salt by different methods have been performed in several studies for kraft lignin solution systems (Lindström 1980, Sundin and Hartler 2000, Norgren *et al.* 2001, Norgren *et al.* 2002). The dependency of the C.C.C. measured for kraft lignin on parameters such as salt concentration, pH, valency of counter ions and temperature observed in these studies can be predicted by the principles behind the C.C.C. concept (see 2.2 Dispersion stability and pair interactions) which, in this case, describe the phase behaviour of negatively-charged polyelectrolytes in aqueous solution.

In an early work, a distinct C.C.C. of 0.4 M NaCl was found at pH 6.2 (Lindström 1980); furthermore, at this condition, it was found to be independent of both the lignin concentration (0.2-0.5 g/L) and temperature (25-60 °C) in the ranges investigated. The phenolic groups can be assumed to be fully protonated at these conditions; the ionised carboxylic groups were used to explain the stabilisation of kraft lignin particles at such low pH-values, since the C.C.C. was also shown to be pH dependent (pH 3-8, 25 °C). However, it was also suggested that other mechanisms influenced the solubility: hydrogen-bonding by protonated carboxylic groups may be the cause of attractive particle interactions, thereby lowering the solubility. It was observed that the stability of the solution was insensitive to the addition of NaCl above pH 9 and already at pH 8, the C.C.C was reported to be 1 M NaCl at 25 °C.

An influence of temperature on the C.C.C. has been found (Norgren *et al.* 2001): measurements were made at alkaline conditions of above pH 10 and salt concentrations up to 1 M NaCl, where the deprotonation degrees of phenolic groups are affected significantly by the temperature-dependent ionisation of water (Norgren and Lindström 2000). It was suggested that the temperature dependencies of the ionisation of both phenolic groups and water could, at least partially, explain the inverse temperature-dependency of the C.C.C. (Norgren *et al.* 2001). Moreover, the concentrations of lignin of 0.3-3 g/L were higher than in the earlier study discussed (Lindström 1980).

In a detailed study of the kinetics of aggregation of Indulin kraft lignin, it was shown that the stability ratio concept could explain the relationship between added salt and the rate of

aggregation that was obtained (Norgren *et al.* 2002). Moreover, the rate of the increase in size of the particles formed was rather slow at 1 M added NaCl, pH 10.5 and temperature 70 °C: the largest particles reached 500 nm in size after 40 min of growth. As the NaCl concentration was increased to 1.1 M, the rate at which particles grew in size increased dramatically and converged to sizes of about 1 µm during a period of 40 min of coagulation time. At 1.2 M NaCl, the sizes of particles reached 1 µm and, at 1.3 M NaCl, which was also determined as the C.C.C., they exceeded 1 µm in less than 10 min. The structures of the particles were fractal flocs (agglomerates), as shown by cryo-TEM images. A correlation between the fractal dimension and the stability ratio could be observed: looser and more porous agglomerates were formed in the diffusion-limited regime and, conversely, denser agglomerates were formed in the reaction-limited regime. This indicates that electrostatic screening strongly influences the phase behaviour of kraft lignin in alkaline aqueous solutions, and that the degree of ionisation and contents of phenolic groups are key properties for the behaviour. It is worth noting that the C.C.C. increased to 1.8 M NaCl when the high and low molecular weight fractions of the lignin were removed by ultrafiltration (the 1< kraft lignin <100 kDa fraction used) prior to the salt-out experiments. It indicates that a high molecular weight fraction has a significantly lower solubility than the rest of the kraft lignin population. As mentioned previously in 1.3 Kraft lignin: Extraction and its properties, the contents of ionisable groups are correlated negatively to the molecular weight, and can have a critical influence on the solubility.

Two later studies presented observations regarding precipitation kinetics that were similar to the above-mentioned (unfractionated) case (Norgren and Mackin 2009, Fritz *et al.* 2017). In the former study, both Indulin and Curan 100 were used as kraft lignin sources for comparison purposes. The latter exhibited a higher solubility and was slightly smaller in size (see 1.3 Kraft lignin: Extraction and its properties): it precipitated at NaCl concentrations $\geq$ 1.2 M at pH 10.5 and 75 °C and, moreover, the rate increased with increasing salt concentration. The effect of the anion in the salt was also tested, *i.e.* the difference in precipitation when adding NaCl or Na_2SO_4 to reach a given Na^+ concentration: the latter salt resulted in precipitation at about 0.6 M for Curan 100 (*cf* 1.2 M for NaCl). This is in agreement with the direct order of the Hofmeister series for a negatively charged and otherwise hydrophobic macromolecule (Schwierz *et al.* 2013) such as kraft lignin. The other study (Fritz *et al.* 2017) used a softwood kraft lignin sourced from the Domtar Inc. Plymouth Pulp Mill (USA). The C.C.C. of NaCl was reported to be 1.2 M at pH 10.5 and 70 °C. Moreover, in agreement with previous results (Norgren *et al.* 2002), the increase in precipitation, correlated to an increase in salt concentration, was associated with an increase in particle size: at 1 M NaCl they exceeded 1 µm.

The effects of mixing on the properties of agglomerate during the precipitation of kraft lignin from black liquors (10-12 wt% kraft lignin, 3.3-4.2 mol Na^+ kg^{-1} water) have been studied (Kannangara *et al.* 2016). Their experiments were conducted in an agitated precipitation vessel (liquor volume 1.8 L), with precipitation performed by sparging CO_2 into the liquid from the bottom until the pH reached 9.8 at 75 °C. The effects of mixing on the properties of the particles were studied during the acidification phase and a following aging phase. *Ex situ* static laser scattering measurements and SEM images of the agglomerates showed that mixing had a strong influence on the shape and size of agglomerates of micron size, which were found to have a two-level structure. The agglomerates (second level) were built up of primary particles (first level) that were 1-2 µm in size, regardless of the mixing conditions. The average fractal dimensions were found

to be 2.45 and 2.51 after acidification (corresponding to high and low mixing speeds, respectively), and shown to decrease to 2.3 and 2.4 after aging. The fractal dimensions measured were assumed to represent the primary particles (1-2 µm), based on the results of another study of two-level agglomerate structures of similar sizes (Ibaseta and Biscans 2010). The similarities of the fractal dimensions between the primary lignin particles formed under Brownian motion without agitation (Norgren *et al.* 2002) and with agitation (Kannangara *et al.* 2016), along with estimations of the mean length scale (125 µm) of a turbulent eddies, suggested that mixing did not had a major impact on the primary particles 1-2 µm in size (Kannangara *et al.* 2016). SEM images of kraft lignin agglomerates, taken in earlier work (Durruty *et al.* 2015), showed that they had similar size distributions and structures comprised of primary particles of about 2 µm, despite the fact that this lignin had been extracted by a different process (LignoBoost).

At this point in time, *in situ* knowledge of the evolvement of the particles size distribution as a function of pH, temperature and salt concentration levels is lacking in the literature. Detailed information on the phase behaviour is currently limited to dilute concentrations of kraft lignin. To the author's knowledge of the current scientific literature, *in situ* monitoring of the precipitation process in the whole relevant pH interval has not yet been investigated. This is, however, of interest since the precipitation process may be sensitive to pH over a wide range of pH values due to variations in the acidity of the ionisable groups on kraft lignin and its polydispersity.

Knowledge of the influence that xylan has on the particle size distribution, and detailed information of the distribution of xylan in co-precipitated and filtered material, are both lacking: they are nevertheless of great importance in promoting understanding of the mechanisms involved in the co-precipitation process of the two macromolecules. This is relevant because the presence of xylan has been shown to have a negative influence on the filterability of xylan-rich suspensions of lignin agglomerates (Wallmo *et al.* 2009). Furthermore, controlling the separation of carbohydrates from lignin is important from a purity perspective: the purity requirement of lignin as a precursor in new products can be high.

Moreover, quantitative theoretical considerations of the particle dispersion stability and the governing inter-particle and molecular interactions have been limited to dilute conditions where the classical Poisson-Boltzmann equation and classical DLVO principle can be considered reasonable. However, black liquor systems typically have high concentration levels of salt; the kraft lignin macromolecules and particles formed by precipitation of the lignin can be considered to be, on average, highly charged at the relevant conditions, not least at alkaline conditions. It may be regarded as important to take these aspects into account in the derivation of models useful in the prediction of the phase behaviour, in order to enhance understanding of the experimental observations made: not least to understand the underlying mechanisms that account for most of the behaviour of kraft lignin in electrolytes.

1.6 Objectives

This study was carried out in order to investigate the precipitation process of kraft lignin from aqueous model solutions, both experimentally and theoretically. The experimental work was mainly conducted as an exploratory effort to gain new *in situ* knowledge about the precipitation process in terms of the formation of particles on the micron scale. This work particularly addressed the investigation of the non-dilute regime, both in terms of lignin and ion concentrations, in a wide range of conditions relevant to industry. The theoretical work was conducted to aid interpretation of the experimental results obtained by allowing quantitative comparisons to be made between observations and theoretically-based predictions, thereby increasing understanding of particle formation. Moreover, the theoretical work aimed at providing additional insight beyond the measurements, *i.e.* particle dispersion stability on the nano-scale, and enable a quantitative evaluation of potential key mechanisms governing it. The objectives and scope of each part are detailed further below.

Experimental

Precipitation experiments were conducted at controlled conditions by means of acidification with acid. The experimental efforts mainly concerned the evolvement of the formation of lignin particles on the micron scale by employing *in situ* monitoring of the chord length distribution (particle-size related) during the experiment. The main goal was to gain deepen understanding of how precipitation is dependent on important process parameters that are relevant in black liquor systems. The parameters chosen for investigation have been predicted as controlling the inter-particle and molecular interactions in black liquor, and thus the phase behaviour of kraft lignin. These parameters are: pH, temperature, ion concentration levels and the anionic specificity (here Cl^- *vs.* SO_4^{2-} was investigated). The parameter ranges investigated were the following: pH 4-13; temperature: 45-77 °C; salt concentration: 1-5.8 mol Na^+ kg^{-1}. Additionally, the influence of small amounts of xylan present in the liquid on the precipitation process, as well as the distribution of them in the precipitated lignin particles obtained, were investigated. The experimental efforts targeted, in particular, detection of the precipitation conditions required to cause the onset of the formation of particles ≥ 1 μm in size and the following formation process of particles at this onset condition. Moreover, significant focus was placed on *in situ* investigation of the changes in the size distribution of the particles formed as the conditions are altered further, primarily by lowering the pH. Analysis of such experimental data provides detailed *in situ* insight into the complex process of precipitation at conditions relevant in industry. The submicron regime has not, however, been directly investigated experimentally. The effects of mixing have not been investigated, either: this parameter is nevertheless considered important, and is mentioned briefly in the interpretation of the results.

Theoretical

The aim of the theoretical work was to predict the magnitude of the interactions between kraft lignin particles on the nano-scale by developing a mathematical model and a numerical scheme. Using these predictions, moreover, the dispersion stability of the nano-scale particles could be evaluated and used to aid interpretation of the experimental observations. The analysis was limited to pairwise interactions of identical particles; its relevance in the context of precipitation is elaborated further in 2 Theory & modelling and

in the results in 4.2.1 Pair interaction potentials. In principle, the pair interactions were modelled as DLVO potentials, albeit extended to some extent. The numerical predictions were made in order to evaluate the dispersion stability of particles in the range 10-1000 nm, and compare them to the onset of formation particles ≥ 1 µm, which was determined experimentally. Special emphasis in the modelling was placed on taking into account important molecular characteristics of the kraft lignin and the properties of the electrolyte in which the macromolecules and particles are immersed. Within the Poisson-Boltzmann framework, modification of the original equation was conducted to account for the conditions of the concentrated electrolyte regime typical for black liquors. An important part was to investigate how such properties and conditions may influence particle interactions via the mechanisms addressed in the model. This was undertaken to evaluate the relevance of these mechanisms as being reasonable candidates for mechanisms governing the dispersion stability of particles on the nano-scale.

1.7 Outline of the thesis

A brief introduction to the relevant theoretical aspects of precipitation is presented in Chapter 2 Theory & modelling. The first part of this chapter concerns the mechanisms of particle formation and the stability of particle dispersions and its relation to particle-particle pair interactions. The second part presents the development of the model conducted in this work and the assumptions made. Finally, utilisation of the model is described by a numerical procedure. The majority of this chapter is associated primarily with **Paper IV**.

The materials used in the experiments are introduced in Chapter 3: Experimental, along with the experimental set-up and the procedure employed (a summary of the corresponding parts in **Papers I-III** and **V**). The main experimental equipment used is also described briefly, *i.e.* Focused Beam Reflectance Measurement and Confocal Laser Scanning Fluorescence Microscopy. Analysis of the results obtained by the former is also presented in more detail.

In the first part of Chapter 4: Results, the experimental results are presented and discussed. It starts with the course of precipitation, which is intended to give an overview of the precipitation process and presents data mainly from **Paper V** but also from **Papers II** and **III**. This is followed by a focused analysis of the "onset of particle formation", here referred to as particles ≥ 1 μm (**Papers II, III** and **V**). The chord length distributions obtained at a wide range of conditions, where the pH was decreased to below the onset point, are also analysed (**Papers III** and **V**). Finally, the influence of xylan on chord length distribution (**Paper III**) and its distribution in precipitated lignin particles (**Paper I**) are presented and discussed.

The second part of Chapter 4 presents the numerical results obtained by applying the model and numerical procedure presented in Chapter 2: Theory & modelling, developed in **Paper IV.** However, the numerical results in this thesis are new and correspond to the conditions in **Paper V**, rather than to the cases analysed in **Paper IV**. The numerical results are compared here to the experimental results, and further analysis of the mechanisms are accounted for in the model and their potential relevance in this context.

The final part of this thesis presents the main conclusions drawn from this study and some reflections as to future work.

2 Theory & modelling

This chapter briefly introduces the basic principles relevant to this thesis, along with the modelling that was conducted and then utilised in the analysis. It starts at the top level of the particle formation mechanisms and the forces governing them before going down in scale to the interactions on the molecular level which, in turn, regulate the former forces. Often it is the phenomena that occur on the molecular level, in the vicinity of the particle surfaces, that are found to be significant.

2.1 Precipitation: Nucleation, particle growth and agglomeration

The course taken when organic components are precipitated out of an aqueous solution may be divided into the following three stages: the initial dissolved state, nucleation and particle growth/agglomeration. In the transition between the initial state and nucleation, however, a solid phase may be formed and disintegrated again in a dynamic manner without the net result being a stable solid phase. The nucleation stage is reached when stable nuclei are formed, *i.e.* there is a stable solid phase of particles formed. There are two types of nucleation mechanisms: homogenous and heterogeneous. The former concerns the formation of the nucleus directly from the components dissolved in the solution while the latter is aided by foreign surfaces, which may be the glass-wall of a beaker, the baffles in a vessel or other particles present.

When the stable nuclei have formed, they may undergo particle growth and/or agglomeration. The former refers to the process of sorption of dissolved components from the aqueous phase onto existing particles, whereas the latter is the process of adhesion of solid particles that form all the more larger particles/agglomerates. These two processes are illustrated schematically in Figure 2-1.

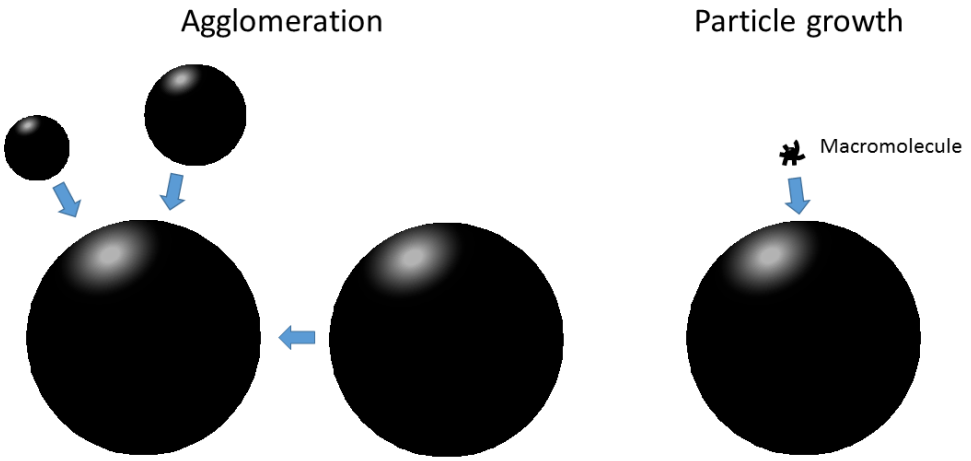

Figure 2-1. Schematic illustration of agglomeration (left) and particle growth (right).

Nucleation, particle growth and agglomeration may also proceed simultaneously and, consequently, the kinetics of each of them govern the outcome of the precipitation process, *e.g.* the particle morphology and size distribution. The kinetics are governed by the forces acting between the particles and the dissolved species as well as their concentrations, all of which influence the frequencies of collision and successful adhesion. Precipitated particulate structures may therefore be path-dependent, *i.e.* being dependent on the history of the precipitation (for instance if conditions have changed during the course of events).

The systems considered in this work involved dissolved or dispersed macromolecules and particles of kraft lignin in electrolyte solutions at relatively high concentrations. It is essential to understand inter-particle and molecular interactions in order to predict the phase behaviour of kraft lignin. These interactions, and their influence on the dispersion stability of macromolecules and particles immersed in the electrolyte phase, are further elaborated in the following sections.

2.2 Dispersion stability and pair interactions

The dispersion stability of particles immersed in an electrolyte is governed by their particle-particles interactions and has been studied intensely for a long period of time, with pioneering contributions reaching back several decades (Derjaguin and Landau 1941, Verwey 1947). The most famous theory is the Derjaguin-Lindau-Verwey-Overbeek (DLVO) theory. It describes the overall interaction potential of two charged particles/surfaces immersed in an electrolyte at a given distance from each other (Israelachvili 2011). This overall mean-potential consists of the electric double layer and the van der Waals interaction between the surfaces. The theory predicts the stability of a particle dispersion to be lower at higher ionic strength and lower pH for weakly acidic macromolecules such as kraft lignin. Regulated by these parameters, the electrostatic potential around the molecule induced by the ionisable surface groups affects particle-particle repulsion. The disjoining pressure, P, between two charged surfaces can be expressed as (Parsons *et al.* 2011):

$$P = P_{\text{entropic}} + P_{\text{electrostatic}} + P_{\text{dispersion}} \tag{2.1}$$

where the three pressure terms are the entropic (osmotic), electrostatic and dispersion components, respectively. The potential energy of interaction between two flat surfaces at a surface-to-surface separation, D (m), W_{flat} (J m^{-2}), can be obtained by integrating the pressure-integrand from infinite separation to D (Israelachvili 2011):

$$W_{\mathrm{flat}} = -\int_{\infty}^{D} P(D')dD' \tag{2.2}$$

To evaluate the potential energy between two identical spherical particles, W_{pair} (J), having a radius, R_{p} (m), that is much larger than the separation distance, the Derjaguin approximation can be applied (Derjaguin 1940):

$$W_{\mathrm{pair}} = \pi R_{\mathrm{p}} \iint_{\infty\infty}^{DD} P(D')dD'dD' \tag{2.3}$$

The pressure that the two particles experience as the separation distance decreases has to be known in order to estimate the pair interaction potential in Eq. (2.3). In the classical DLVO theory, the double layer repulsion and the dispersive interaction can be separated: the latter may be accounted for by a van der Waals interaction for like-particle interactions immersed in a liquid medium, separated by distance D (Hamaker 1937, Israelachvili 2011):

$$W_{\mathrm{vdW}} = -\frac{H}{6}\left[\frac{2R_{\mathrm{p}}^2}{(4R_{\mathrm{p}}+D)D} + \frac{2R_{\mathrm{p}}^2}{(2R_{\mathrm{p}}+D)^2} + \ln\left(\frac{(4R_{\mathrm{p}}+D)D}{(2R_{\mathrm{p}}+D)^2}\right)\right] \tag{2.4}$$

where H is the Hamaker constant. This expression is, in fact, not restricted to $R_{\mathrm{p}} \gg D$, but reduces to:

$$W_{\mathrm{vdW}} = -\frac{HR_{\mathrm{p}}}{12D} \tag{2.5}$$

as the separation distance becomes negligible to the particle radius, *i.e.* within the constraint of the Derjaguin approximation.

The value of the pair interaction potential at D may be used to evaluate the stability of a particle dispersion and is commonly given in number of *kT*, which places it in proportion to the thermal energy. k (J K^{-1}) is the Boltzmann constant and T (K) the temperature. If the potential is sufficiently high (positive), the overall interaction between the particles is strongly repulsive and thereby provides a barrier for precipitation; there is no strict limit for stability, since it is a stochastic system that is being considered. However, potentials > 10 *kT* are regarded as sufficient barriers to stabilise the dispersion in practice, and the dispersions are called stable/stabilised. These states are commonly referred to as "kinetically stabilised" (Israelachvili 2011) if a lower energy state is possible at particle-particle contact. Obviously, the higher the barrier the more stable the dispersion. If, on the other hand, the pair interaction potential is zero, it is at the tipping point and the system is unstable: this is also the case for negative values. For a negatively charged particle in an electrolyte, added salt screens the surface charges and reduces double layer repulsion. The

salt needed to decrease the pair interaction potential to zero predicts the critical coagulation concentration (C.C.C.) of salt.

The C.C.C., and thus also to the DLVO theory, is connected to another common concept: the stability ratio (Reerink and Overbeek 1954, Evans and Wennerström 1999). This divides the kinetics of the precipitation process into two regimes, namely reaction and diffusion-limited, that are controlled by *e.g.* the electrostatic surface potential and, consequently, the parameters affecting it (such as pH, ionic strength and surface charge density). Aggregation in the reaction-limited regime occurs at a low frequency, because not every collision between the macromolecules/particles results in a stable aggregate being formed. In the diffusion-limited regime, on the other hand, each collision does result in a stable aggregate. In the latter regime, the speed of the Brownian motion of the molecules/particles is the rate-determining step of the precipitation in an unstable dispersion, and the kinetics are comparably fast. The transition point between the two regimes is found at the C.C.C. and can be investigated experimentally as well as theoretically (as outlined above). The rate of particle adhesion is strongly related to the height of the repulsive barrier (Holthoff *et al.* 1996). Although the rate decreases gradually as the barrier high increases, the precipitation may proceed relatively slowly at barriers in order magnitude of a few *kT*.

2.3 Poisson-Boltzmann cell model

Charged surfaces immersed in electrolyte render, to a large degree, heterogeneous distributions of ionic species due to electrostatic interactions. This has important consequences for the properties of such a system and gives rise to phenomena such as electrostatic double layer repulsion, which is one of components of the DLVO interaction mentioned earlier. Although called an electrostatic interaction it is, in fact, entropic and related to the concentration distribution of ions at the vicinity of a charged surface. It is, therefore, necessary to determine the concentration distributions of ionic species if double layer repulsion is to be analysed further.

In a very dilute system of charged particles immersed in an electrolyte solution, the Poisson-Boltzmann equation may be used to predict the mean ion concentration distributions around the particles. It relates the electrostatic mean-field potential to mean concentration distributions as:

$$\nabla^2\psi = -\frac{e}{\varepsilon_0\varepsilon_\mathrm{r}}\sum_i z_i c_{i,0}\exp\left(-\frac{z_i e\psi}{kT}\right) \tag{2.6}$$

where ψ (V) is the electrostatic mean-field potential, e is the elementary charge (C), ε_0 (F m^{-1}) is the permittivity in vacuum and z_i (-) and $c_{i,0}$ (m^{-3}) are the valency of the ionic species, i, and the concentration of it at a reference condition (*e.g.* the bulk), respectively. The solvent, being *e.g.* water, is simplified to a dielectric continuum the properties of which are expressed in the relative permittivity or dielectric constant, ε_r (-).

In a system of identical spherical particles of radius R_p (m), dispersed in an electrolyte solution due to strong and long-ranged repulsive interactions, it can be assumed that they are in a state of even distribution. The average volume per particle can be used to determine

the volume of a spherical cell where the particle is concentrically placed. A schematic illustration of such a system is shown in Figure 2-2.

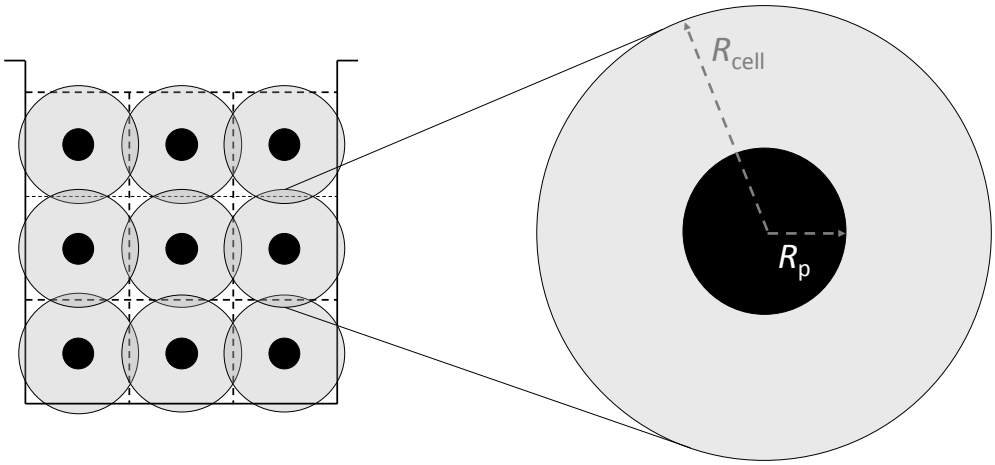

Figure 2-2. Schematic illustration of dispersed particles immersed in an electrolyte. The system is divided into equal spherical cells containing a concentric spherical particle. Each cell represent a Poisson-Boltzmann cell. R_{cell} *and* R_p *are the radii of the PB cell and the particle, respectively.*

The Poisson-Boltzmann equation in Eq. (2.6), expressed in spherical coordinates, may be applied to the liquid domain in a spherical cell, with suitable boundary conditions:

$$\frac{d^2\psi}{dr^2} + \frac{2}{r}\frac{d\psi}{dr} = -\frac{e}{\varepsilon_0 \varepsilon_\mathrm{r}} \sum_i z_i c_{i,0} \exp\left(-\frac{z_i e \psi(r)}{kT}\right) \tag{2.7}$$

Boundary conditions: $\left.\frac{d\psi}{dr}\right|_{r=R_\mathrm{in}} = -\frac{\sigma}{\varepsilon_0 \varepsilon_\mathrm{r}}$, $\left.\frac{d\psi}{dr}\right|_{r=R_\mathrm{cell}} = 0$

where σ (C m^{-2}) is the surface charge density of the particle, R_cell (m) is the radius of the cell and R_in (m) is that at the inner boundary, which may be chosen as the particle radius, R_p. The whole system can be divided into an ensemble of equal cells and, due to the periodical repetitiveness of the system, it is sufficient to consider one cell at least to a first approximation (Deserno and Holm 2001). The outer boundary condition implies that the electric field is zero at the boundary and that the cells carry no net charge: the whole system is consequently electroneutral.

For a dispersion of strongly long-ranged repulsive monodisperse particles, as indicated above, it is realistic to assume that their distribution in the liquid is homogenous and that the properties of a cell can be obtained from the solution of the Poisson-Boltzmann equation in Eq. (2.7). The dispersion can be viewed schematically as a "solid-like" structure because the strong repulsion between particles renders maximum separation of the particles as being the most favourable configuration (Hallez *et al.* 2014). A constraint of the approximation is that the range of the repulsive interaction must be greater than the cell radius, *i.e.* $\kappa R_\mathrm{cell} < 1$, where the Debye screening length κ^{-1} (m) is given by:

$$\kappa^{-1} = \sqrt{\frac{\varepsilon_0 \varepsilon_r kT}{e^2 2I}} \quad , \quad I = \frac{1}{2}\sum_i z_i{}^2 c_{i,0}. \tag{2.8}$$

where I (m^{-3}) is the volumetric ionic strength of the aqueous solution at the bulk condition. It provides a characteristic length of the range of the double layer within the Poisson-Boltzmann theory. Its physical significance emerges naturally in the derivation of the Debye-Hückel equation from the linearized Poisson-Boltzmann equation, accurate as $c_{i,0} \rightarrow 0$ (infinitely dilute solutions) and for $|e\psi/kT|<<1$ (Hill 1986). As deviations from the criteria mentioned above become significant, the descriptive power of this length in relation to the range of the double layer interactions becomes alternated (see 2.5 Modification of the Poisson-Boltzmann equation).

Obviously, the case described above ($\kappa R_{\text{cell}} < 1$) implies that a particle interacts with several other neighbouring particles simultaneously (Wennerström 2017). Consequently, the analysis of particle interactions becomes a many-body problem, being per definition different from the pure pair-interaction problem. In the opposite regime, on the other hand, when the range of the repulsive interaction between particles is much shorter than half of the average separation distance (the state of homogenously distributed particles), pair interactions become a reasonable approximation. Here, the particles' positions can deviate significantly from those corresponding to the state of homogenous distribution, and only interact strongly at relatively short separation distances. In this case, many-body interactions are negligible in relation to pairwise interactions (discussed in 2.2 Dispersion stability and pair interactions) and it is sufficient to consider just the latter (Wennerström 2017). An approach that utilises the Poisson-Boltzmann cell model to estimate pair interactions is outlined in 2.6 Numerical procedure.

2.4 Charge regulation

The ionisable functional groups on a weakly acidic polyelectrolyte such as kraft lignin, may be partially ionised depending on the solution conditions, for instance the pH-value (Norgren and Lindström 2000). The contribution that the phenolic groups make to the surface charge density can be expressed as:

$$\sigma = \alpha\sigma_0 \tag{2.9}$$

where α (-) is the ionisation degree of the phenolic groups and σ_0 ($C\ m^{-2}$) is the maximum surface charge density that they contribute when fully ionised. The equilibrium between protonation and deprotonation reactions of the phenolic groups determines the ionisation degree and can be expressed according to the mass action law (Israelachvili 2011):

$$K_a = \frac{\alpha}{1-\alpha}\{H^+\} \tag{2.10}$$

where K_a (-) is the intrinsic equilibrium constant for the reaction and $\{H^+\}$ (-) is the proton activity at the particle surface. The deprotonation of the phenolic groups and the equilibrium constant at the actual temperature for the reactions can be approximated via the van't Hoff relation:

$$K_{\mathrm{a}}(T) = K_{\mathrm{a}}(T_{\mathrm{ref}})\exp\left(-\frac{\Delta H_{\mathrm{a}}}{kN_{\mathrm{A}}}\left(\frac{1}{T}-\frac{1}{T_{\mathrm{ref}}}\right)\right) \tag{2.11}$$

where ΔH_{a} (J mol^{-1}) is the ionisation enthalpy, which here is approximated to be that of phenol, *i.e.* 20.0 kJ mol^{-1}. N_{A} (mol^{-1}) is the Avogadro's number and T_{ref} (K) is the reference temperature corresponding to the reference equilibrium constant. The constant for the phenolic groups was assumed to be that for phenol, which has a pK_{a} of about 10.0 at 25 °C. This estimate agrees rather well with experimental data (Norgren and Lindström 2000, Ragnar *et al.* 2000).

The protons, or more precisely H_3O^+, are attracted by the negatively charged surface, which can be accounted for by introducing a Boltzmann factor to relate the proton activity in the bulk liquid to that at the surface:

$$\{H^+\}_{R_{\mathrm{in}}} = \{H^+\}_0\exp\left(-\frac{e\psi(R_{\mathrm{in}})}{kT}\right) \tag{2.12}$$

Moreover, the pH is also temperature dependent and the value measured at 25 °C can be related to the actual pH at elevated temperature in a similar manner as in Eq. (2.11). The corresponding expression for the ionisation of water is:

$$K_{\mathrm{w}}(T) = K_{\mathrm{w}}(T_{\mathrm{ref}})\exp\left(-\frac{\Delta H_{\mathrm{w}}}{kN_{\mathrm{A}}}\left(\frac{1}{T}-\frac{1}{T_{\mathrm{ref}}}\right)\right) \tag{2.13}$$

where ΔH_{w} (J mol^{-1}) is the ionisation enthalpy, assumed temperature-independent taking the value of 56 kJ/mol (Olofsson and Olofsson 1977) and the pK_{w} was assumed to be 14.0 at 25 °C.

An explicit expression to account for the phenolic contribution to surface charge density can be obtained by combining Eqs. (2.9) to (2.13). Together with the carboxylic group contribution, it yields the total charge density as:

$$\sigma = \frac{K_{\mathrm{a}}(T)\sigma_0^{\mathrm{Phen}}}{K_{\mathrm{a}}(T) + \exp\left(-\frac{\Delta H_{\mathrm{w}}}{kN_{\mathrm{A}}}\left(\frac{1}{T}-\frac{1}{T_{\mathrm{ref}}}\right)-\frac{e\psi(R_{\mathrm{in}})}{kT}\right)10^{-(\mathrm{pH})_{0,T_{\mathrm{ref}}}}} + \sigma_0^{\mathrm{COOH}}, \tag{2.14}$$

$$K_{\mathrm{a}}(T) = K_{\mathrm{a}}(T_{\mathrm{ref}})\exp\left(-\frac{\Delta H_{\mathrm{a}}}{kN_{\mathrm{A}}}\left(\frac{1}{T}-\frac{1}{T_{\mathrm{ref}}}\right)\right)$$

where σ_0^{Phen} and σ_0^{COOH} are the contributions to the total surface charge density by the phenolic groups and carboxylic groups, respectively, being fully ionised. T_{ref} is 298.15 K or 25 °C and the overall effect of the temperature on the charge densities of the phenolic groups is strongly dependent on the relative magnitudes of the ionisation enthalpies, ΔH_{a} and ΔH_{w}. The latter is higher, with the result that the ionisation degree of the phenolic groups, and consequently the overall charge density, decreases with increased temperature at alkaline conditions (Norgren and Lindström 2000).

2.5 Modification of the Poisson-Boltzmann equation

As indicated earlier in 2.3, the Poisson-Boltzmann cell model, Eq. (2.7), neglects interactions between the ions and allows them to interact only with the mean electrostatic potential: it is thus restricted to very dilute solution. In fact, the classical Poisson-Boltzmann equation is a special case of the general, so called exact Poisson-Boltzmann equation (Hill 1986), which includes activity coefficients of the ionic species of which may deviate from unity:

$$\nabla^2\psi(r) = -\frac{e}{\varepsilon_0\varepsilon_\mathrm{r}}\sum_i \frac{\gamma_{i,0}}{\gamma_i(r)} z_i c_{i,0} \exp\left(-\frac{z_i e\psi(r)}{kT}\right) \tag{2.15}$$

The activity coefficients $\gamma_i(r)$ and $\gamma_{i,0}$ are the local activity coefficients at r (m) and at a reference condition (in this case, the bulk), respectively. As the concentration of ions increases, inter-ionic interactions become increasingly important and have to be taken into account. This can be done by the implicit incorporation of an Debye-Hückel model to estimate the local activity coefficients (Delville *et al.* 1982). However, these approaches are limited to rather dilute systems too.

Another more systematic approach for including various inter-ionic and molecular interactions is to reconsider the free energy of the system and include the effects explicitly at this level. For an open system such as the PB cell, a favourable starting point is the grand potential, Φ (J), defined as (Balian 1991):

$$\Phi \equiv A - \mu N \tag{2.16}$$

where A (J) is the Helmholtz free energy, μ (J) is the chemical potential and N (-) is the number of molecules. Due to the heterogeneous distributions of ionic species in the liquid domain, the more general density functional form of the grand potential ought to be considered, which allows spatial variations of ion concentrations, $c_i(\boldsymbol{r})$ (m^{-3}), within the domain. Adding specific ion-surface interactions (Schwierz *et al.* 2013) and steric effects of the excluded volumes of ions and solvent (Borukhov *et al.* 1997), it can be expressed as:

$$\Phi = \int\left[-\frac{1}{2}\varepsilon_0\varepsilon_\mathrm{r}|\nabla\psi(\boldsymbol{r})|^2 + e\sum_i z_i c_i(\boldsymbol{r})\psi(\boldsymbol{r}) - \sum_i \mu_i c_i(\boldsymbol{r})\right]d\boldsymbol{r}$$

$$+\frac{kT}{a^3}\int\left[a^3\sum_i c_i(\boldsymbol{r})\ln\left(a^3 c_i(\boldsymbol{r})\right) + \left(1 - a^3\sum_i c_i(\boldsymbol{r})\right)\ln\left(1 - a^3\sum_i c_i(\boldsymbol{r})\right)\right]d\boldsymbol{r}$$

$$+\int\left[\sum_i c_i(\boldsymbol{r})\left(\xi V_i^{\mathrm{phob}}(\boldsymbol{r}) + (1-\xi)V_i^{\mathrm{phil}}(\boldsymbol{r})\right)\right]d\boldsymbol{r}. \tag{2.17}$$

The first integral on the right-hand side of Eq. (2.17) contains three terms that involve the following contributions, in consecutive order: the energy of the electric field itself, the electrostatic potential energies of the ions in the electric field and the equilibrium constraint of the chemical potential of ions to the bulk condition (the second term on the right-hand

side in Eq. (2.16)). The second integral accounts for the entropic contributions of the ions and the solvent, taking into account the excluded volume and thus steric effects. The above-mentioned terms have been formulated previously (Borukhov *et al.* 1997), where a lattice site is of the size, a (m), and may be chosen to correspond to a hydrated ion. All ions are given the same size in the current expression, so ion-specific effects are therefore not introduced in this regard. In this work, a was chosen to be 7 Å, which corresponds to the diameter of a hydrated Na^+ ion (Mancinelli *et al.* 2007, Mähler and Persson 2012). An important consequence of the steric effects is the maximum packing degree of the ions, which is governed by the value of a, and becomes particularly important at highly charged surfaces. This is lacking in the classical Poisson-Boltzmann equation because the ions are treated as point-charges, and may therefore yield unreasonably high concentrations close to a surface of high surface charge density.

The last integral on the right-hand side of Eq. (2.17) introduces the interactions between ions and the parts of the particle surface other than its charges: these interactions can be specific both to the surface and the ions involved. The surface is divided into hydrophilic and hydrophobic parts, here distributed evenly on the molecular level, in contrast to having distinct meso-patches. The degree of hydrophobicity, ξ (-) [0, 1], determines the proportions of the two categories of surface characteristics. Specific ion-surface interactions with a hydrophilic and a hydrophobic surface can be accounted for by the potentials of mean force, V_i^{phil} and V_i^{phob} (J), respectively. These distance-dependent potentials have been determined elsewhere (Schwierz *et al.* 2013) from water-explicit atomistic molecular dynamics simulations. They are essentially free energies of interaction between an ion and a surface immersed in water because the effect of the water is implicit in the potentials, albeit at infinitely dilute solutions of ions. In these simulations, the hydrophilic and hydrophobic surfaces were OH and CH_3 terminated, respectively. The inclusion of the potentials in the Poisson-Boltzmann equation (without surface charges present) was verified successfully in the same study, against molecular dynamics simulations at 1 M NaCl in bulk concentration. This implies that the use of the potentials is not limited to infinitely dilute solutions.

Having all the contributions expressed in the grand potential, its partial derivatives, with respect to the electrostatic potential and the ion concentrations, respectively, may be evaluated and set equal to zero. This provides a set of equations from which the equilibrium conditions can be determined for a system that allows molecular and thermal exchange with the bulk reservoir. The partial derivative with respect to the electrostatic potential yields Poisson's equation as in earlier sources (Borukhov *et al.* 1997, Ben-Yaakov *et al.* 2011), because no additional terms involving the electrostatic potential has been added here. The partial derivatives with respect to the ion concentrations, i, on the other hand, yield the Boltzmann distributions of mean ion concentrations, which are modified further (ion-surface potentials) beyond the steric effects of ions (Borukhov *et al.* 1997). This procedure is outlined in the Appendix. Poisson's equation and the modified Boltzmann distributions can be combined to form a modified Poisson-Boltzmann equation. In the spherical coordinate system of a Poisson Boltzmann cell model it reads:

$$\frac{\mathrm{d}^2\psi}{dr^2}+\frac{2}{r}\frac{d\psi}{dr}=$$

$$-\frac{e}{\varepsilon_0\varepsilon_\mathrm{r}}\frac{\sum_i z_i c_{i,0}\exp\left(-\frac{z_i e\psi(r)}{kT}-\xi\frac{V_i^{\mathrm{phob}}}{kT}-(1-\xi)\frac{V_i^{\mathrm{phil}}}{kT}\right)}{\left[1+a^3\sum_i c_{i,0}\left(\exp\left(-\frac{z_i e\psi(r)}{kT}-\xi\frac{V_i^{\mathrm{phob}}}{kT}-(1-\xi)\frac{V_i^{\mathrm{phil}}}{kT}\right)-1\right)\right]} \tag{2.18}$$

Boundary conditions: $\left.\frac{d\psi}{dr}\right|_{r=R_\mathrm{in}}=-\frac{\sigma}{\varepsilon_0\varepsilon_\mathrm{r}}$, $\left.\frac{d\psi}{dr}\right|_{r=R_\mathrm{cell}}=0$

2.6 Numerical procedure

In order to make predictions of the pair interaction potentials by employing Eq. (2.3), the osmotic pressure due to ions between two charged surfaces has to be known. For pairwise interaction between identical particles, symmetry applies at the midpoint between the particle-surfaces. It means that the electrostatic component in the disjoining pressure in Eq. (2.1) at the midpoint vanishes. Consequently, the concentration of ions at the midpoint between two surfaces, *i.e.* at $D/2$, renders the osmotic repulsion. Since the bulk concentration of ions is finite, the net osmotic pressure at a given separation distance gives P_{entropic} in Eq. (2.3). It is expressed as a function of the difference between the midpoint concentration and the bulk concentration, *i.e.*:

$$P_{\mathrm{entropic}}(D/2)=kT\sum_i\left(c_i(D/2)-c_{i,0}\right). \tag{2.19}$$

Together with the attractive van der Waals component, this yields the disjoining pressure and the pair interaction potential may be expressed as:

$$W_{\mathrm{pair}}=4\pi R_\mathrm{p}\int_{\infty}^{\left(\frac{D}{2}\right)}\int_{\infty}^{\left(\frac{D}{2}\right)}kT\sum_i\left(c_i(D'/2)-c_{i,0}\right)d(D'/2)d(D'/2)+W_{\mathrm{vdW}}. \tag{2.20}$$

To solve Eq. (2.20), the midpoint concentrations need to be determined as a function of the separation distance. For non-dilute electrolyte solutions, as is of interest here, the modified Poisson-Boltzmann equation outlined in the previous section can be employed to estimate the midpoint concentrations. If the concentration distributions in the spherical system are approximately equal to those for the flat surface geometry at a given distance from the surface, then $R_{\mathrm{cell}}=D/2$, where the outer boundary concentration of ions provides the midpoint concentration. This has shown to be the case for similar conditions evaluated in Paper IV. It should be noted that the surface charge density in the inner boundary condition

in Eq. (2.18) has to be determined implicitly because it is a function of the electrostatic potential at the surface, see Eq. (2.14).

Dispersion effects enter implicitly in the estimation of midpoint concentrations due to ion-surface potentials introduced in the modified Poisson-Boltzmann equation (Eq. (2.18)). However, they also have a direct influence on the van der Waals contribution to the disjoining pressure in Eq. (2.1), *i.e.* a van der Waals interaction between the surface (non-electrostatic part) and the dispersive part of the ions. This interaction may, in fact, even be repulsive for cations near a hydrocarbon-surface. Nevertheless, it is typically small in relation to the indirect effect it has on the entropic pressure contribution of the ions (Parsons *et al.* 2011), and thus has been neglected here. What remains is the classical van der Waals potential of attraction (Hamaker 1937), *i.e.* the last term in Eq. (2.20). The lignin-water-lignin Hamaker constant of 4.2 *kT* was used (Hollertz *et al.* 2013), although the value could potentially be significantly lower in a strong electrolyte. This is due to the screening of the zero-frequency contribution of van der Waals interaction that could lead to a significant reduction in the Hamaker constant (Israelachvili 2011). For hydrocarbons, this contribution is in the order of $3kT/4$, which provides an indication of the order of the possible reduction.

The degree of hydrophobicity of the kraft lignin particles was assumed to be 88 %, *i.e.* assumed to be the same as in Paper IV. The surface charge densities were estimated based on the average contents of phenolic and carboxylic groups for the kraft lignin source utilised in the experimental study (see 3.1 Materials). The parameters of the solution condition in the estimations were also chosen to correspond, as close as possible, to the precipitation conditions in Paper V. Moreover, the ion-surface potentials used were those for interactions of Na^+, Cl^- and F^- with a hydrophobic and hydrophilic surface, respectively. F^- potentials were used because potentials for SO_4^{2-} and OH^- ions, which were present in the experiments in Paper V, were lacking in the literature source utilised (Schwierz *et al.* 2013): they were instead approximated with F^- potentials. Nevertheless, all three of these ions are characterised as being quite similar in the Hofmeister series (Parsons *et al.* 2011), and are sometimes classified as strongly-hydrated kosmotropic ions, although this is merely a qualitative description (Salis and Ninham 2014).

A sufficiently dilute dispersion of particles is required for many-body interactions between them to be negligible, so that pair interactions may be regarded as being sufficient to be considered (see 2.3 Poisson-Boltzmann cell model). It is thus useful to have an idea of the ranges of Poisson-Boltzmann cell radii corresponding to the homogenously dispersed state that can be expected, for purposes of comparison with the range of the pair potentials (the latter of which are known first after the numerical results have been retrieved). Consider the following hypothetical test case: a suspension consisting of 9 wt% kraft lignin, of which the volume fraction (solidosity) of the solid part of the spherical kraft lignin agglomerates are 50 % lignin. If all of the particles had a radius of 10, 100, or 1000 nm then, hypothetically, the corresponding $D/2$ values would be 9, 88 and 883 nm, respectively (see the calculation in the Appendix). These values ought to be much larger than the range of the pair interactions to satisfy the requirement of the assumption of pairwise interactions.

3 Experimental

This chapter presents the materials, preparations and experimental set-up used in the experiments conducted. Moreover, it describes briefly the principles of the main equipment utilised in the experiments, namely Focused Beam Reflectance Measurement (FBRM) and Confocal laser Scanning Florescence Microscopy.

3.1 Materials

Lignin

A softwood kraft lignin, sourced from a Nordic pulp mill and extracted by LignoBoost™ technology, was used in this study. Lignin from the same batch as used here has been characterised by others regarding ionisable functional groups (Aminzadeh *et al.* 2017). The contents of phenolic groups and carboxylic groups were found to be 4.27 mol/kg and 0.45 mol/kg, respectively. The residual content of xylan on the lignin used in the current study was determined to be 0.35 %. The estimated content of residual xylan was based on measurements of the xylose concentration after acid hydrolysis with sulphuric acid using a methodology that can be found elsewhere (Jedvert *et al.* 2012). The concentration of xylose was measured using a Dionex ICS-5000 system equipped with CarboPac™ PA1 columns. An electrochemical detector was used; the eluents were NaOH and NaOH+NaAc (0.2 M).

The molecular weight distribution of the kraft lignin was determined from measurements using gel-permeation chromatography (GPC), which is a size-exclusion chromatography (SEC) method. The unit was a PL-GPC 50 plus equipped with a PolarGel-M column and a guard column (300x7.5 mm/50 x 7.5 mm, 8 µm). A DMSO/LiBr mixture of 10 mM LiBr was used as the mobile phase and the external calibration curve-fit was based on standards of Pullulan of the type: polysaccharide calibration kit, Varian. Four samples were taken of the LignoBoost powder of kraft lignin from the stored batch source and run in the GPC unit. The results from these runs are shown in Figure 3-1 as relative intensities of various molecular weights.

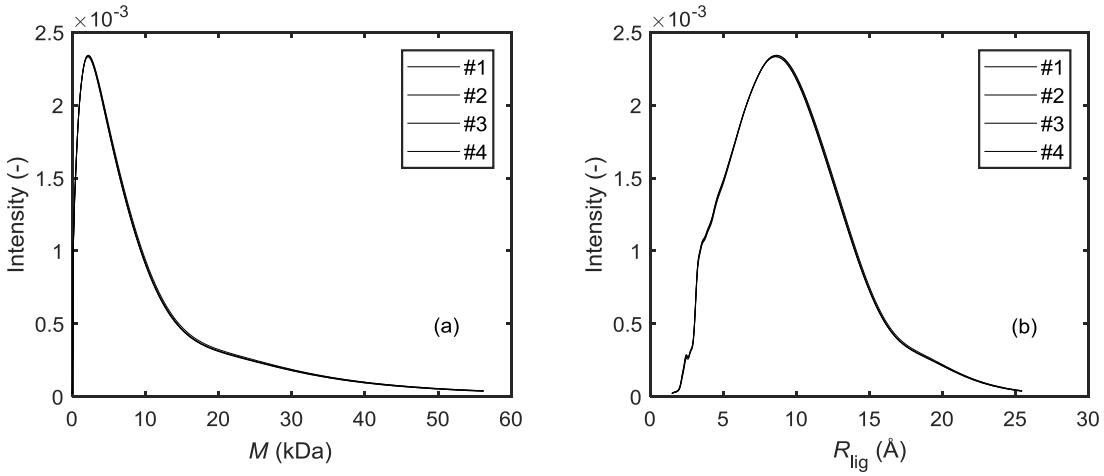

Figure 3-1. ***(a)*** *Molecular weight and* ***(b)*** *estimated macromolecular size distributions of the initial kraft lignin powder sampled four times (#1-4). The average M_n and M_w are 3.1 and 11.3 kDa, respectively.*

The results in Figure 3-1 indicate a widely polydisperse material with the most common molecules belonging to the low molecular weight fraction below 10 kDa, although there is a significant tail in the distribution of high molecular weight material. In order to provide an idea of the corresponding molecular size, a rough estimate of the corresponding molecular size distribution is shown in Figure 3-1: the mode-value of the distribution is about 1 nm. The procedure and assumptions made to estimate the molecular weight and size distributions are presented below.

The number and weight-averaged molecular weights, M_n and M_w, respectively, were determined according to:

$$M_\mathrm{n} = \sum_i n_i M_i \tag{3.1}$$

$$M_\mathrm{w} = \sum_i n_i M_i^2 \left(\sum_i n_i M_i \right)^{-1} \tag{3.2}$$

where n_i is the normalised intensity response measured in the ultra-violet region corresponding to molecular weight M_i. For the four distributions, the average values of M_n and M_w were 3.1 (± 0.03) and 11.3 (± 0.09) kDa, respectively, which yields a polydispersity of 3.6. It ought to be mentioned that it is difficult to determine the molecular weight of kraft lignin, and especially so from the indirect measurements made here. The values obtained are always specific to the instrument system and calibration curve used.

Assuming that kraft lignin macromolecules are compact and spherical, the size distribution of the molecules may be estimated according to:

$$R_{\mathrm{lig},i} = \left(\frac{3}{4\pi} \frac{M_i}{N_\mathrm{A} \rho_\mathrm{lig}} \right)^{1/3} \tag{3.3}$$

where $R_{\mathrm{lig},i}$ is the estimated radius of the lignin molecule with molecular weight, M_i, and ρ_{lig} is the density of lignin, 1350 kg m^{-3} (Norgren and Lindström 2000).

Xylan

The xylan added to the solutions used in the precipitation experiments was a beechwood xylan (Lot 141202, P-XYLNBE, Megazyme) with a glucuronic acid content, according to the supplier, of 13.0 wt% .

Chemicals

Aqueous model solutions for use in the precipitation experiments were prepared by mixing NaOH (Sigma Aldrich, purity ≥ 98%) with either Na_2SO_4 (Fisher Chemical, purity > 99.5 %) or NaCl (Sigma Aldrich, purity ≥ 99.5%) and deionised water. The two acids used for acidification was made by diluting concentrated sulphuric acid (Scharlau, 95-97 %) and hydrochloric acid (VWR, 37 %) to solutions of 6 M.

3.2 Preparation and set-up

The preparation and experimental set-up have, in principle, been the same throughout the work. The main steps in the experimental procedure are illustrated in Figure 3-2. Papers II, III and V have focused on the monitoring of the precipitation process: the steps involved are shown in the upper part in the chart. The work presented from Paper I concerns the analysis of the distribution of xylan that was conducted on the filter cake material of kraft lignin: this material was retrieved from filtration following after the precipitation stage.

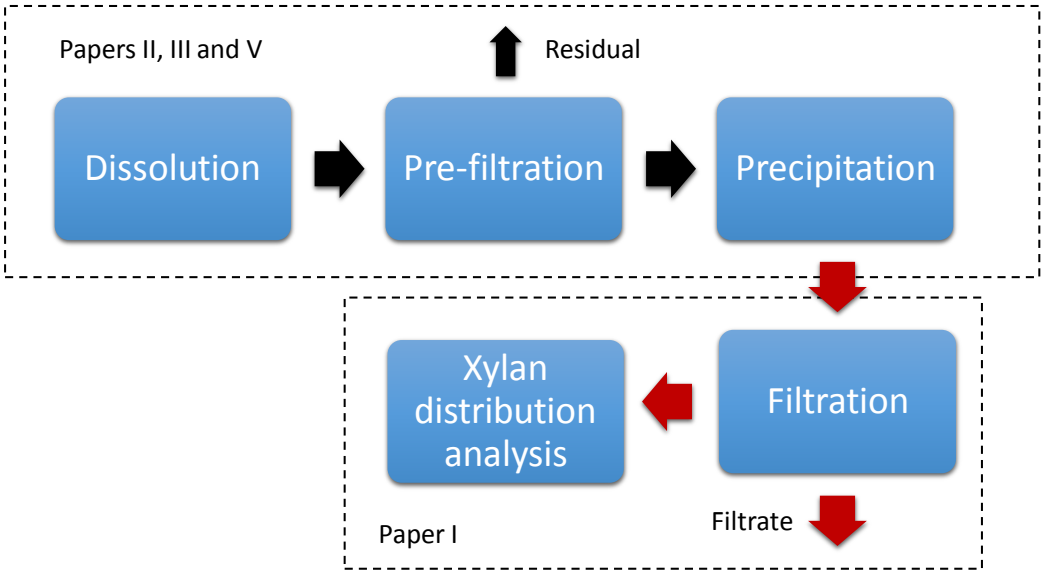

Figure 3-2. Overview of steps in the experimental procedure.

Preparations for the precipitation experiments

The first step in the experimental procedure was the dissolution of the kraft lignin powder in 1.0 M NaOH aqueous solution for a minimum of 16 hours; the pH during the dissolution stage was >13. In Papers III and V, all mixtures were pre-filtered after the dissolution period

at room temperature. In Paper II, some mixtures were prefiltered and others were not, in order to investigate the effect of this stage on precipitation. The pre-filtration was performed using a Buchner funnel connected to the top of a glass flask by vacuum suction: the filter paper was a Sartorius stedim, Type 184 (regenerated cellulose), having a nominal cut-off of 0.45 µm. In all cases, less than 1.6 % of the organic mass was filtered off although, in most cases, the loss was around 1 %. The filtrate had a concentration of 0.1 g lignin per g water when it was added to the precipitation vessel with a pH > 13 (Papers II and III) or about 12.3 (most cases in Paper V).

The precipitation vessel

The precipitation vessel was a 0.5 L jacketed glass vessel of inner diameter (96 mm). It was baffled along the walls and equipped with a pitched-blade impeller (diameter 50 mm/blade with 10 mm), positioned 15 mm from the bottom, to provide good mixing conditions. The agitation speed was 250 rpm (Papers 1, III and V) or 150 rpm (Paper II), and the direction of the flow was downwards. The temperature of the interior volume was controlled by indirect heating via the jacket. The FBRM probe was inserted at an angle of about 35 ° towards the direction of the flow to ensure the sufficient impingement of particles on the window located on its tip, yet preventing lignin from clogging the window during measurement (for a further description see 3.3 Focused Beam Reflectance Measurement (FBRM)). An illustration of the vessel is provided in Figure 3-3.

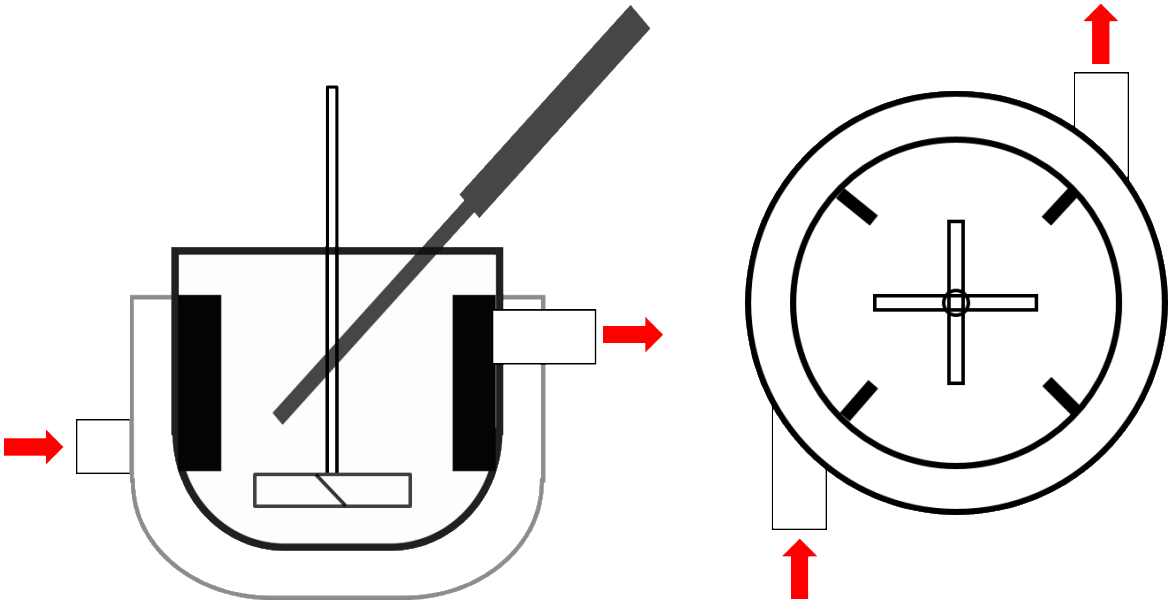

Figure 3-3. Schematic diagram of precipitation vessel employed. Red arrows indicate the inlet and outlet flows of the heating fluid used to heat the vessel indirectly.

Acidification and pH measurements

Precipitation was performed by the addition of 6 M sulphuric or hydrochloric acid in a dropwise and sequential manner to allow the pH of the system to equilibrate in between the sequences. When the pH value was stable after the addition of an amount of acid, the liquid was assumed to be in chemical equilibrium with the surfaces of the particles in the system (*e.g.* the equilibrium protonation reaction of ionisable groups). Measurement of the pH was made at different times during each experiment by withdrawing a sample of 10 ml from the vessel, cooling it to about 25 °C and then using a pH meter calibrated at room temperature.

The sample was re-heated to the precipitation temperature after the pH measurement was complete and returned to the precipitation vessel. This procedure, whereby the sample was returned to the vessel, had no influence on the chord length distribution that was measured during the experiments.

Analysis of the distribution of xylan in particles

Other precipitation experiments were performed where the pH was lowered by adding sulphuric acid (6 M) in one stage. After precipitation occurred, the heat was turned off and the vessel was allowed to cool to room temperature before the suspension was filtered and the cake collected. The filter cake was used to analyse the distribution of xylan in the particles that composed the cake. Samples from the cakes were taken for later analysis on the microscopic level (see 3.5 Confocal Laser Scanning Florescence Microscopy). Slices taken from layers at different heights in the cake were used to analyse the content of xylan at different positions within it. The content of xylan in the samples taken from the slices could be estimated from the content of xylose after treating the samples with a highly concentrated solution of sulphuric acid and quantifying the xylose content with High Performance Anion Exchange Chromatography (HPAEC) analysis using a Dionex ICS 5000 system equipped with CarboPac^{TM} PA1 columns and an electrochemical detector. The procedure for this quantification of xylose can be found elsewhere (Jedvert *et al.* 2012).

3.3 Focused Beam Reflectance Measurement (FBRM)

FBRM is a laser-based technique used for the particle-size analysis of a system both *in situ* and in real time. More precisely, it measures the chord lengths of particles and, during a predetermined time interval, reports the numbers of chord lengths being allocated to bins (#1-100) with predefined bin edges. The allocation setting used in this work is known as "primary" and focuses the resolution of the chord length dimension to smaller particles, *i.e.* the bin-width increases along the dimension according to a geometric series. The unit used here, a G400 from Mettler Toledo, reports the numbers of particle chord lengths measured during a predefined sampling time as "counts" (#/s). It is these counts that, when allocated to different chord length-bins, result in the chord length distribution. The technique utilises scattering and interference phenomena of light for the measurement of chord lengths by focusing a beam at a point very close to the window on the tip of the FBRM probe immersed into the fluid under investigation, *e.g.* a fluid comprised of solid particles suspended in a liquid. The focused beam scans the suspension in a fixed circular path at high speed (2 m/s); the chords of the particles measured are reported in the 1-1000 µm range. The equipment utilises the time elapsed by the back-scattered light, which results in a pulse, as the focused beam passes across a particle. The velocity of the scanning motion of the focused beam and the duration of the pulse then determine the chord length. A schematic diagram of this measurement technique is shown in Figure 3-4.

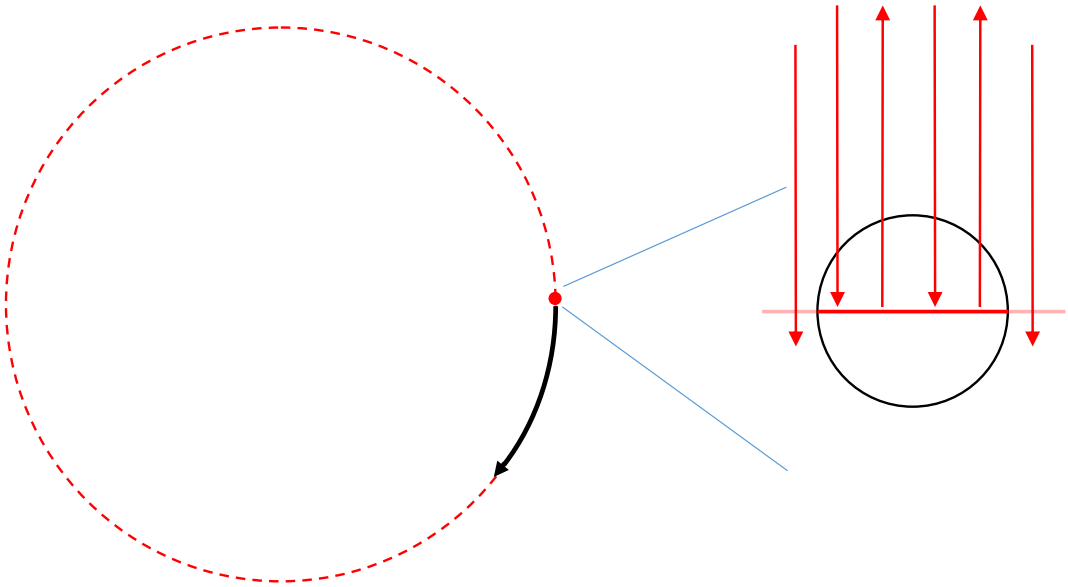

Figure 3-4. Schematic diagram of the Focused Beam Reflectance Measurement (FBRM) technique. The laser beam is focused on a point located just outside the probe window in the fluid being analysed. The focal point moves along a circular path at a fixed speed and, as a particle passes it, back-scattering of light occurs. This is returned to the probe and measured by the equipment.

3.4 Analysis of chord length counts

The onset of the formation of stable particles of size ≥ 1 µm was determined from the precipitation experiments in this work by analysing the counts of chords measured during the *in situ* monitoring of the precipitation process with the FBRM equipment. As acidification was being performed in an experiment, an increase in counts could often be observed as a consequence of particles being formed. In the early stages of the acidification sequence, when the onset condition had not yet been reached, the count levels decayed again to the baseline and resulted in a "count-peak": this is not regarded as being the onset. If, on the other hand, the count levels remained elevated above the baseline after an increase in counts, then that rise in counts was regarded as the onset of the formation of stable particles ≥ 1 µm. This, and the estimation of the time-scale of particle formation on the micron scale, is illustrated schematically in Figure 3-5.

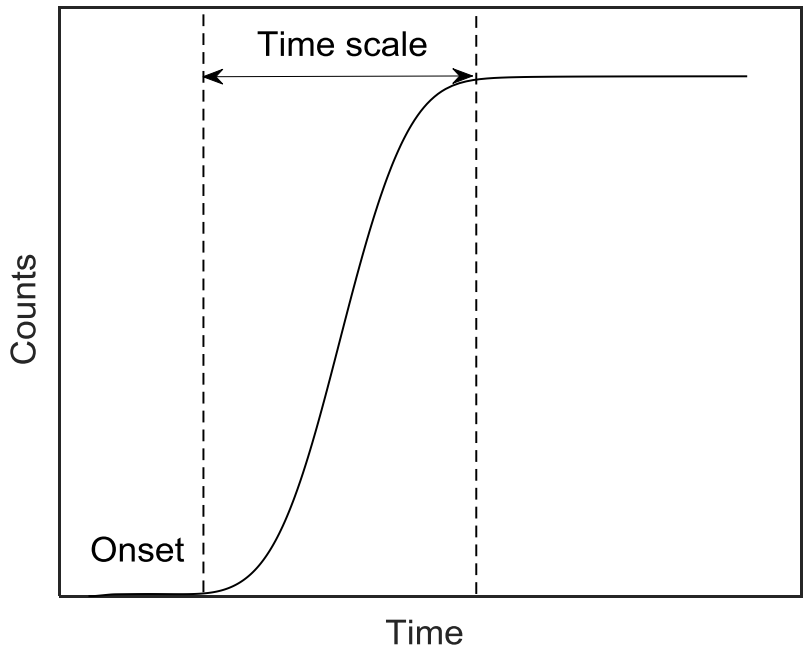

Figure 3-5. Schematic illustration of the onset of the formation of stable particles ≥ 1 µm and the evolvement of the following formation of particles on the micron scale, quantified as "counts" of the chords measured. The kinetics of the precipitation process levelled out, from which a time scale could be determined.

For some analyses it can be beneficial to have approximately equal bin-widths of chord lengths classes so that the relative abundance of particles belonging to various size-classes can be compared, and not merely the relative changes in the chord length distributions. The bin-width was therefore chosen to be approximately 5 µm; the original chord length-classes from the output of the equipment were allocated, as accurately as possible, to the new classes with approximately equal bin-widths. The bin-width remained at approximately 5 µm, up to about 30 µm, after which virtual deviations occurred and increased along the dimension (see 4.1.4 Chord length distributions).

The chord length distribution is number-based but it can, however, be used to construct a volume-based distribution for particles ≥ 1 µm if certain assumptions are made. If the particles are assumed to be spherical, and the chord length being measured is their diameter, then the volume fraction of a size class can be estimated as:

$$vol.\%\ (d_{i_1} \leq d_i \leq d_{i_2}) = 100\left(\sum_{i=i_1}^{i_2} d_i^3\, N_i\right)\left(\sum_{i=1}^{i_{\max}} d_i^3\, N_i\right)^{-1} \tag{3.4}$$

where d_i is the diameter or chord length from the original chord length distribution, i, of particles of N_i counts and the indices i_1 and i_2 represent the bin-edges of the size-class. The index i runs from 1 to $i_{\max}$ which is the largest cord length reported by the equipment (1000 µm). If it is further assumed that the volumetric densities (solidosity) of the particles are equal, the class also represents the volume fraction of the lignin precipitated among the particles on the micron scale.

3.5 Confocal Laser Scanning Florescence Microscopy

This microscopy method has been used widely for studying (micro) biological systems and in food science in order to reveal the structure and/or distribution of the various constituents of a sample. A monochrome laser beam illuminates a sample containing florescent constituents: the radiation is adsorbed and light of lower wavelengths is emitted that can be detected by the instrument. Typically, a spectrum of emitted light is obtained, the intensity of which can be examined in different regions of wavelength in the spectrum. It is a useful technique for detecting the locations of one or more florescent constituents in a sample by contrast imaging. Since lignin is auto-florescent, it is possible to dye xylan by the chemical attachment of a florescent side group that preferably emits light of relatively high intensity in a region of the spectrum where the intensity of the auto-florescence of lignin is relatively low. Xylan and lignin can thus be located in the sample by means of contrast imaging, and information on the distribution of the constituents in the sample can thereby be gained.

In this work, a Confocal Laser Scanning Microscope of type Leica TCS SP5 II from Wetzlar, Germany, was used. The laser used for illuminating the samples was a 488 nm argon laser; the depth of the scanning layer was about 0.8 µm. An upright set was used in which the illumination source hits the sample target from above, whilst the laser scans the sample, layer by layer, in a plane within a chosen region. Thus, three-dimensional imaging can be obtained of the florescent matter emitting light in the wavelength region of interest. The xylan was dyed by attaching Remazol Brilliant Blue R (RBBR) to it using a synthesis procedure, resulting in an ether bond between the xylan and the RBBR. The dye emits light with wavelengths found predominantly in a spectrum where its intensity profile is shifted towards wavelengths higher than the region in which the lignin emits most light. Images of the distribution of lignin and xylan may then be obtained by imaging the location of emittance in the chosen regions of 500-540 (which is dominated by lignin) and 620-720 (where the difference in emittance between BRRB and lignin is the greatest), and by co-localising the emittance of the two intervals of wavelengths.

4 Results

This chapter summarises the experimental and numerical results presented in this thesis. It starts with the experimental results, which are summarised from Papers I-III and V. The numerical results, which are based on the model and numerical scheme in Paper IV, are thereafter presented.

4.1 Experimental results

This section primarily concerns the precipitation experiments conducted in a precipitation vessel monitored by FBRM. Firstly, an overview of the course of precipitation is outlined. Then the onset of precipitation of particles ≥ 1 µm is presented and discussed in more detail, followed by the analysis that was carried out of the chord length distributions. Finally, the results of the co-precipitation of kraft lignin with xylan are shown and the effect of the latter is evaluated. As well as the FBRM results, the analysis of the distribution of xylan in the precipitated lignin is also presented here where, for instance, confocal laser scanning florescence microscopy was used.

4.1.1 Course of precipitation

The precipitation of kraft lignin is influenced by parameters such as pH, ion concentrations in the aqueous solution and temperature. The experimental procedure employed provided the possibility of monitoring the course of precipitation as the conditions were changed which, in this work, was primarily by decreasing the pH. Figure 4-1 illustrates the course of precipitation during an experiment as a consequence of the addition of the salt, followed by the subsequent addition of acid. The pH decreased from the initial pH (in this case pH 12.0) as all the more acid was added. At sufficiently high pH, it can be observed that an increase in counts usually followed after an addition of acid. However, the count levels decreased quickly again to the baseline, resulting in a "count-peak". This behaviour is not regarded as being an onset point of stable particles ≥ 1 µm. The locally acidic areas in the liquid where the acid was added would temporarily have a lower pH than the surrounding liquid, which could result in local precipitation being observed as the count-rise. As the pH gradient evened out, the lignin particles that formed were unstable and either disintegrated or redissolved. It was not until the pH decreased to a critical point that a distinct increase in count levels could be observed that is not followed by a decay in the levels to the baseline: this was identified as the "the onset of formation of stable particles ≥ 1 µm". From

the pH measurements made close to this point in time, an onset pH could be determined. In Figure 4-1 the evolution of the entire experiment is shown in the upper image, whereas the lower image displays a close-up on the early stage before onset and at its occurrence (*i.e.* the distinct count-rise at about 300 min). Judging by the relatively small amount of acid needed to go from the baseline to the rapid formation of particles ≥ 1 µm, it seems that the stability of the lignin dispersion was very sensitive to the pH-level, at least at these conditions (1.2 mol Na^+ kg^{-1} water and 65 °C). As can be seen in the following figures further below, the onset pH can be less clear in the data and precipitation kinetics can be much slower.

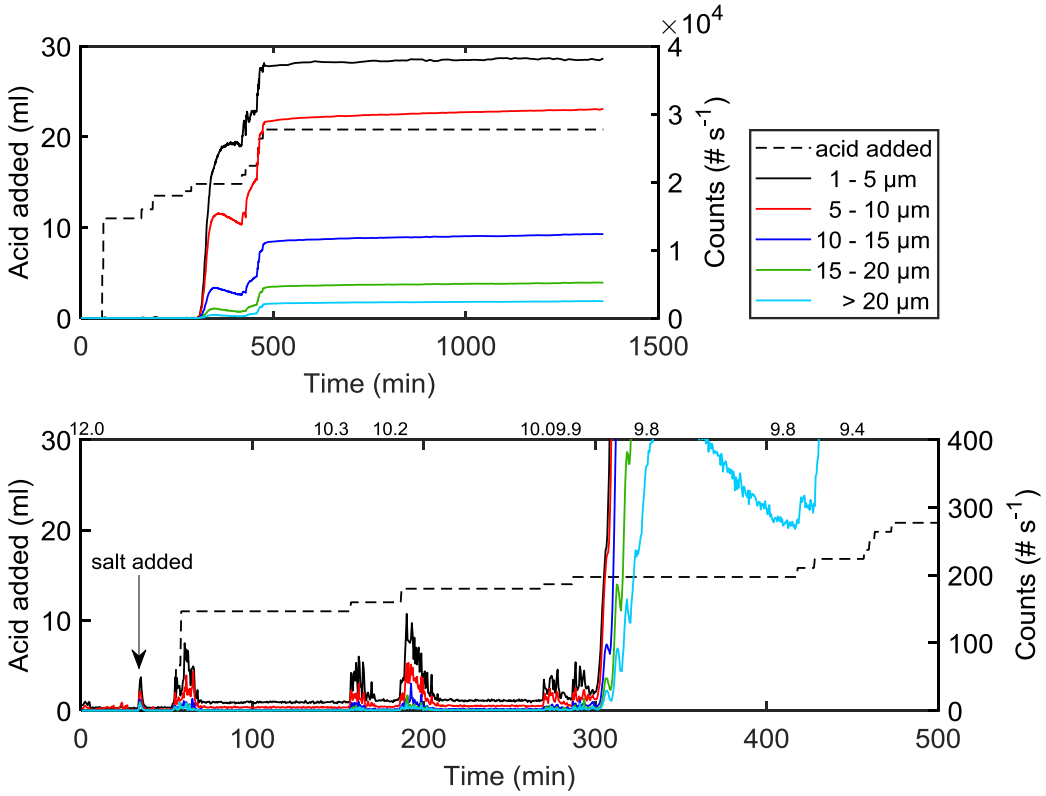

Figure 4-1. The course of precipitation. The line of numbers above the lower image are the pH values measured at 25 °C at various times throughout the experiment. Precipitation conditions: 65 °C, 1.2 mol Na^+ kg^{-1} water and Cl^- as the anion.

The course of precipitation, at a range of conditions in terms of Na^+ concentration and anion-type in the added salt, from the point of addition of the salt at the initial pH, the subsequent addition of acid in sequences and to the end pH, are presented in Figure 4-2 to Figure 4-7. It can be observed that when adding NaCl at an initial pH of about 12.3 (Paper V), the formation of stable micron-sized particles occurred at Na^+ concentrations of 2 mol kg^{-1} water or higher, while this was not the case when Na_2SO_4 was added (*cf.* Figure 4-2 to Figure 4-5). The experiment at the high concentration level of salt with NaCl added (4.0 mol Na^+ kg^{-1} water) was repeated without lignin: the count-peak after the salt addition disappeared quickly and returned to the baseline. This indicates that the initial count levels mentioned previously, observed after the addition of NaCl, were probably not for salt crystals but rather the lignin particles that had formed.

In the case, with SO_4^{2-} as the anion, on the other hand, acidification was necessary to cause the formation of stable micron-sized particles. However, at the high salt level (4 mol Na^+ kg^{-1} water), a mere decrease in pH to a level of 11.7 was sufficient to generate a slow but observable formation of stable micron-sized particles. It was not until the pH had been decreased to about 11.3 that a significant formation of micron-sized particles could be observed: this characteristic event is regarded as being "the onset of the formation of particles ≥ 1 µm by means of acidification". Obviously, these observations do not exclude the possibility that submicron-sized particles were formed at an earlier stage, *i.e.* at a pH higher than the onset pH, but such particles cannot be reported by the experimental equipment used. Figure 4-6 and Figure 4-7 show experiments with an initial pH >13 and having SO_4^{2-} as the anion in the added salt. Here, it can also be observed that no stable micron-sized particles were formed after the addition of the salt: significant acidification was required to cause the onset of the formation of stable micron-sized particles.

The observations discussed above indicate that there is a specificity in the precipitation depending on which anion is present in the solution (in this case Cl^- or SO_4^{2-}). It appears to be easier to form micron-size particles when Cl^- is present compared to SO_4^{2-}, although it cannot be determined if this relation also applies to the formation of the first stable solid nuclei on the nano-scale. Another study (Norgren and Mackin 2009) indicated that the reverse order may apply regarding the formation of the first stable solid phase, *i.e.* that SO_4^{2-} salts out kraft lignin easier than Cl^-. It should be mentioned, however, that the source of kraft lignin and its concentrations were different to those used in this study. Furthermore, this may not necessarily contradict the findings of this work: the effects had by various anions on precipitation may differ for different length-scales and/or at different concentration ranges of salt (Zhang and Cremer 2009). In this work, the salt concentrations were shifted to higher values; ion-specific differences can be observed in the range of 2-4 mol Na^+ kg^{-1} water. This is discussed further in 4.2.3 Comparisons with experimental observations: further considerations.

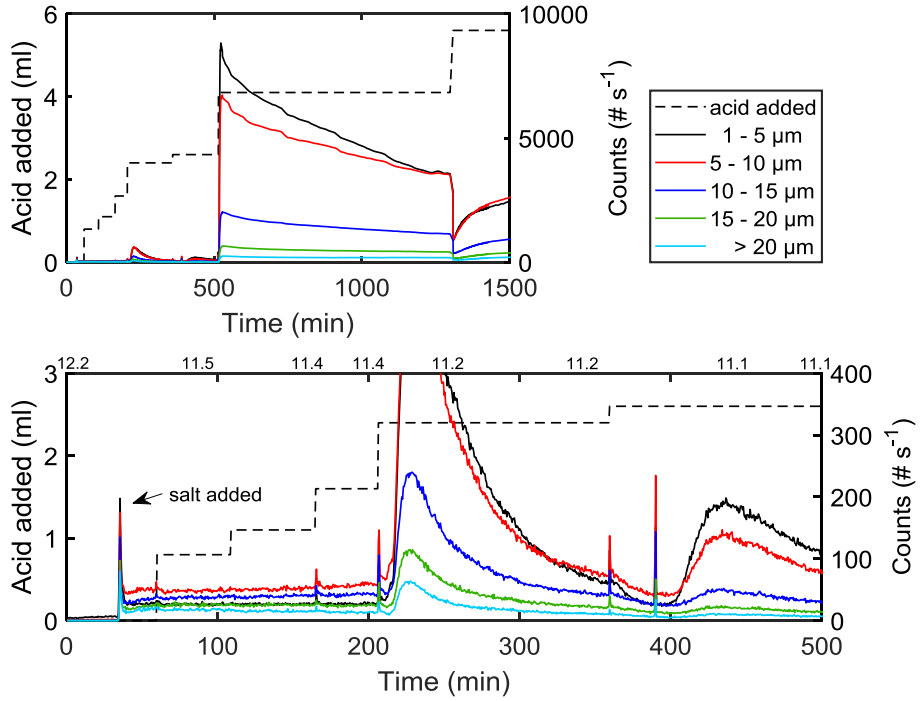

Figure 4-2. The course of precipitation. The line of numbers above the lower image are the pH values measured at 25 °C at various times throughout the experiment. Precipitation conditions: 65 °C, 3.9 mol Na^+ kg^{-1} water and Cl^- as the anion.

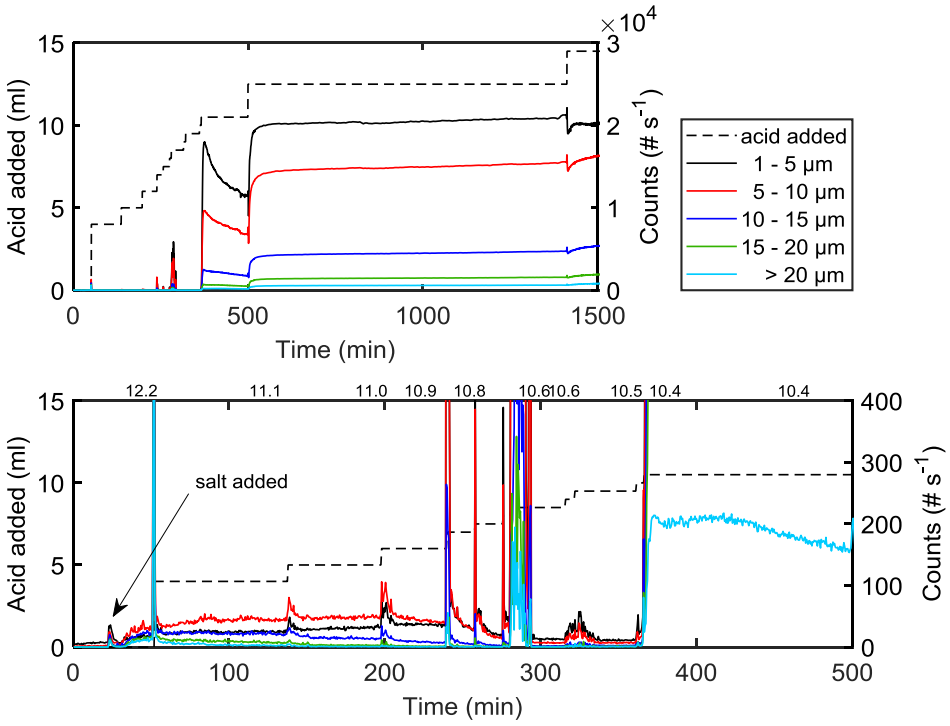

Figure 4-3. The course of precipitation. The line of numbers above the lower image are the pH values measured at 25 °C at various times throughout the experiment. Precipitation conditions: 65 °C, 2.0 mol Na^+ kg^{-1} water and Cl^- as the anion.

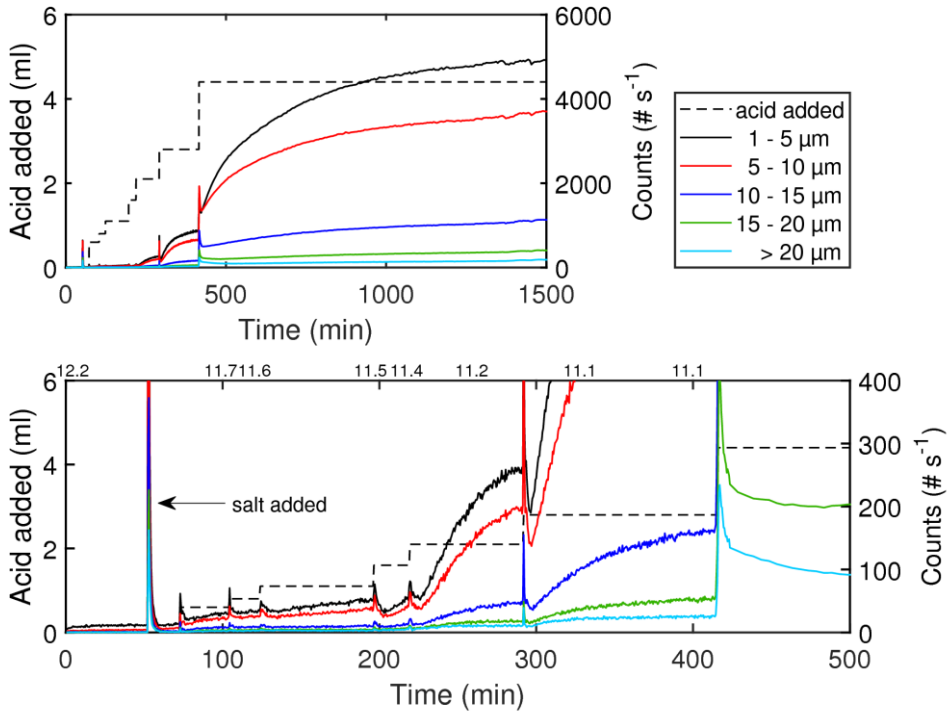

Figure 4-4. The course of precipitation. The line of numbers above the lower image are the pH values measured at 25 °C at various times throughout the experiment. Precipitation conditions: 65 °C, 4.0 mol Na^+ kg^{-1} water and SO_4^{2-} as the anion.

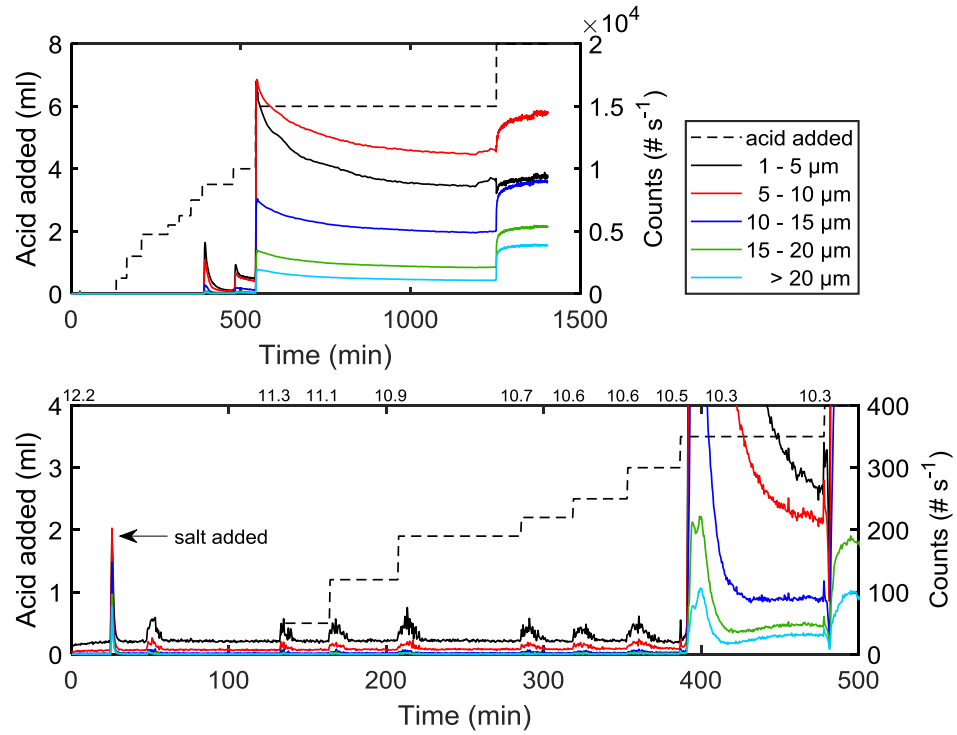

Figure 4-5. The course of precipitation. The line of numbers above the lower image are the pH values measured at 25 °C at various times throughout the experiment. Precipitation conditions: 65 °C, 2.0 mol Na^+ kg^{-1} water and SO_4^{2-} as the anion.

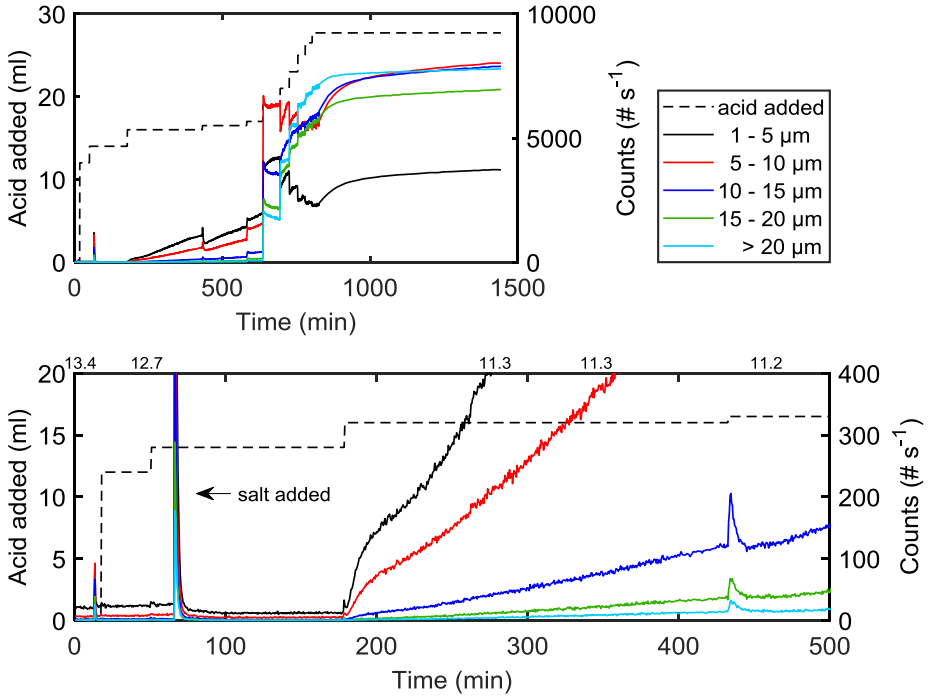

Figure 4-6. The course of precipitation. The line of numbers above the lower image are the pH values measured at 25 °C at various times throughout the experiment. Precipitation conditions: 77 °C, 4.0 mol Na^+ kg^{-1} water and SO_4^{2-} as the anion.

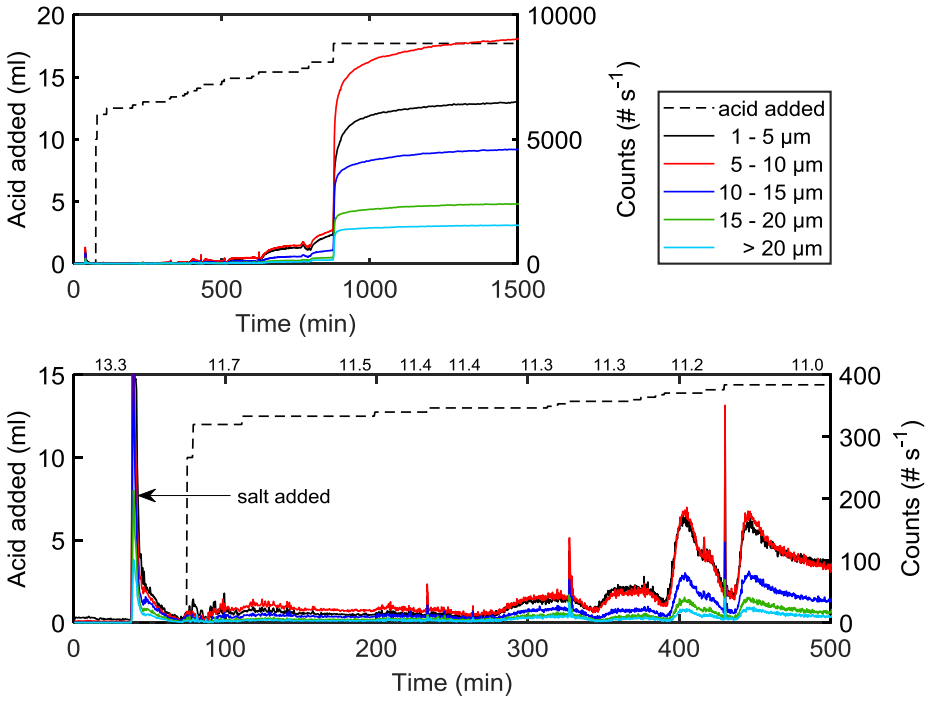

Figure 4-7. The course of precipitation. The line of numbers above the lower image are the pH values measured at 25 °C at various times throughout the experiment. Precipitation conditions: 45 °C, 4.0 mol Na^+ kg^{-1} water and SO_4^{2-} as the anion.

4.1.2 Onset of particle formation

A compilation of "the onset of the formation of particles ≥ 1 µm" in this work and the C.C.C. of NaCl determined in other studies found in the literature are shown in Figure 4-8. Moreover, in one of the literature sources (Norgren *et al.* 2002), the formation of particles ≥ 1 µm and the C.C.C. clearly coincided; another (Fritz *et al.* 2017) pointed in the same direction, albeit less clearly. It is apparent that the onset pH is strongly dependent on the Na^+ concentration in a wide range of conditions. In general, the combined effect of the pH and the Na^+ concentration suggests that electrostatics play a significant role: precipitation may be caused by either lowering the pH or increasing the Na^+ concentration. Some of the more subtle differences may be due to differences in the experimental set-up and/or the source of the kraft lignin used. For instance, one data point (Norgren *et al.* 2002), corresponding to the precipitation of Indulin at non-agitated conditions, reports the formation of micron-sized particles at pH 10.5, 1.3 mol Na^+ kg^{-1} water and 70 °C, whilst the corresponding onset condition in the present work was pH 9.8 at 1.2 mol Na^+ kg^{-1} water. In the latter case, agitation was employed, which may influence the stability of agglomerates and especially so in the micron range; moreover, LignoBoost kraft lignin was used (see 3.1 Materials).

At the initial pH of about 12.3 and 2.0 mol Na^+ kg^{-1} water or higher (specifically with NaCl), the lignin, salted out as micron-sized particles, suggests that different lignin fractions exhibit different phase behaviour. High molecular weight kraft lignin has been found to precipitate more easily than its low molecular weight counterparts (Norgren *et al.* 2001, Norgren *et al.* 2002, Zhu *et al.* 2016). Furthermore, it has been suggested that the high molecular weight factions may behave as colloids (Norgren *et al.* 2002), being destabilised first when either an addition of salt is made or the pH is lowered. In the other end of the molecular weight distribution, the lignin molecules may be rather small and require a lower pH or higher salt concentration to precipitate compared to colloidal-like lignins. The results reported in 4.1.2 Onset of particle formation show that the number of particles formed increases with decreased pH and/or increased Na^+ concentration. This may be a consequence of the heterogeneity in the molecular properties of the kraft lignin: as the dissolution conditions for the lignin becomes worse, in terms of the levels of pH and salt concentration, all the more kraft lignin gradually precipitates.

In most of the studies in this work, the precipitation temperature was elevated (45-77 °C). However, although the data in the lower range of Na^+ concentrations (Lindström 1980) corresponds to 25 °C, the data point at pH 6.2 applied to the range 25-60 °C (see data set of red-edged circles in Figure 4-8). It is possible that the points at lower pH may also do so because the effect of temperature on pH is negligible at acidic conditions. The data point at about 2 mol kg^{-1} water, which deviates from the rest of the data at similar magnitudes of Na^+ concentration, corresponds to 25 °C. A significantly lower pH was however required at this condition to reach a C.C.C. of 2 mol kg^{-1} water: the temperature level may be the main reason for this because a higher temperature has been found to destabilise kraft lignin dispersions at alkaline conditions (Norgren *et al.* 2001). An observation (unpublished data) pointing towards a similar effect was made in a recent experiment using the same experimental scheme as in this work: when an attempt was made to salt-out the lignin at room temperature by adding Na_2SO_4 at pH 9.6, no formation of particles ≥ 1 µm was observed during the subsequent addition of salt. Instead, the system underwent gelation at about 1.4 mol Na^+ kg^{-1} water. Submicron-sized particles and/or macromolecules had

probably become stabilised and prevented from growing into the micron range: the system underwent gelation without forming particles ≥ 1 µm. Those observations indicate that it may be difficult for particles ≥ 1 µm to form at room temperature. Consequently, a sufficiently elevated temperature is required in order to achieve sufficient growth in the size of the particles rather than gelation. Gelation has also been observed in this study (Paper III), at around pH 9 at 45 °C and 1 mol Na^+ kg^{-1} water. At higher salt concentrations, however, this was not observed. It suggests that the lower limit in temperature prior to gelation may be dependent on the other two main parameters: pH and salt concentration. The principles determining whether kraft lignin undergoes gelation or precipitates as suspended solid particles are currently not understood.

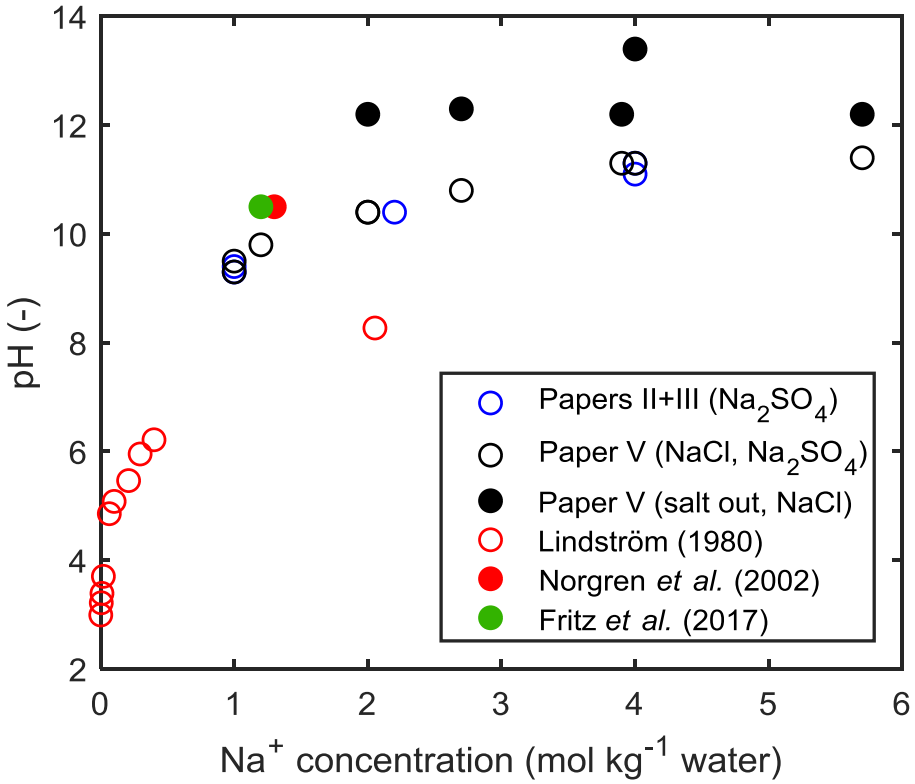

Figure 4-8. The pH value at the onset of the formation of particles ≥ 1 µm or C.C.C. (literature sources) of Na^+ concentration.

4.1.3 Pre-existence of particles prior to acidification

The presence of pre-existing micron-sized particles suspended in the liquid prior to acidification has a mere, yet observable, influence on the onset pH (see Figure 4-9): the count-value of all particles ≥ 1 µm is virtually zero due to prefiltration, and the onset pH decreases by about 0.2 pH units compared to non-prefiltered cases. In the absence of pre-existing micron-sized particles, a lower pH was required to cause the onset of the formation of new micron-sized particles. This was observed at the two lower salt concentration levels, *i.e.* 1.0 and 2.0 mol Na^+ kg^{-1} water, but not, however, at the higher level of 4.0 mol Na^+ kg^{-1} water (Na_2SO_4 was used to regulate the Na^+ concentration in all of these cases). As already discussed in 4.1.2 Onset of particle formation, one interpretation that can be made for high salt concentrations, *e.g.* 4.0 mol Na^+ kg^{-1} water and also using SO_4^{2-}, is that a substantial

amount of submicron particles may have been formed already at the initial pH (>13) when the salt was added. In the prefiltered case at 4.0 mol Na^+ kg^{-1} water in Figure 4-9, sufficient amounts of submicron particles may thus have been formed after the addition of salt, but were not detectable during acidification towards the onset. It is possible that the onset occurred at a pH similar to that of the corresponding non-prefiltered cases, as a lower pH was not required due to the presence of the submicron population. In the corresponding cases with Cl^- as the anion at 4 and 2 mol Na^+ kg^{-1} water, however, no indication could be found that the mere presence of the presumably salted-out lignin caused a shift in the onset pH of the formation of micron-scale particles: the onset pH due to acidification was approximately the same as for the cases with SO_4^{2-} (*cf.* Figure 4-3 and Figure 4-5). This observation does not provide further support for the fact that the presence of pre-existing particles necessarily shifts the onset pH.

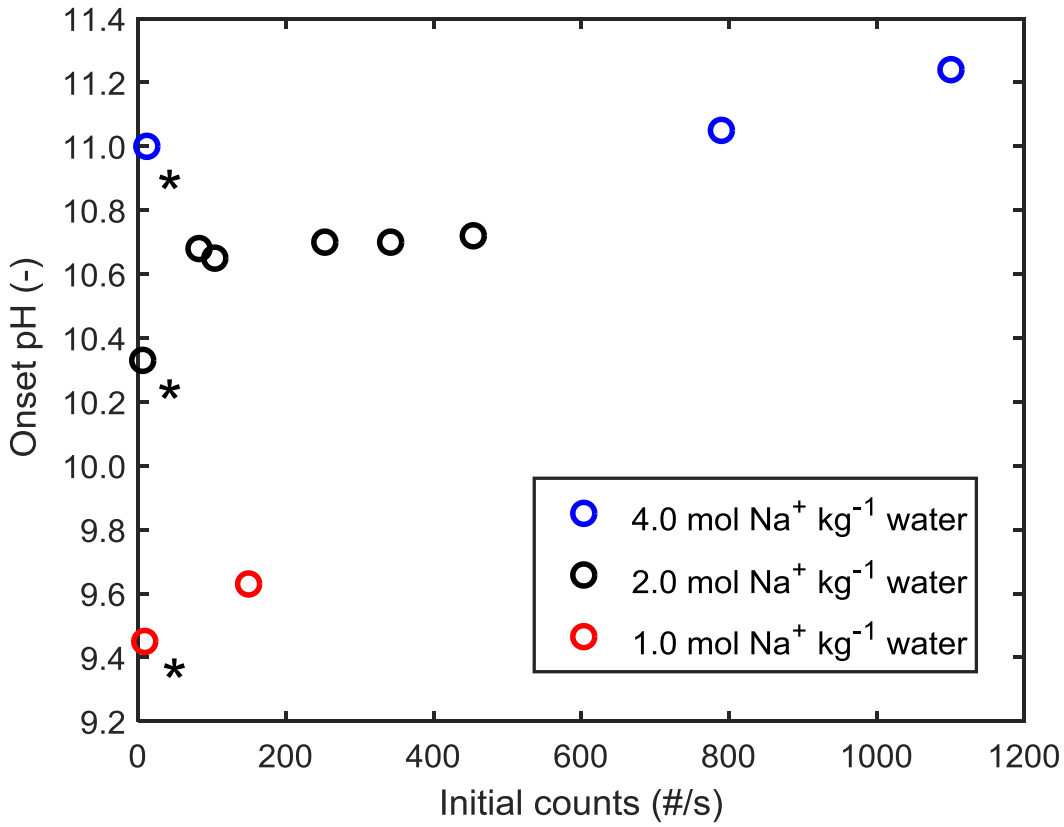

Figure 4-9. The onset pH of the formation of particles ≥ 1 µm due to acidification at various concentrations of salt and amounts (initial counts) of pre-existing particles (≥ 1 µm) prior to acidification. Precipitation temperature: 45 °C. pH value at 25 °C. The lignin solution was prefiltered prior to acidification. Salt added: Na_2SO_4.*

The rate of precipitation was, however, found to increase when pre-existing particles were present: the higher the initial count of all particles ≥ 1 µm prior to acidification, the shorter the precipitation time scale (see Figure 4-10 and the definition of the time scale in 3.4 Analysis of chord length counts). It is possible that the rate of precipitation was predominantly dependent on the availability of the surface area of particles as sites for heterogeneous nucleation, particle growth and/or agglomeration.

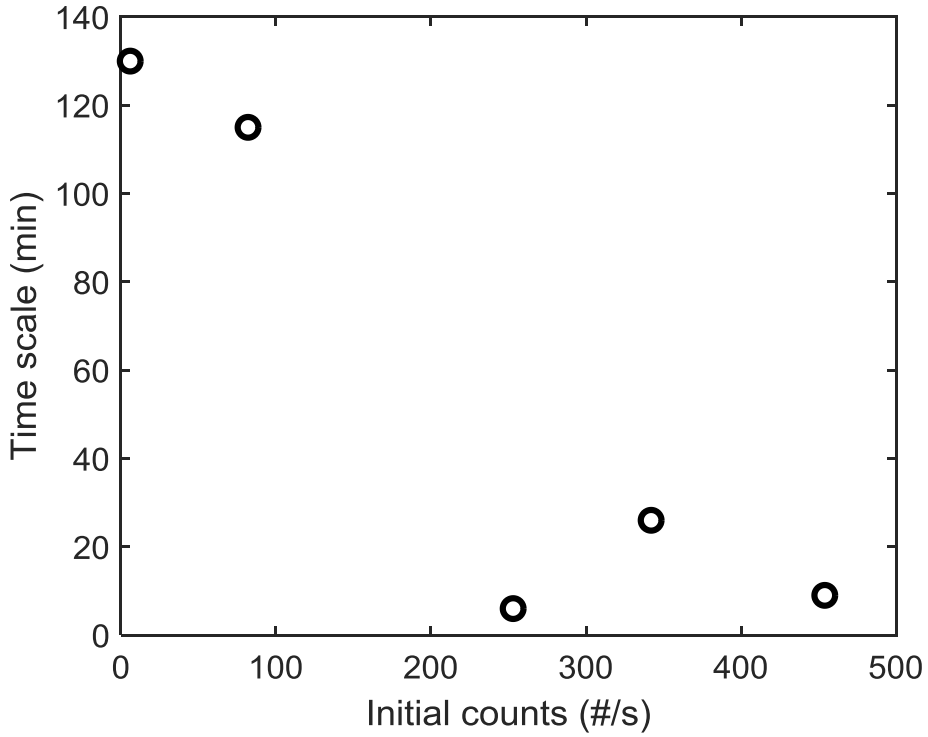

Figure 4-10. The time scale of precipitation vs. the initial counts of all particles ≥ 1 µm prior to acidification. Salt added: Na_2SO_4.

4.1.4 Chord length distributions

The number and volume-based chord length distributions of the particles in a wide range of precipitation conditions are shown in Figure 4-11 to Figure 4-13. The main parameters investigated were the pH, salt concentration level and temperature.

Figure 4-11 shows that the pH level at a high concentration of Na^+ (4 mol kg^{-1} water) influences the chord length distribution significantly: it is affected all the way from about pH 11, *i.e.* just below the onset pH of particles ≥ 1 µm, to pH 4. More particles are formed the lower the pH becomes (upper left graph in Figure 4-11); they are also larger, to some degree at the expense of smaller particles. The volume-based distributions (upper right graph in Figure 4-11) show the shift towards larger particles as the pH decreases: although the relative weight of the volume of small micron-sized particles (1-10 µm) is rather significant at pH 11, it has however decreased by about an order of magnitude at pH 10.5 and almost vanished at pH 4. Considering the bell shape of the volume-based distribution curve (upper right graph in Figure 4-11), along with the rather low relative volume of the particles 1-10 µm in size, it would be reasonable to assume that almost all of the solid lignin particles will be found in the micron-range unless the full size distribution is significantly bimodal, with an enormous population of submicron particles. One single agglomerate of at least 1 µm may be comprised of about 10^3 particles that are 0.1 µm in size.

The fact that pH affects in such a wide range of conditions even at very high concentrations of salt (4 mol Na^+ kg^{-1} water) indicates that the kraft lignin's surface charges are of great relevance. The rather abundant phenolic groups contribute with charges in the alkaline regime and the less abundant carboxylic groups can contribute all the way down to quite

acidic conditions. The latter is strengthened when the effect of the Na^+ concentration on the chord length distribution at pH 4 (the lower panel in Figure 4-11) is considered: with respect to both number and volume, the particle chord length distribution is shifted to larger particles as the Na^+ concentration increases from 1 to 4 mol kg^{-1} water. Phenolic groups ought to be fully protonated at this point, so the carboxylic groups, still being (partly) charged at this pH, are therefore a probable candidate for being the root cause of the shift.

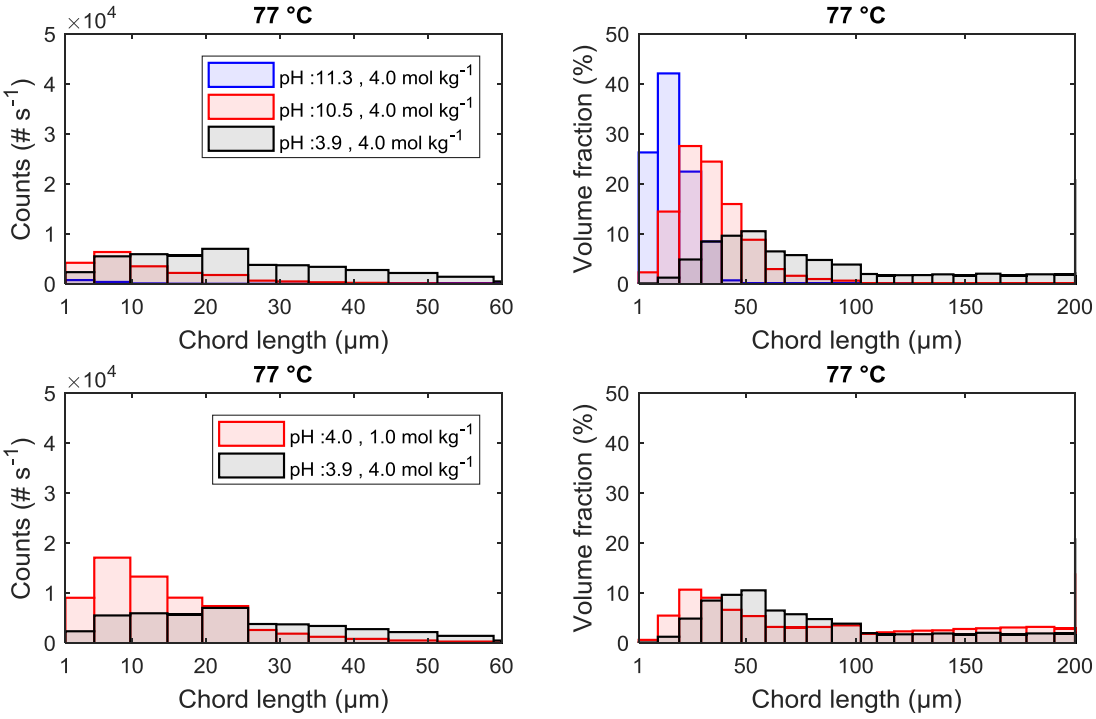

Figure 4-11. Number (counts) and volume-based chord length distributions at 77 °C. Upper panel: the influence of pH at 4 mol Na^+ kg^{-1} water. Lower panel: the influence of Na^+ concentration at about pH 4.

The general trend is that more small particles were formed at 65 °C compared to 77 °C (see Figure 4-12). At near-neutral conditions (pH ~ 7.7), the number of particles was higher at 65 °C compared to 77 °C, but the volume-based chord length distribution showed a shift towards larger particles (50-100 µm) at the higher temperature. At pH 4 the shift towards larger particles at 77 °C compared to 65 °C in both number and volume is clear, see Figure 4-12. The volume-based distribution was also found to be very broad: a long tail continues from about 60 µm at a rather constant level of a few volume % at least up to 200 µm. An explanation as to why larger particles become relatively more abundant at 77 °C compared to 65 °C cannot be put forward at the moment. However, it has been observed that the properties of kraft lignin can change at temperatures around 85 °C and form "soft and tacky" large clumps (Uloth and Wearing 1989). Moreover, the relationship between the chord length distributions at 77 °C and 65 °C obtained in this work resembles that found in another study at 80 and 70 °C, after precipitation of kraft lignin from black liquor at about pH 9.7 (Öhman and Theliander 2007), *i.e.* that larger particles form at the higher temperature. Comparisons of the chord length distributions at 45 °C and 65 °C not only show that more micron-sized particles were formed at 45 °C than at 65 °C, but also indicate that larger particles were formed at 45 °C, volume-wise (see Figure 4-12).

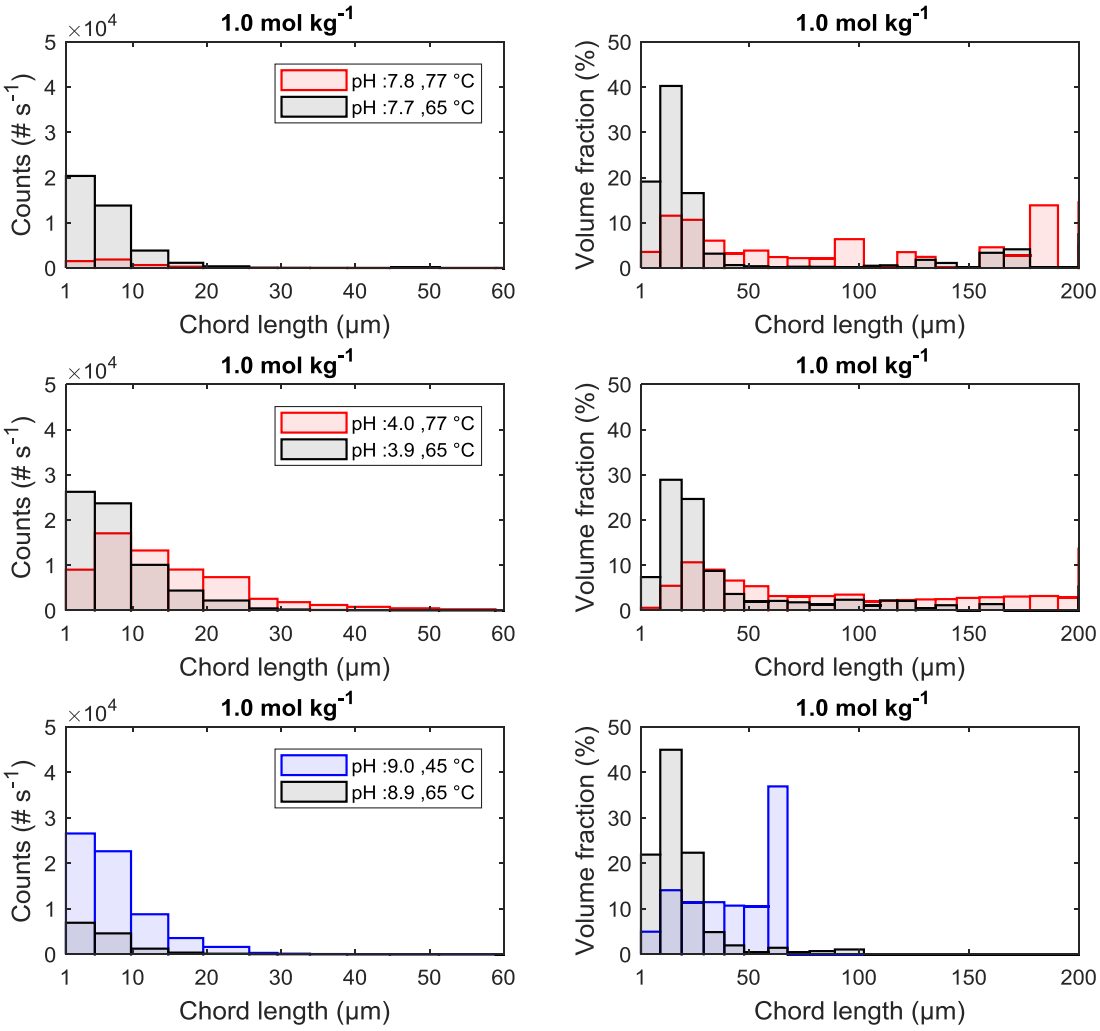

Figure 4-12. Number (counts) and volume-based chord length distributions at 45°C, 65 °C and 77 °C and at various pH levels. The Na^+ concentration was 1.0 mol kg^{-1} water.

The number-based chord length distributions given in Figure 4-13 show that the amount of particles ≥ 1 µm increases as the pH is decreased. Based on the shape of the number-based distributions, and the fact that the most common class of particles in the chord length distribution was found to be in the 1-5 µm class, it is deemed reasonable to assume that the actual size-distribution has been truncated at 1 µm due to instrumental limits, and therefore submicron particles may also co-exist. The extent of submicron particles cannot, however, be assessed further using the present data alone. In Figure 4-13, the number of particles ≥ 1 µm appears to decrease at an increased concentration of Na^+. It is nevertheless possible, considering the shift towards larger particles in the volume-based distributions (see the right panel in Figure 4-13) at increased Na^+ concentration, that particles in the range 1-20 µm (the most frequently populated classes) underwent agglomeration and/or particle growth and therefore appeared as much fewer, but larger, particles. For instance, if 8,000 spherical particles of size 1 µm were to agglomerate, they would compose a highly dense particle-agglomerate with a diameter of at least 20 µm, and $6.4*10^4$ particles would yield a corresponding agglomerate of at least 40 µm. Thus, a significant decrease in the number of

particles in the range of a few microns may result in a minor increase in the numbers of particles merely tenfold in size: such an increase would not, in effect, be observable when depicted in the number-based distribution. In some of the cases with Cl^- as the anion, the counts are higher than for the corresponding case with SO_4^{2-}. However, the pH values were also slightly lower in the latter, and thus it cannot be certain that the difference in count level is not due to the anion specificity.

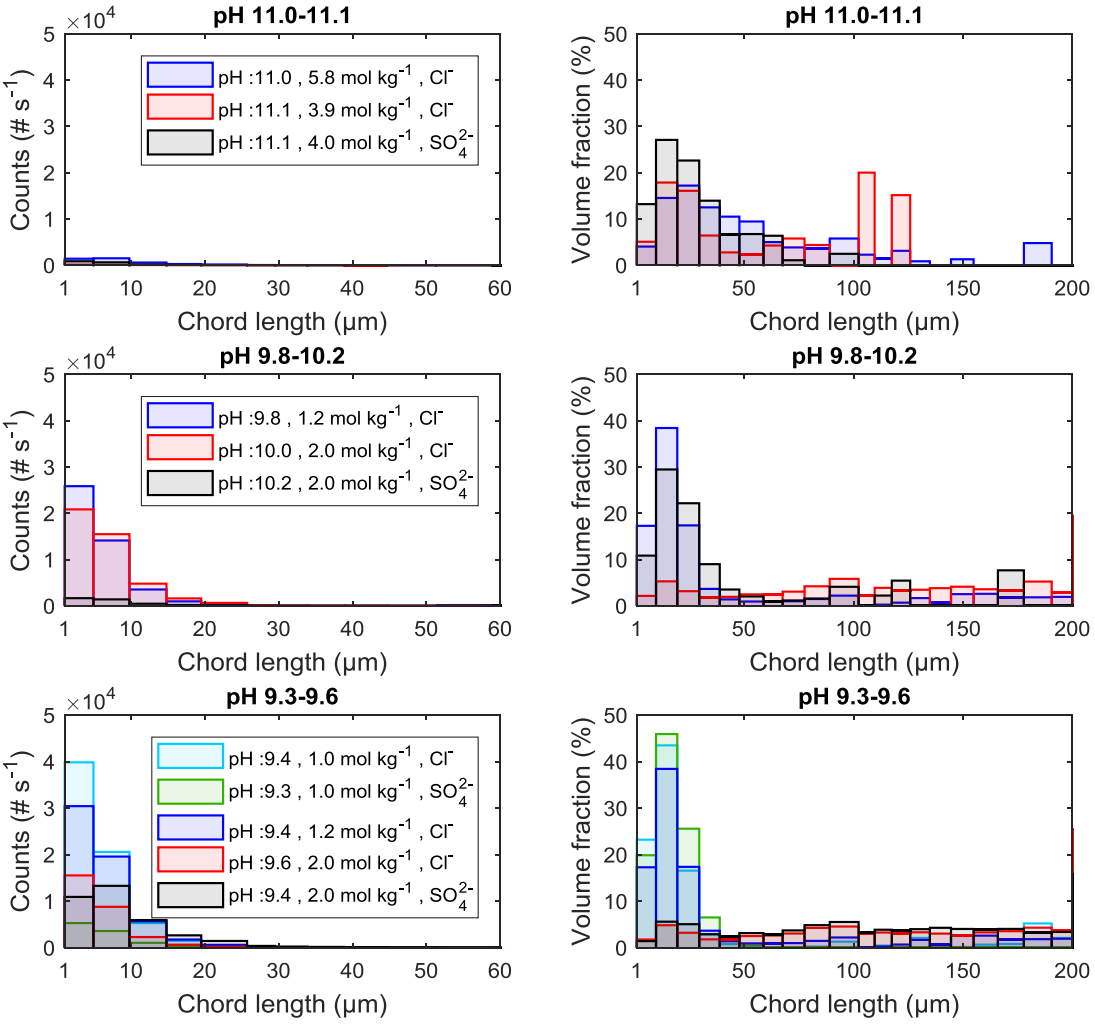

Figure 4-13. Number (counts) and volume-based chord length distributions at 65 °C. The influence of Na^+ concentration and anionic type (SO_4^{2-} and Cl^-) is shown at three pH levels (~11, ~10, and ~9.4).

The image that emerges from the observations made above is that both the pH and the concentration level of Na^+ affect the precipitation in a manner that is typical when electrostatic effects are involved. The combination of the two parameters determines, to a large extent, the condition required for the onset of the formation of particles ≥ 1 µm in a wide range of conditions according to Figure 4-8. Below this onset limit, the precipitation process proceeds further if either the pH is decreased or the concentration of salt is increased. This point is also illustrated in Figure 4-14: generally speaking, the total volume

of particles on the micron-scale increases as the pH decreases and/or the concentration of Na^+ increases.

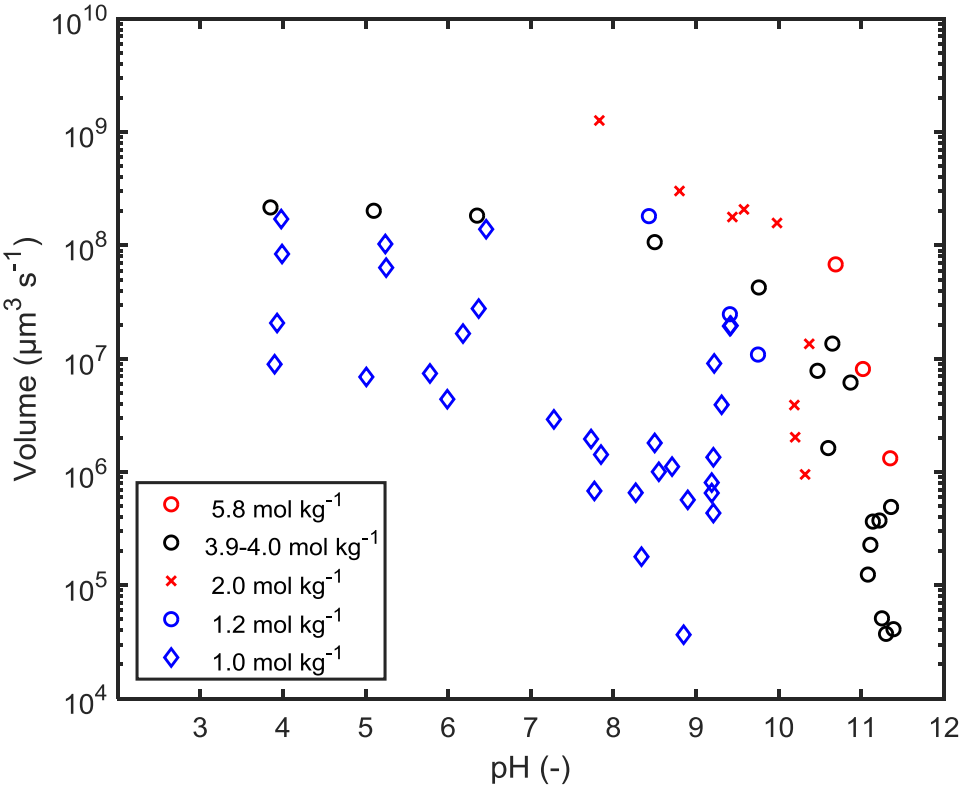

Figure 4-14. The total volume of particles (≥1 µm) measured per second with the FBRM vs. the pH level (measured at 25 °C). The volume-estimates were based on the chord length distributions (see 3.4 Analysis of chord length counts).

4.1.5 Co-precipitation with xylan

Distribution of xylan in lignin-particles

In this work (Paper I), the distribution of xylan on kraft lignin was investigated both on the macroscopic (in a filter cake) and microscopic (on particles) scales. On the micro-level, a confocal laser scanning fluorescence microscope was used to study two samples of lignin taken from experiments in which kraft lignin was co-precipitated with dyed xylan. Spots of high intensity in the wavelength interval where dyed xylan has its strongest emittance were only observed in two cases: one of these is shown in Figure 4-15. These spots are most likely areas with a high density of xylan, but just a few detectible spots cannot account for the significant content of xylan present in the cake. A reasonable interpretation of the result is therefore that most of the xylan was dispersed finely in the cake material to such an extent that its intensity became too weak to distinguish between it and lignin: it means that the xylan was evenly distributed on the microscopic scale. This result strengthens further the hypothesis that xylan sorbs onto agglomerates of lignin, and thereby becomes incorporated into the structure (Durruty *et al.* 2017). It ought to be mentioned here that the acidification procedure used for the precipitation experiments in which analysis of the xylan content of the filter cake was made was harsh, since all the acid was added at once, which is in direct contrast to the experiments monitored *in situ* with FBRM. Nevertheless,

the observations made of the chord length distributions of the agglomerates (as shown below) and the distribution of xylan in the filter cakes indicate the possibility that xylan becomes incorporated into the lignin agglomerates.

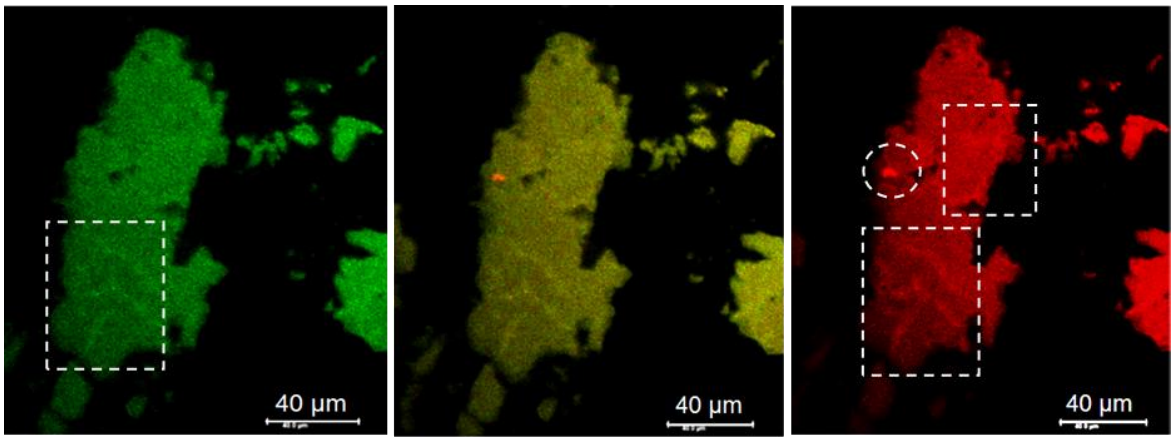

(a) Emission range assigned to lignin, collected from 500-540 nm.

(b) Co-localization of both collected emission ranges.

(c) Emission range assigned to stained xylan, collected from 620-722 nm.

Figure 4-15. Images of the intensity landscape of emitted light collected in different wavelength intervals: ***(a)*** *light emission range collected predominantly from auto-florescent lignin;* ***(b)*** *superimposed images of collection ranges assigned to lignin and dyed/stained xylan and* ***(c)*** *wavelength span corresponding to the strongest emittance from dyed xylan.*

Measurements of the xylose concentration in slices of filter cake taken at different heights showed that xylan was trapped in the cake and distributed evenly along its height, see Figure 4-16. This observation shows that the xylan was aslo distributed evenly in the cake on a macroscopic scale.

Figure 4-16. Xylose concentration in slices taken at different heights in the filter cakes of lignin co-precipitated with xylan. Three cakes were examined: two with non-dyed xylan (L-X) and one with dyed xylan (L-dX). See Paper I.

Influence of xylan on the chord length distribution

The influence of xylan on the formation of particles on the micron scale can be observed in Figure 4-17 (at 77 °C) and Figure 4-18 (at 65 °C). The influence is most clear at the higher temperature, where smaller particles are formed in the case with xylan added. The shift in the distribution between the case with and without xylan was found to be consistent in the pH range 4-6: at these pH values, the ionisation degree of the carboxylic groups can be expected to be influenced by the pH. It is possible that the xylan sorbed onto the particles contribute to a reduction in the particle size. It is unclear at which conditions xylan may sorb onto lignin particles but, when they do, they can become incorporated into particles of kraft lignin because these particles grow in size by further lignin-sorption or the agglomeration of particles. Xylan-rich particles may retard their tendency to agglomerate further, compared to pure lignin counterparts, due to electrostatic or steric effects that xylan may induce. At 65 °C, the main observation in Figure 4-18 is that the count levels were generally lower in the presence of added xylan; the differences in the distributions can be seen already at pH 8-9.

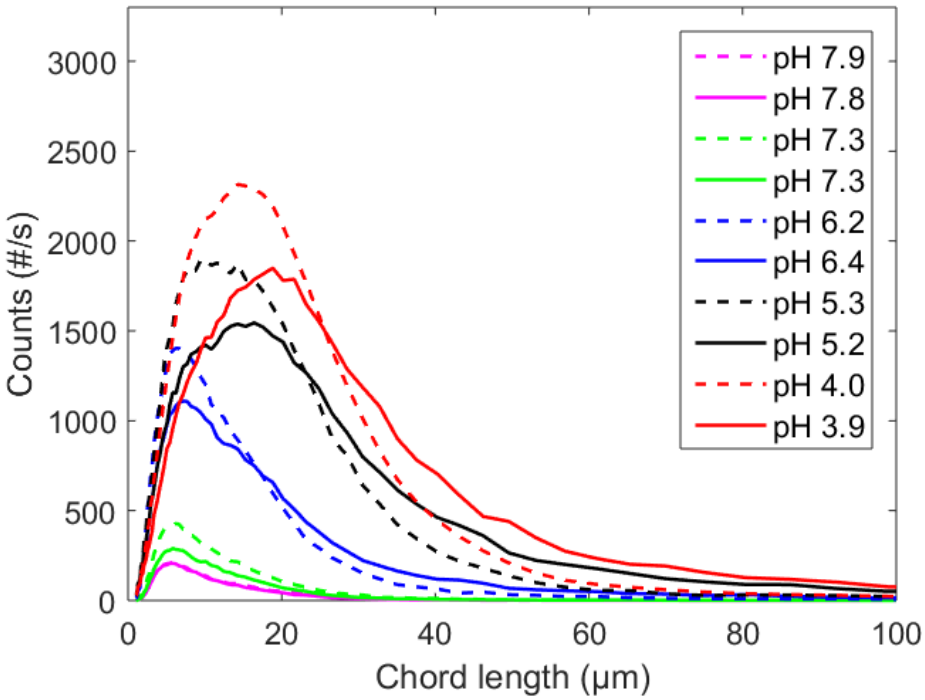

Figure 4-17. Comparison of chord length distributions with (dashed line ---) and without (full line ——) xylan added. Na^+ concentration: 1.0 mol kg^{-1} water. Precipitation temperature: 77 °C.

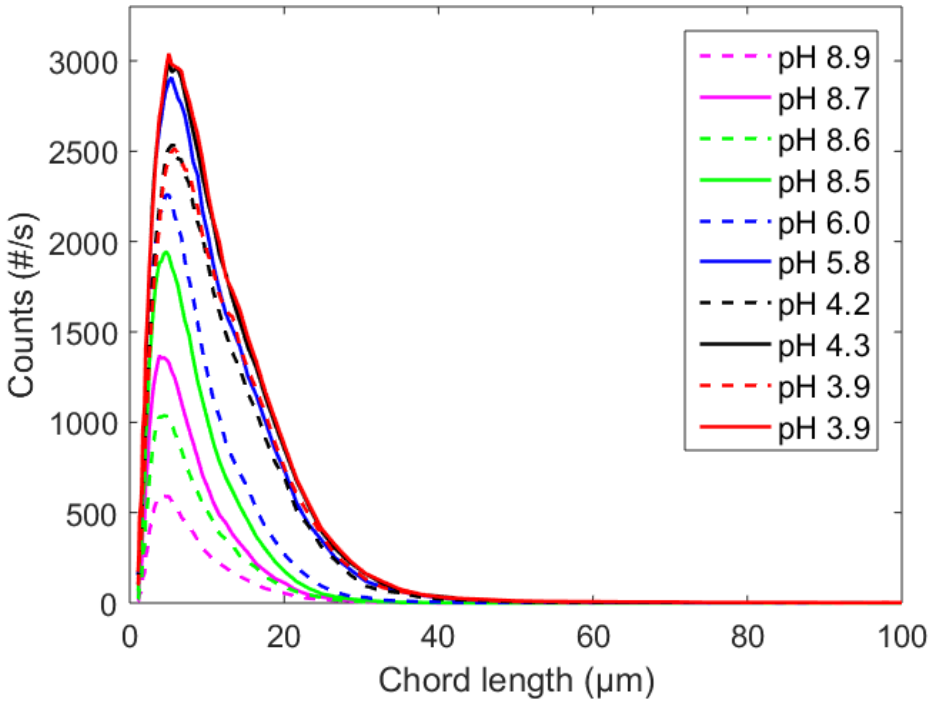

Figure 4-18. Comparison of chord length distributions with (dashed line ---) and without (full line ——) xylan added. Na^+ concentration: 1.0 mol kg^{-1} water. Precipitation temperature: 65 °C.

4.2 Numerical results

The results of the numerical predictions of the pair interaction potentials estimated according to the procedure in 2.6 Numerical procedure are discussed below. This is followed by a presentation of some of the results pertaining to the charge regulation and the ion concentration profiles from the solutions of the modified Poisson-Boltzmann equation given in Eq. (2.18), which provides the input data for the predictions of pair potentials.

4.2.1 Pair interaction potentials

Repulsive barriers reflect the resistance of two particles to adhere to each other and thereby undergo agglomeration: they are an indication of the stability of the particle dispersion. Results from the predictions of pair interaction potentials between two identical kraft lignin particles on the nano-scale are shown in Figure 4-19 and Figure 4-20. They are presented as repulsive barriers, or the absence thereof, if the interaction potentials are <0, at various levels of pOH and concentrations of salt (the Na^+ concentration). Predictions were made for Na^+ concentration levels in the range 1-2.5 M. 0.5 M of the Na^+ ions originated from NaOH in all cases and the remainder from NaCl: *i.e.* mimicking the experimental concentrations in Paper V. The contents of phenolic and carboxylic groups were 4.27 and 0.45 mol kg^{-1} lignin, respectively, corresponding to the average values for the LignoBoost lignin used in the experiments conducted in this work. The temperature was 65 °C in all cases.

The repulsive barriers are predicted to stabilise the nano-scale particles (> 10 *kT*) up to concentrations of about 2 M Na^+ at 1 pOH, although barriers for particles of about 10 nm are below 10 *kT* at this Na^+ concentration. At pOH 1.5, however, the barriers are reduced, but the dispersion of particles remains stabilised on the nano-scale up to 2 M Na^+. The exception is nanoparticles with a radius of about 10 nm as these may agglomerate slowly, since the barriers are merely a few *kT*. At pOH 2, on the other hand, the particle dispersion is predicted as being destabilised at the salt concentration of 2 M but stabilised at about 1.8 M at this pOH (at least particles with radii of about 100 nm). These predictions agree reasonably well with the experimental observations made in this work when NaCl was used as the added salt. The experimental results showed that micron-sized particles were formed at about pOH 1.7 at 2 mol Na^+ or higher, *i.e.* close to the numerical predictions. Particle dispersions on the nano-scale are predicted to remain rather stable at 1.5 M at further increased pOH up to about pOH 3.5: at this condition, only particles with radii of about 1 µm are predicted to remain significantly stabilised. At further increased levels of pOH, up to pOH 4, these are also destabilised at 1.5 M. In an experiment at pOH 4.2, *i.e.* comparable to the previous condition, the onset of formation of particles ≥ 1 µm was observed to occur at the Na^+ concentration of 1.2 M (Figure 4-1). The predicted and experimental values are quite close.

At 1.2 M Na^+, nanoparticle dispersions (*e.g.* with radii of 100 nm) are predicted to be stabilised both at pOH 4 and 4.5. In an experiment, however, as mentioned above, the pOH had to be increased to about 4.2 before the formation of micron-sized particles could be observed. Moreover, it can be seen in Figure 4-20 that no significant change in the barriers are predicted in the pOH range 4-4.5, and this persists as the pOH is decreased further, *e.g.* to 5.5. This prediction is due to the fully ionised carboxylic groups in the model, because the phenolic groups are virtually fully protonated at such a high pOH. The numerical results suggest that the carboxylic groups can have a significant effect on the dispersion stability. This is a reasonable assumption considering the effect that pOH at 1 mol Na^+ kg^{-1} water has on the chord length distributions at pOH > 5. The numerical results at 1.2 M Na^+ do, however, overestimate the dispersion stability when compared to the experimental data; possible explanations for this are discussed later in 4.2.3 Comparisons with experimental observations: further considerations.

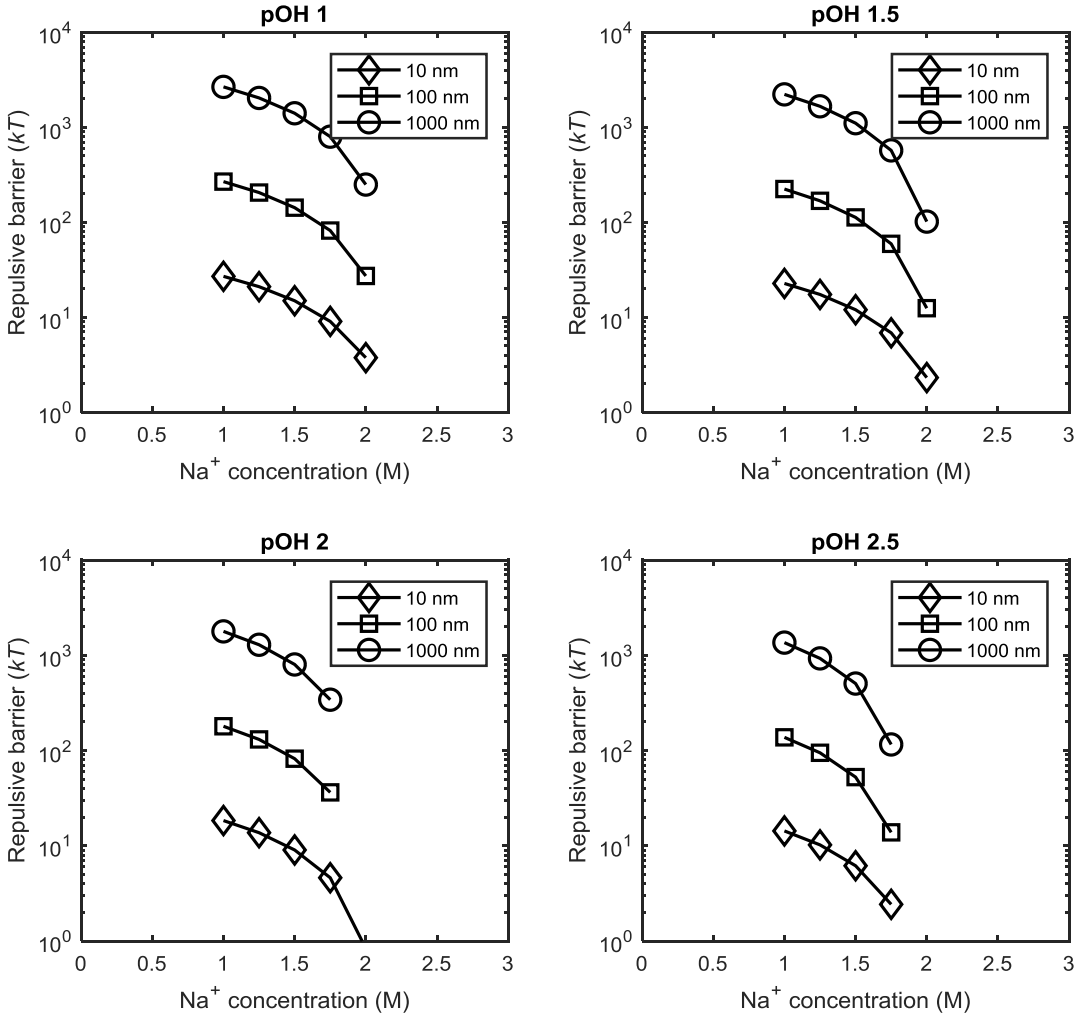

Figure 4-19. Pair interaction potentials between kraft lignin particles of radii 10, 100, and 1000 nm at various levels of salt concentration (Na^+) with Cl^- as the anion in the added salt. The pOH is in the range 1-2.5 and the temperature is 65 °C. The contents of phenolic and carboxylic groups (mol kg^{-1} lignin) are 4.27 and 0.45, respectively.

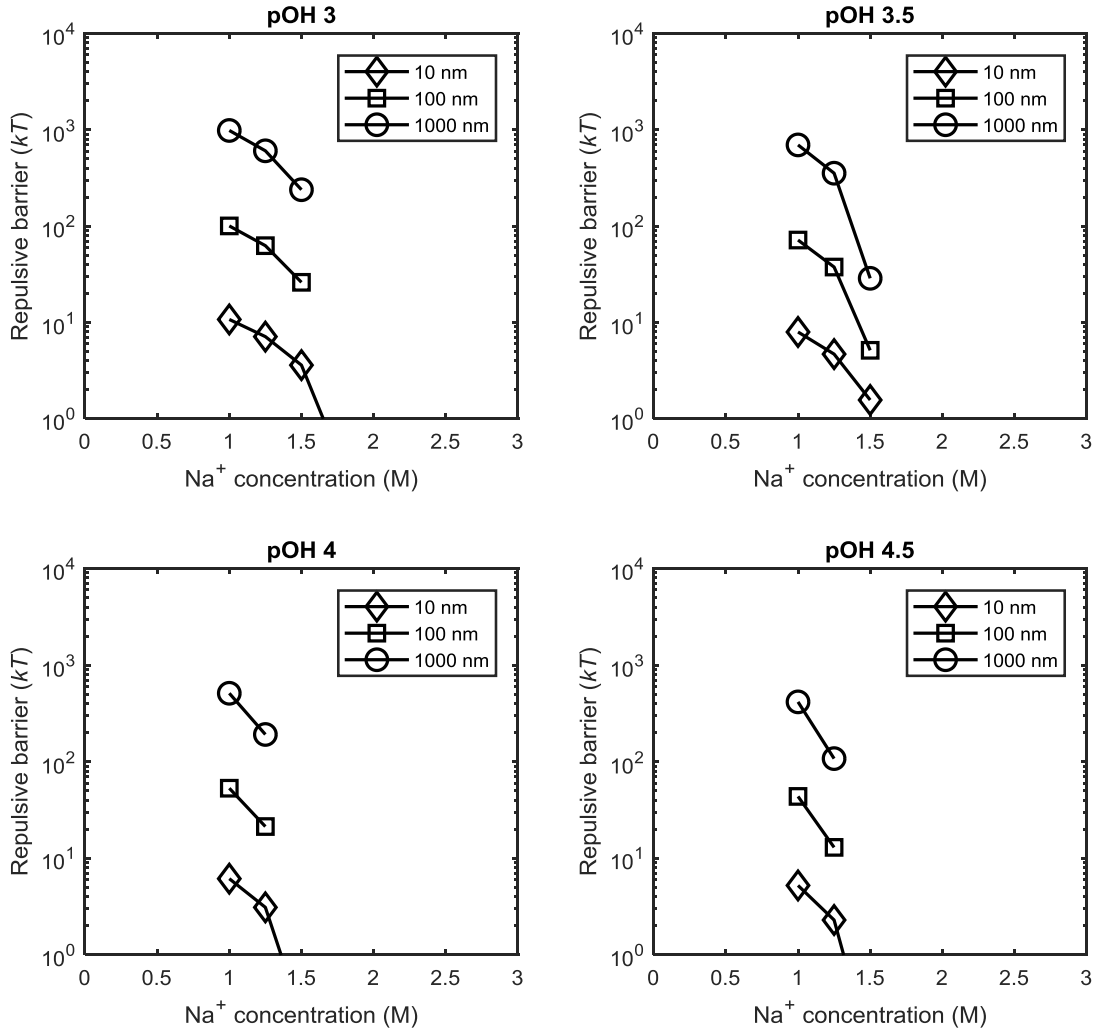

Figure 4-20. Pair interaction potentials between kraft lignin particles of radii 10, 100, and 1000 nm at various levels of salt concentration (Na^+) with Cl^- as the anion in the added salt. The pOH is in the range 3-4.5 and the temperature is 65 °C. The content of phenolic and carboxylic groups (mol kg^{-1} lignin) are 4.27 and 0.45, respectively.

The corresponding barriers when SO_4^{2-} is the anion in the added salt are shown in Figure 4-21 and Figure 4-22. Again, the Na^+ concentration levels were in the range 1-2.5 M and, in all cases, 0.5 M of the Na^+ ions originated from NaOH. Here, however, the remainder comes from Na_2SO_4, *i.e.* mimicking the experimental concentrations in Paper V where SO_4^{2-} were the anion. Generally, at low pOH levels, the ability of the system to retain a nano-scale dispersion of particles is predicted to increase when SO_4^{2-} is the anion in the added salt rather than Cl^-. This agrees with the observation that the addition of NaCl to reach 2 mol Na^+ kg^{-1} water caused the formation of particles ≥ 1 µm at about pOH 2, while the corresponding addition of Na_2SO_4 did not: *i.e.* Cl^- has a greater ability than SO_4^{2-} to salt-out the kraft lignin dispersion. For instance, the nanoparticle dispersion is predicted to be stabilised at pOH 2 in the latter case (see *e.g.* the particles of radii 100 nm in Figure 4-21). Moreover, the dispersion is predicted to remain stable at pOH 2.5 as well at the Na^+

concentration of 2 M, but unstable at pOH 3. This prediction is about 0.5 pOH units higher than the value determined experimentally (*cf* Figure 4-5).

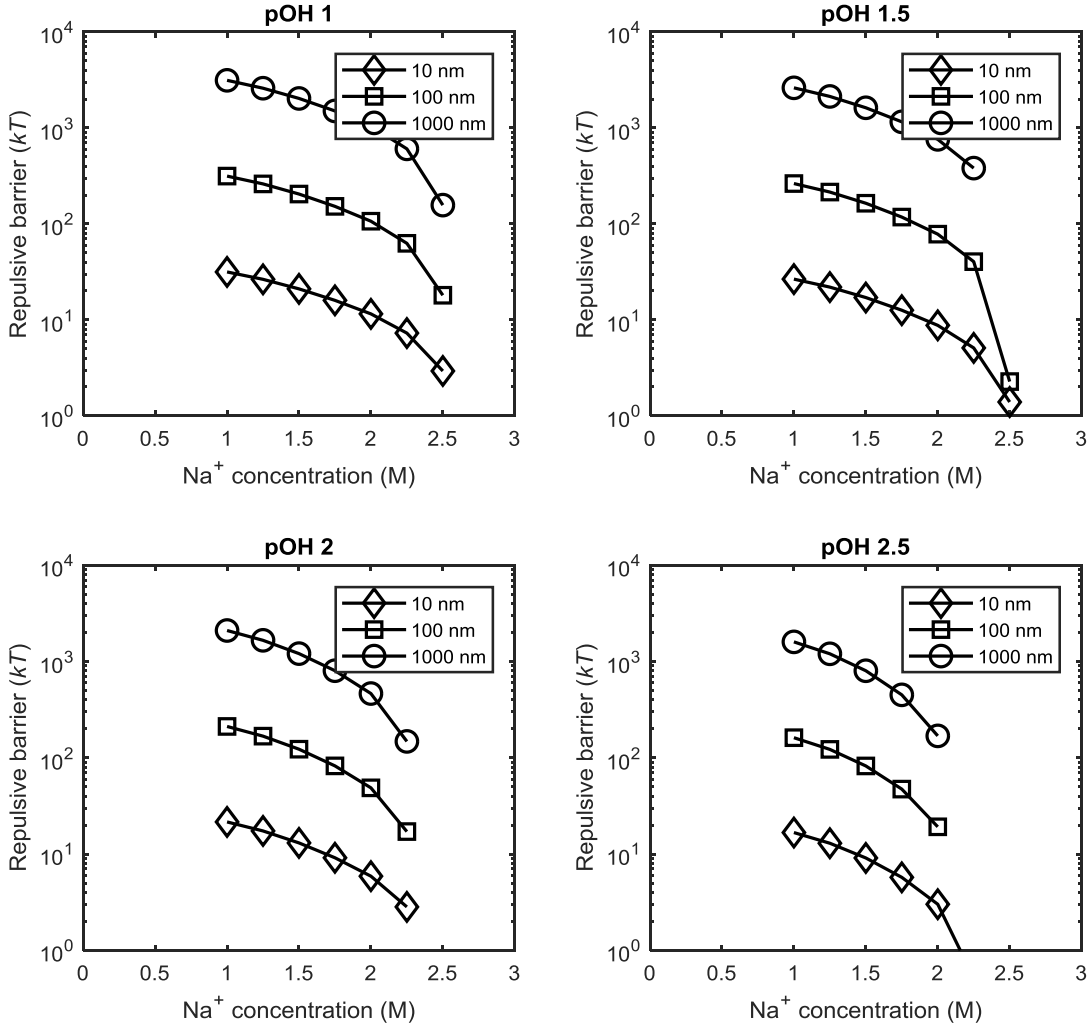

Figure 4-21. Pair interaction potentials between kraft lignin particles of radii 10, 100, and 1000 nm at various levels of salt concentration (Na^+) with SO_4^{2-} as the anion in the added salt. The pOH is in the range 1-2.5 and the temperature is 65 °C. The contents of phenolic and carboxylic groups (mol kg^{-1} lignin) are 4.27 and 0.45, respectively.

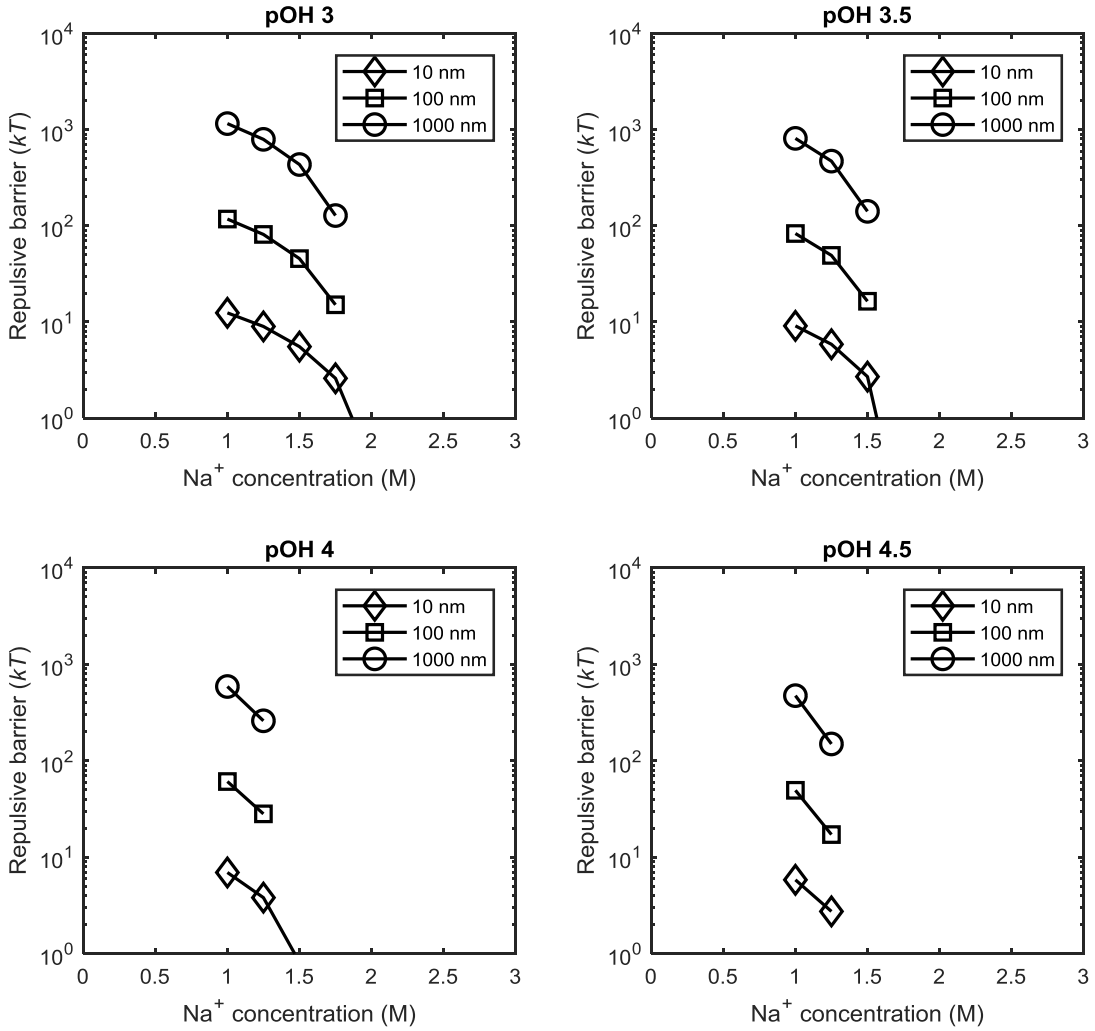

Figure 4-22. Pair interaction potentials between kraft lignin particles of radii 10, 100, and 1000 nm at various levels of salt concentration (Na^+) with SO_4^{2-} as the anion in the added salt. The pOH is in the range 3-4.5 and the temperature is 65 °C. The contents of phenolic and carboxylic groups (mol kg^{-1} lignin) are 4.27 and 0.45, respectively.

The pair interaction potentials for particles of radii 1000, 100 and 10 nm, respectively, at pOH 2 and at a series of Na^+ concentrations (1-2.5 M) for the NaCl-case, are shown in Figure 4-23. As is typical for DLVO potentials: the larger the particles, the stronger the repulsive and attractive forces. However, due to the limited range of repulsive interaction (double layer) as a consequence of screening, van der Waals attraction dominates at larger distances and causes a local energy minimum at a separation D of 40 Å, which is common for screened systems (Israelachvili 2011). Although this minimum is rather deep (~-70 kT) for particles of radius 1 µm, and even significant for 100 nm particles (~-10 kT), it is small for 10 nm particles (> -kT). The two larger size-classes are, consequently, prone to flocculation according to the predictions, *i.e.* forming loose agglomerates, at salt concentration levels < 2 M. The 10 nm particles, on the other hand, are not predicted to flocculate in this manner (see the insert in the graph on the right hand side in Figure 4-23). The potentials are rather similar for the Na_2SO_4 case in terms of the prediction of a local

minimum at a few nm from the surface even though, as mentioned previously, the repulsive barriers are larger. It ought to be mentioned here that sorption of dissolved kraft lignin macromolecules onto the much larger nanoparticles may take place: the repulsive barriers for sorption may be in the order of magnitude of a few *kT* , thus, indicating potential slow particle growth (Paper IV). The range of the potentials in Figure 4-23 ought to be compared to the characteristic cell sizes estimated for the three particle classes in 2.6 Numerical procedure. The range of significant pair interactions is much shorter than the length scale of the average particle-to-particle distance from the cell size estimates for uniformly distributed particles. Pair interactions should, thus, be a reasonable assumption for kraft lignin particles on the nano-scale at those lignin concentrations.

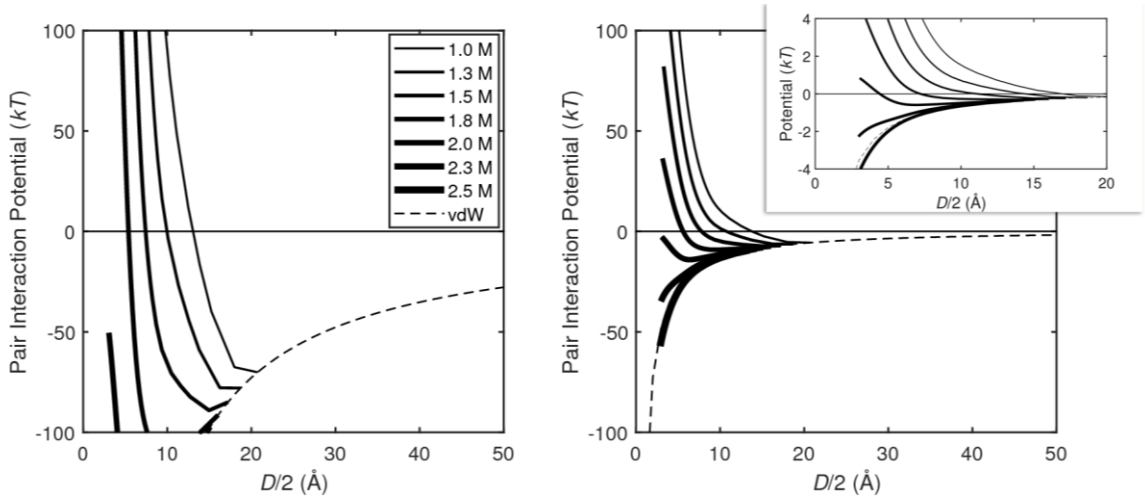

Figure 4-23. Pair interaction potentials at various half separation distances, D/2. Left: 1000 nm particles. Right: 100 nm particles. Insert: 10 nm particles. Bulk pOH: 2. The concentrations in the legend are of Na^+. Type of salt added: NaCl. vdW: van der Waals attraction component to the potential.

4.2.2 Charge regulation and ion concentration profiles

As indicated above by the pOH dependency of the dispersion stability of kraft lignin particles, the surface charge density is predicted to influence the stability significantly, which the salt concentration level is also predicted to do. It was assumed that the surface pH regulates the ionisation degree of phenolic groups according to the reaction equilibrium of protonation *vs.* deprotonation. The surface pH decreases at increased temperature and, moreover, depends on the electrostatic potential between the bulk condition and the particle/macromolecule surface (recall Eq. (2.14)). Thus, the surface pH may be significantly lower compared to the bulk value. Figure 4-24 shows the predicted surface pH as a function of the half separation-distance between two similar kraft lignin particles/molecules at 65 °C. As the two surfaces approach each other, the surface pH decreases as a result of the simultaneous decrease in the electrostatic potential at the surface (more negative). At each separation distance, the electrolyte solution was assumed to be in equilibrium; the Poisson-Boltzmann cell remained electroneutral, *i.e.* the counterions in the cell balanced the charged surface.

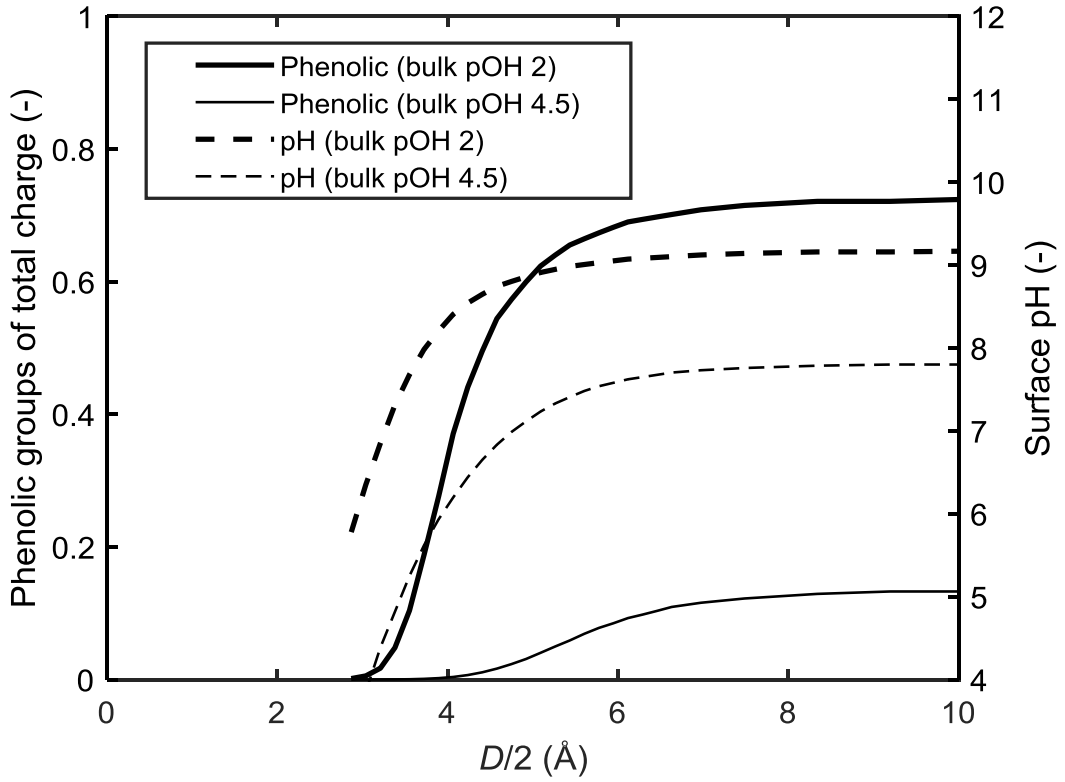

Figure 4-24. Fractions of charges from phenolic groups of total charge density (left y-axis) and surface pH (right y-axis) at various half separation-distances between two interacting kraft lignin particles/ macromolecules. Bulk conditions: pOH 2 and 4.5. Temperature: 65 °C.

These interlinked properties, *i.e.* charge regulation, surface pH and electrostatics, influence the distribution of ion concentrations in the vicinity of the surfaces (see Figure 4-25). They therefore determine the concentration of ions at the midpoint between the surfaces which gives the osmotic pressure experienced by the particles as they approach each other. The development of the midpoint concentration as the separation distance decreases is seen in Figure 4-25 as the endpoints on the right-hand side of the curves of Na^+ concentration. Figure 4-25 thus illustrates how the double layer is compressed: it consists predominantly of the Na^+ counterions at short distances, reaching a maximum Na^+ concentration of almost 5 M. This maximum is a consequence of the steric effects in the modified Poisson-Boltzmann model, which allows a maximum close packing of ions determined by the choice of the lattice size or ionic diameter: a in Eq. (2.17). Moreover, the diffuse layer of crowded Na^+ is somewhat shifted away from the surface by the hydrophobic ion-surface interactions of the lignin. These distance-dependent interactions can compete with the electrostatic attraction of the counterions induced by the surface charges on the lignin; close to the surface, they even dominate the ion-lignin interaction. This effect renders the prediction of the increased range of salt concentrations possible, where the double layer repulsion still overcomes the attractive van der Waals interaction (see Figure 4-19 to Figure 4-22). The modifications made to the Poisson-Boltzmann equation, which manifest themselves in the above-mentioned effects, suggest that charged-particle systems of increased salt concentration may be analysed with the model, whereas the classical Poisson-Boltzmann equation would be inadequate.

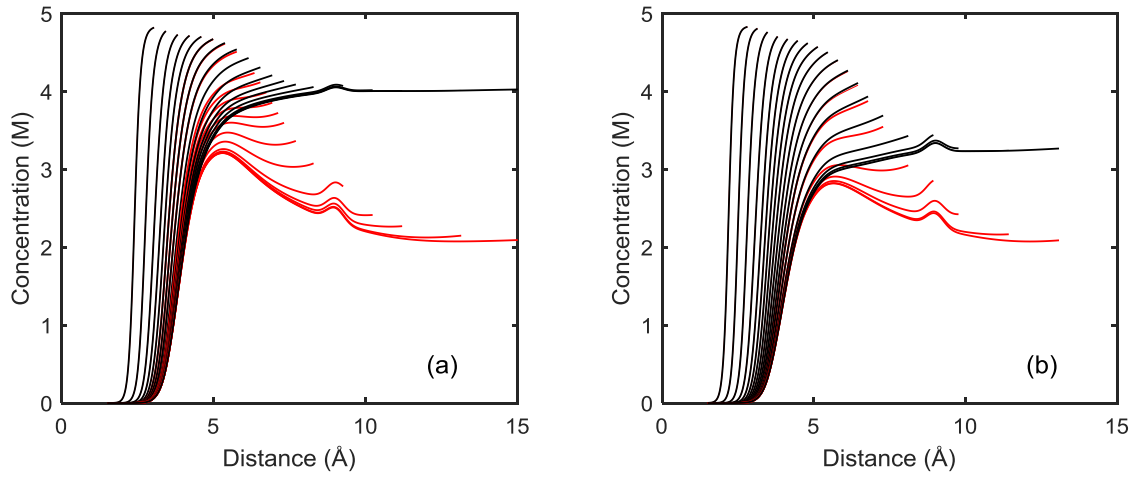

Figure 4-25. Concentration of ion vs. distance from the surface at various half-separation distances, D/2 (the end-points on right-hand side of each curve). Black curves: total ion concentration profiles. Red curves: Na^+ contribution made. Concentration of Na^+ in the bulk: 2.0 M. pOH: 2.0. ***(a)*** *NaCl case.* ***(b)*** *Na_2SO_4 case.*

It is nevertheless important to note that the repulsive double layer interaction vanishes at Na^+ bulk concentrations greater than ~2.7 and ~3.2 M for the NaCl and Na_2SO_4 cases, respectively, for a lattice cell size of 7 Å (*i.e.* the diameter of the hydrated Na^+ ion). As the Na^+ concentration in the bulk increases beyond this concentration, the total bulk concentration of the ions approaches the maximum concentration of the ionic atmosphere: the net osmotic pressure, which drives the repulsive interaction, therefore vanishes.

4.2.3 Comparisons with experimental observations: further considerations

The predictions presented in 4.2.1 Pair interaction potentials agree reasonably well with the experimental observations made regarding the formation of particles ≥ 1 µm at several conditions. Some noteworthy deviations were, however, found at some conditions. Considering that the particles are described as perfect hard spheres having average properties in terms of hydrophobicity and charge density (contents of ionisable groups), the model used can be regarded as an extensively simplified representation of the actual case. Yet it predicts the trends observed in the experiments relatively well. Given that the predictions have this level of accuracy, the results suggest that double layer repulsion, or a mechanism that resembles it to a large extent, may be a reasonable candidate for the significant mechanism, or at least one of them, that stabilises kraft lignin particle dispersions on the nano-scale; even at rather high concentration levels of salt of about 2.5-3 mol Na^+ kg^{-1} water.

It should also be mentioned that the predictions are representative for particles that contain ionisable groups corresponding to an average kraft lignin macromolecule: the contents of phenolic and carboxylic groups assumed here were the averages of the whole population of the lignin material used in the experiments (see 3.1 Materials). The dispersion stability and precipitation are probably more complex than illustrated in the predictions, not least as a consequence of the heterogeneity in the molecular properties of kraft lignin. Macromolecules of kraft lignin with a high molecular weight probably precipitate first, as they usually have lower contents of phenolic and carboxylic groups compared to fractions

of lower molecular weight: the latter fractions may require a subsequent lower pH or higher salt concentration levels in order to precipitate. Charge density may be one reason for this, although there may be others as well because, in general, the molecular weight of a polymer correlates with its solubility (Hill 1986). As a consequence, the properties of the dissolved and precipitated lignin may vary at different conditions. This was also observed experimentally in the precipitation of kraft lignin from fractionated industrial softwood black liquors (Paper IV), see Figure 4-26. It shows that, as the precipitation yield increases as a consequence of the increase in pOH, the phenolic group content in the precipitated lignin increases. It also indicates that the phenolic group content varies with the molecular weight, which is correlated to the yield too. Such aspects may explain some of the deviations observed between the predictions made of the stability of particle dispersion and experimental observations regarding the onset of the formation of micron-sized particles. For instance, deviations are seen at pOH 4-5 at about 1-1.5 M of Na^+, where the carboxylic groups are predicted to dominate the charging of the lignin. An alternative, in that case, is that the ionisation degree of the carboxylic groups should be taken into account at a short particle-particle-separation distance: the surface pH predicted becomes rather low here already at weakly alkaline bulk conditions (Figure 4-24).

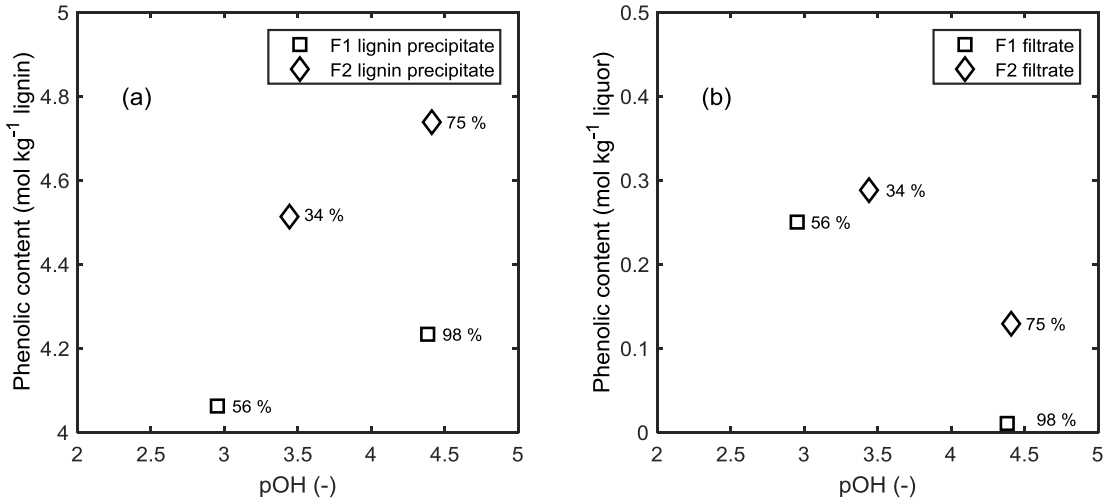

Figure 4-26. Contents of phenolic groups ***(a)*** *in the precipitated kraft lignin from black liquor factions (30 wt% dry content) and* ***(b)*** *in the remaining liquor, vs.* the pOH *(from Paper IV). The gravimetric yields at the corresponding conditions are given in percentage. F1 and F2 are a high and medium molecular weight fraction, respectively, with respect to the original unfractionated softwood black liquor.*

Figure 4-25 indicates that there is an upper limit of when the double layer repulsion can be considered realistic: the case of 4 mol Na^+ kg^{-1} water is certainly beyond this limit. Experimental results show nonetheless that no stable particles ≥ 1 µm were formed when Na_2SO_4 was added to reach a Na^+ concentration of 4 mol Na^+ kg^{-1} water, *e.g.* at about pOH 1.7. Figure 4-23 implies that there is the possibility that a local minimum in the pair potential may render flocculation and weaker agglomerate structures. SO_4^{2-} may lead to weaker structures (looser flocs) than in the case with Cl^-, since the repulsive barriers are higher in the former. This, in turn, may cause agglomerates to disintegrate to a larger degree when subjected to agitation, thus retarding the formation of micron-sized particles: the influence of agitation on the formation of particles at salt concentrations in this range can

be found elsewhere (Kannangara *et al.* 2016), although there it was suggested that particles of ~ 1 μm would be unaffected by agitation. In any case, double layer repulsion ought to vanish at concentrations as high as 4 mol Na^+ kg^{-1} and therefore cannot provide an explanation why micron-sized particles are absent until pOH values as high as 2.5-3 are reached in the SO_4^{2-} cases. The speculation may be made that there are other ion-specific effects of electrostatic/steric origin which influence the agglomerates. Should this be so, they may even provide other significant candidates to explain the observations: this is possible, since some discrepancies were found between the predictions and the observations made. Clearly, further investigation is needed here.

Nevertheless, the distributions of ion concentration presented previously (Figure 4-25) indicate a possible mechanism that may lie behind, at least to some degree, the higher dispersion stability when using SO_4^{2-} compared to Cl^-. The preconditions necessary for a significant anion-specific effect of this type are twofold: firstly, the surface charge has to be sufficiently high so that a close packing of counterions is attained close to the surface. Secondly, the salt concentration has to be high so that the difference in total ion concentration in the bulk between the two cases becomes large, which is due to the difference in valency of anions (Cl^- *vs.* SO_4^{2-}).

Improvements can be made to the model, regardless, to investigate the above-mentioned case further. The ion-surface interactions for SO_4^{2-} have been approximated using those for F^- (Eq. (2.17). Despite the fact that both are classified as kosmotropic (Salis and Ninham 2014), this approximation introduces some uncertainty in the prediction. Theoretical studies of ion-specific interactions that involve divalent species are currently limited, but they are desirable in order to bring clarity to those specific effects (Schwierz *et al.* 2013). Another improvement would be to include ion-specific ion-ion correlations, as they have been neglected in the current model.

5 Conclusions

The formation and growth of kraft lignin particles/agglomerates ≥ 1 µm in aqueous model solutions have been studied *in situ* using a FBRM instrument. The experimental methodology developed has provided valuable insights regarding the formation of the first micron-sized particles/agglomerates and the following evolvement of the chord length distribution during the precipitation process, *i.e.* changes in the concentration of particles/ agglomerates of various size-classes during the course of precipitation.

It was found from the analysis, and in agreement with earlier studies, that the precipitation of kraft lignin remains sensitive to pH even at high salt concentrations: at least up to 4 mol Na^+ kg^{-1} water. The level of salt concentration controls, to a large extent, the onset pH for the formation of micron-sized particles: the higher the salt concentration level, the higher the onset pH. At a pH value below the onset pH, an increase in the salt concentration renders a shift in the chord length distribution on the micron-scale to larger particles/agglomerates. The same effect was obtained when the pH was lowered further: depending on the concentration level of the salt, changes in the chord length distribution were observed in a very wide range of pH values, namely 4-13. This suggests that the electrostatic effects of the ionisable groups on kraft lignin (phenolic and carboxylic) are of significant importance to the particle formation process even at high salt concentration levels (1-4 mol Na^+ kg^{-1} water). Temperature has also been shown to be important for the sizes of the particles formed. A tendency for the system to undergo gelation was observed in the range 25-45 °C, although at 45 °C this was dependent on the pH and salt concentration level. At 65 °C, this phenomenon was not observed and, at 77°C, the particles became larger than at 65 °C. Temperature is therefore important to the formation of micron-sized particles. Furthermore, small amounts of xylan present during co-precipitation with kraft lignin (5 g/95 g lignin) indicated a retardation in particle formation to a minor extent; xylan was also found to be distributed evenly in the precipitated lignin.

Predictions of the dispersion stability of kraft lignin nanoparticles were made by employing a modified Poisson-Boltzmann model for the estimation of pair interaction potentials (an extended DLVO model). Taking into account steric effects of the ions and non-electrostatic ion-surface interactions (most importantly hydrophobic) led to that the repulsive part of the pair interactions was increased, compared to the classical Poisson-Boltzmann predictions.

As a consequence, the dispersion stabilities of nanoparticles were predicted to be high at low pOH (*e.g.* 1), even at high concentrations of ions, *i.e.* up to ~2-2.5 mol Na^+ kg^{-1} water, depending on the anion used. Comparisons of the predictions to the onset of the formation of particles ≥ 1 µm determined experimentally agreed reasonably well for the case with NaCl added to obtain various levels of Na^+ concentrations (1-4 mol kg^{-1} water). The corresponding predictions for Na_2SO_4 provided at least a partial explanation of the differences in particle formation observed experimentally when the different salts were added to obtain high concentrations of salt (2-4 mol Na^+ kg^{-1} water). Nevertheless, the model used predicted a lower nanoparticle dispersion stability in that salt concentration-range with Na_2SO_4 as the added salt compared to the corresponding observations made in the experiments for particles ≥ 1 µm.

It is expected that the rather abundant phenolic groups contribute to the charging, and thus phase behaviour, of kraft lignin, which this study also supports. However, both the experimental and theoretical results indicate that the less abundant carboxylic groups may also influence the formation of particles significantly, especially in the neutral-to-acidic regime (where the phenolic groups ought to be protonated), if salt concentrations levels are not too extreme, *e.g.* about 1 M Na^+.

6 Future work

In an industrial setting, the use of the FBRM technique for the online monitoring of particle size can be considered a promising choice of method, based on the results in this thesis. It may, for instance, be inserted into vessels and pipes to conduct online monitoring and offline analysis of various unit operations and streams in industry. In an industrial context, it could not only aid in quality control but also be used in pilot-scale trials, *e.g.* in process development.

From a scientific perspective, a similar resolution in time and particle-size dimension of the particle formation process, as obtained in this work, is desirable on the nano-scale. The precipitation process on this scale provides the boundary conditions for the micron-level processes that has been studied in detail here. Such knowledge is thus relevant to understanding not only precipitation operations similar to those conducted here but also other types of processes that are dependent on the phase behaviour of kraft lignin on the nano-scale. The data currently available on this scale is limited to dilute concentrations of kraft lignin, providing poorly resolved information on the particle size distribution during the course of precipitation.

Investigation into the ways mixing influences the particle size distribution, both experimentally and theoretically, would provide further knowledge and understanding relevant to industrial operations and process design.

In situ information of the shape of the particles would also be valuable for understanding the process of particle formation. Moreover, such data would be useful in comprehending the packing behaviour of particles during the dewatering of kraft lignin suspensions.

As implied in this work, improvements can be made to the modified Poisson-Boltzmann model. Specific ion-surface potentials for SO_4^{2-} ions can be added to increase the certainty in the predictions. Furthermore, specific ion-ion correlations can also be included, as they are neglected in the current model.

7 Acknowledgement

The work presented in this thesis has been conducted within the Wallenberg Wood Science Center and the financial support from the Knut and Alice Wallenberg Foundation is gratefully acknowledged.

Many people have contributed in various ways throughout this PhD project. My special thanks go to the following people:

First and foremost my supervisor Hans Theliander, for your engagement and guidance throughout my PhD study, as well as, for providing the chance to develop as a researcher.

Julie Durruty for great team work during experimental campaigns and Weizhen Zhu (Daniel) for good collaboration and enjoyable time working together.

Maria Sedin for fruitful and amusing discussions, on and off-topic, and your valuable advice.

Helene Schneider and Lynn Schneider for your excellent work in your master thesis project at SIKT and Joakim Thorstensson for your efforts in challenging experiments.

Tuve Mattsson for good discussions and input to papers.

Annika Altskär for the help with conducting the confocal laser scanning fluorescence microscopy measurements.

Maureen Sondell for thorough and rapid linguistic reviews of the thesis and papers.

All the colleagues (past and present) at the Division of the Chemical Engineering, especially at SIKT, for creating a great atmosphere. Jonas Wetterling and Anders Ahlbom: thank you for the great company and many good laughs during the time sharing an office with you. Anders Åkesjö, for your generous help with all types of image-editing issues and the dinner-discussions. Malin Larsson and Eva Kristenson, for your help, not only regarding the administrative matters. Ximena Rozo Sevilla for your engagement in the laboratory working environment.

All the colleagues at Wallenberg Wood Science Center for the interesting meetings and conferences, as well as the enjoyable activities we have shared together. This network has given me a good insight into the research topics related to biorefining and materials.

Last, but not least, Preshanthi and my family for their support.

8 Appendix

8.1 Modified Boltzmann distribution

Setting the partial derivative of the grand potential in Eq. (2.17), with respect to the specific ion concentration, $c_j(\boldsymbol{r})$ ($j \in i$), equal to zero, yields:

$$0 = ez_j\psi(\boldsymbol{r}) - \mu_j + \xi V_j^{\text{phob}}(\boldsymbol{r}) + (1-\xi)V_j^{\text{phil}}(\boldsymbol{r}) + kT\left[\ln\left(a^3 c_j(\boldsymbol{r})\right) + 1 - \frac{1}{1-a^3\sum_i c_i(\boldsymbol{r})} - \ln\left(1 - a^3\sum_i c_i(\boldsymbol{r})\right) + \frac{a^3\sum_i c_i(\boldsymbol{r})}{1-a^3\sum_i c_i(\boldsymbol{r})}\right]. \quad \text{(A.1)}$$

After simplification of Eq. (A1), the following expression is obtained:

$$0 = ez_j\psi(\boldsymbol{r}) - \mu_j + \xi V_j^{\text{phob}}(\boldsymbol{r}) + (1-\xi)V_j^{\text{phil}}(\boldsymbol{r}) + kT\left[\ln\left(a^3 c_j(\boldsymbol{r})\right) - \ln\left(1 - a^3\sum_i c_i(\boldsymbol{r})\right)\right]. \quad \text{(A.2)}$$

The chemical potential of ion j is equal to that of the bulk condition where the electrostatic and ion-surface potentials vanishes, thus:

$$\mu_j = kT\ln\left(a^3 c_{j,0}\right) - kT\ln\left(1 - a^3\sum_i c_{i,0}\right) \quad \text{(A.3)}$$

Eqs. (A.2) and (A.3) yields:

$$\ln\left(\frac{a^3 c_j(\boldsymbol{r})}{\left(1 - a^3 \sum_i c_i(\boldsymbol{r})\right)}\right) =$$

$$\ln\left(\frac{a^3 c_{j,0}}{1 - a^3 \sum_i c_{i,0}}\right) - \beta e z_j \psi(\boldsymbol{r}) - \beta \xi V_j^{\text{phob}}(\boldsymbol{r}) - \beta(1-\xi) V_j^{\text{phil}}(\boldsymbol{r}) \tag{A.4}$$

or

$$\frac{c_j(\boldsymbol{r})}{1 - a^3 \sum_i c_i(\boldsymbol{r})} = \frac{c_{j,0} \exp\left(-\beta e z_j \psi(\boldsymbol{r}) - \beta \xi V_j^{\text{phob}}(\boldsymbol{r}) - \beta(1-\xi) V_j^{\text{phil}}(\boldsymbol{r})\right)}{1 - a^3 \sum_i c_{i,0}(\boldsymbol{r})} \tag{A.5}$$

where $\beta = 1/(kT)$. The concentration of j in the Boltzmann distribution is given implicitly in Eq. A5. However, summation over all ionic species leads to:

$$\frac{\sum_i c_i(\boldsymbol{r})}{1 - a^3 \sum_i c_i(\boldsymbol{r})} =$$

$$\frac{\sum_i c_{i,0} \exp\left(-\beta e z_i \psi(\boldsymbol{r}) - \beta \xi V_i^{\text{phob}}(\boldsymbol{r}) - \beta(1-\xi) V_i^{\text{phil}}(\boldsymbol{r})\right)}{1 - a^3 \sum_i c_{i,0}} \tag{A.6}$$

The following substitutions can made:

$$x = \sum_i c_i(\boldsymbol{r}) \tag{A.7}$$

$$B_i(\boldsymbol{r}) = \exp\left(-\beta e z_i \psi(\boldsymbol{r}) - \beta \xi V_i^{\text{phob}}(\boldsymbol{r}) - \beta(1-\xi) V_i^{\text{phil}}(\boldsymbol{r})\right) \tag{A.8}$$

which leads to:

$$\frac{x}{1 - a^3 x} = \frac{\sum_i c_{i,0} B_i(\boldsymbol{r})}{1 - a^3 \sum_i c_{i,0}}. \tag{A.9}$$

Rearrangement yields:

$$x\left(1 + \frac{a^3 \sum_i c_{i,0} B_i(\boldsymbol{r})}{1 - a^3 \sum_i c_{i,0}}\right) = \frac{\sum_i c_{i,0} B_i(\boldsymbol{r})}{1 - a^3 \sum_i c_{i,0}}. \tag{A.10}$$

Then x can be extracted:

$$x = \frac{\sum_i c_{i,0} B_i(\boldsymbol{r})}{1 - a^3 \sum_i c_{i,0}} \left(1 + \frac{a^3 \sum_i c_{i,0} B_i(\boldsymbol{r})}{1 - a^3 \sum_i c_{i,0}}\right)^{-1}. \tag{A.11}$$

Re-substitution gives:

$$\sum_i c_i(\boldsymbol{r}) = \frac{\sum_i c_{i,0}\, B_i(\boldsymbol{r})}{1 - a^3 \sum_i c_{i,0}} \left(1 + \frac{a^3 \sum_i c_{i,0}\, B_i(\boldsymbol{r})}{1 - a^3 \sum_i c_{i,0}}\right)^{-1} =$$

$$\sum_i c_{i,0}\, B_i(\boldsymbol{r}) \left(1 + a^3 \sum_i c_{i,0}\, (B_i(\boldsymbol{r}) - 1)\right)^{-1}. \tag{A.12}$$

After removing the summations, the modified Boltzmann distribution is obtained:

$$c_j(\boldsymbol{r}) = c_{j,0} B_j(\boldsymbol{r}) \left(1 + a^3 \sum_i c_{i,0}\, (B_i(\boldsymbol{r}) - 1)\right)^{-1}, \tag{A.13}$$

$$B_i(\boldsymbol{r}) = \exp\left(-\beta e z_i \psi(\boldsymbol{r}) - \beta \xi V_i^{\text{phob}}(\boldsymbol{r}) - \beta(1 - \xi) V_i^{\text{phil}}(\boldsymbol{r})\right).$$

8.2 Average separation distance between nanoparticles

The volume fraction of identical particles in a system, ϕ (-), can be expressed as:

$$\phi = \frac{V_{\text{p}}^{\text{cell}}}{V^{\text{cell}}} \tag{A.14}$$

where V^{cell} (m^3) and $V_{\text{p}}^{\text{cell}}$ (m^3) are the volume of a cell and a particle which is contained in it, respectively. An average half separation distance between the particles can be approximated as, $(D/2)_{\text{m}} \approx R_{\text{cell}} - R_{\text{p}}$, and can be estimated from the cell radius, R_{cell}. The radius can be expressed as:

$$R_{\text{cell}} = \frac{R_{\text{p}}}{\phi^{1/3}} \tag{A.15}$$

The volume fraction of the particles can be estimated from:

$$\phi = \frac{m_{\text{p}} \rho_{\text{p}}^{-1}}{m_{\text{p}} \rho_{\text{p}}^{-1} + m_{\text{liq}} \rho_{\text{sol}}^{-1}} \tag{A.16}$$

where ρ_{p} (kg m^{-3}) and ρ_{sol} (kg m^{-3}) are the average density of the particles and the aqueous solution, respectively (the values can be found below). m_{p} (kg) is the total mass of the particles (kraft lignin and liquid in the void) and m_{liq} (kg) is the free liquid of the salt solution. The mass of particles is the sum of that of the lignin, m_{L} (kg), and the confined aqueous salt solution in the void, $m_{\text{sol}}^{\text{p}}$ (kg), thus:

$$m_{\text{p}} = m_{\text{L}} + m_{\text{sol}}^{\text{p}}. \tag{A.17}$$

Consequently, the free liquid mass can be expressed as:

$$m_{\mathrm{liq}} = m_{\mathrm{sol}} - m_{\mathrm{sol}}^{\mathrm{p}} \tag{A.18}$$

where m_{sol} (kg) is the total mass of the liquid part of the system. The volume fraction of lignin in the particles or solidosity, $\phi_{\mathrm{L}}^{\mathrm{p}}$ (-), can be used to determine the mass of the aqueous solution confined in them according to:

$$\phi_{\mathrm{L}}^{\mathrm{p}} = \frac{m_{\mathrm{L}}\rho_{\mathrm{L}}^{-1}}{m_{\mathrm{L}}\rho_{\mathrm{L}}^{-1} + m_{\mathrm{sol}}^{\mathrm{p}}\rho_{\mathrm{sol}}^{-1}}. \tag{A.19}$$

The mass of the solution confined in the particles is then:

$$m_{\mathrm{sol}}^{\mathrm{p}} = m_{\mathrm{L}}\left(1 - \phi_{\mathrm{L}}^{\mathrm{p}}\right)/\phi_{\mathrm{L}}^{\mathrm{p}}. \tag{A.20}$$

Combining Eqs. (A.16), (A.17), (A.18) and (A.20) yield:

$$\phi = \frac{m_{\mathrm{L}}\left(1 + \left(1 - \phi_{\mathrm{L}}^{\mathrm{p}}\right)/\phi_{\mathrm{L}}^{\mathrm{p}}\right)\rho_{\mathrm{p}}^{-1}}{m_{\mathrm{L}}\left(1 + \left(1 - \phi_{\mathrm{L}}^{\mathrm{p}}\right)/\phi_{\mathrm{L}}^{\mathrm{p}}\right)\rho_{\mathrm{p}}^{-1} + \left(m_{\mathrm{sol}} - m_{\mathrm{L}}\left(1 - \phi_{\mathrm{L}}^{\mathrm{p}}\right)/\phi_{\mathrm{L}}^{\mathrm{p}}\right)\rho_{\mathrm{sol}}^{-1}}. \tag{A.21}$$

From the lignin, water, and salt amounts (m_{L}, m_{w} and m_{salt}), the weight percentage of lignin in the suspension is given by:

$$wt\ \% = 100\frac{m_{\mathrm{L}}}{m_{\mathrm{L}} + m_{\mathrm{sol}}} = 100\frac{m_{\mathrm{L}}}{m_{\mathrm{L}} + m_{\mathrm{w}} + m_{\mathrm{salt}}}. \tag{A.22}$$

The density of the particles may be approximated by:

$$\rho_{\mathrm{p}} \approx \phi_{\mathrm{L}}^{\mathrm{p}}\rho_{\mathrm{L}} + \left(1 - \phi_{\mathrm{L}}^{\mathrm{p}}\right)\rho_{\mathrm{sol}} \tag{A.23}$$

where ρ_{L} and ρ_{sol} were assumed to be 1350 kg m^{-3} and 1100 kg m^{-3}.

References

Alén, R., P. Patja and E. Sjöstrom (1979). "Carbon dioxide precipitation of lignin from pine kraft black liquor " Tappi **62**(11): 108-110.

Argyropoulos, D. S. (1994). "Quantitative Phosphorus-31 NMR Analysis of Six Soluble Lignins." Journal of Wood Chemistry and Technology **14**(1): 65-82.

Balian, R. (1991). Thermodynamics Revisited. From Microphysics to Macrophysics: Methods and Applications of Statistical Physics. Berlin, Heidelberg, Springer Berlin Heidelberg**:** 181-239.

Ben-Yaakov, D., D. Andelman, R. Podgornik and D. Harries (2011). "Ion-specific hydration effects: Extending the Poisson-Boltzmann theory." Current Opinion in Colloid & Interface Science **16**(6): 542-550.

Bialik, M., P. Sedin and H. Theliander (2008). "Boiling Point Rise Calculations in Sodium Salt Solutions." Industrial & Engineering Chemistry Research **47**(4): 1283-1287.

Borukhov, I., D. Andelman and H. Orland (1997). "Steric Effects in Electrolytes: A Modified Poisson-Boltzmann Equation." Physical Review Letters **79**(3): 435-438.

Crestini, C., H. Lange, M. Sette and D. S. Argyropoulos (2017). "On the structure of softwood kraft lignin." Green Chemistry **19**(17): 4104-4121.

Cusola, O., S. Kivistö, S. Vierros, P. Batys, M. Ago, B. L. Tardy, L. G. Greca, M. B. Roncero, M. Sammalkorpi and O. J. Rojas (2018). "Particulate Coatings via Evaporation-Induced Self-Assembly of Polydisperse Colloidal Lignin on Solid Interfaces." Langmuir **34**(20): 5759-5771.

Dang Binh, T. T., H. Brelid and H. Theliander (2016). The impact of ionic strength on the molecular weight distribution (MWD) of lignin dissolved during softwood kraft cooking in a flow-through reactor. Holzforschung. **70:** 495-501.

Delville, A., H. Gilboa and P. Laszlo (1982). "Calculation of activity coefficients from a novel numerical solution of the Poisson–Boltzmann equation and application to 23Na

NMR of sodium polystyrene sulfonate." The Journal of Chemical Physics **77**(4): 2045-2050.

Derjaguin, B. (1940). "On the repulsive forces between charged colloid particles and on the theory of slow coagulation and stability of lyophobe sols." Transactions of the Faraday Society **35**(0): 203-215.

Derjaguin, B. V. and L. Landau (1941). "Theory of the Stability of Strongly Charged Lyophobic Sols and of the Adhesion of Strongly Charged Particles in Solutions of Electrolytes." Acta Phys. Chim. URSS **14**: 633-662.

Deserno, M. and C. Holm (2001). Cell Model and Poisson-Boltzmann Theory: A Brief Introduction. Electrostatic Effects in Soft Matter and Biophysics. C. Holm et al., Springer Netherlands. **46:** 27-52.

Dong, D., A. L. Fricke, B. M. Moudgil and H. Johnson (1996). "Electrokinetic study of kraft lignin." Tappi J. **79**(7): 191-197.

Durruty, J., T. Mattsson and H. Theliander (2015). "Local and average filtration properties of kraft softwood lignin." Nordic Pulp and Paper Research Journal **30**(1): 132-140.

Durruty, J., T. Mattsson and H. Theliander (2017). "Local filtration properties of Kraft lignin: The influence of residual xylan." Separation and Purification Technology **179**: 455-466.

Evans, D. F. and H. Wennerström (1999). Colloidal stability. The colloidal domain: where physics, chemistry, biology, and technology meet. D. F. Evans et al. Danvers, MA, USA, Wiley-VCH 401-442.

Frederick, J. (1997). Black Liquor Properties. Kraft Recovery Boilers. Atlanta, GA, TAPPI Press**:** 65.

Fritz, C., C. Salas, H. Jameel and O. J. Rojas (2017). "Self-association and aggregation of kraft lignins via electrolyte and nonionic surfactant regulation: stabilization of lignin particles and effects on filtration." Nordic Pulp & Paper Research Journal **32**(4): 572-585.

Froass Peter, M., J. Ragauskas Arthur and E. Jiang Jian (1998). "NMR Studies Part 3: Analysis of Lignins from Modern Kraft Pulping Technologies." Holzforschung - International Journal of the Biology, Chemistry, Physics and Technology of Wood **52**(4): 385.

Garver, T. M. and P. T. Callaghan (1991). "Hydrodynamics of kraft lignins." Macromolecules **24**(2): 420-430.

Gellerstedt, G. and E. Lindfors (1984). "Structural Changes in Lignin During Kraft Pulping." Holzforschung **38**(3): 151-158.

Gellerstedt, G., E. Sjöholm and I. Brodin (2010). "The wood-based biorefinery: a source of carbon fiber?" Open Agriculture Journal **4**(2): 119-124.

Goring, D. A. I. (1962). "The physical chemistry of lignin." Pure and Applied Chemistry **5**(1-2): 233-254.

Goring, D. A. I., R. Vuong, C. Gancet and H. Chanzy (1979). "The flatness of lignosulfonate macromolecules as demonstrated by electron microscopy." Journal of Applied Polymer Science **24**(4): 931-936.

Hallez, Y., J. Diatta and M. Meireles (2014). "Quantitative Assessment of the Accuracy of the Poisson–Boltzmann Cell Model for Salty Suspensions." Langmuir **30**(23): 6721-6729.

Hamaker, H. C. (1937). "The London—van der Waals attraction between spherical particles." Physica **4**(10): 1058-1072.

Henriksson, G. (2008). Lignin. The Ljungberg Textbook Wood Chemistry. Stockholm, Vasastadens Bokbinderi AB.

Hill, T. L. (1986). 18.3 Electrolyte Solutions. Introduction to Statistical Thermodynamics. New York, Dover Publications**:** 334-338.

Hill, T. L. (1986). 21.2 Flory-Huggins polymer solution theory. Introduction to Statistical Thermodynamics. New York, Dover Publications**:** 401-410.

Hollertz, R., H. Arwin, B. Faure, Y. Zhang, L. Bergström and L. Wågberg (2013). "Dielectric properties of lignin and glucomannan as determined by spectroscopic ellipsometry and Lifshitz estimates of non-retarded Hamaker constants." Cellulose **20**(4): 1639-1648.

Holthoff, H., S. U. Egelhaaf, M. Borkovec, P. Schurtenberger and H. Sticher (1996). "Coagulation Rate Measurements of Colloidal Particles by Simultaneous Static and Dynamic Light Scattering." Langmuir **12**(23): 5541-5549.

Hu, Z., X. Du, J. Liu, H.-m. Chang and H. Jameel (2016). "Structural Characterization of Pine Kraft Lignin: BioChoice Lignin vs Indulin AT." Journal of Wood Chemistry and Technology **36**(6): 432-446.

Ibaseta, N. and B. Biscans (2010). "Fractal dimension of fumed silica: Comparison of light scattering and electron microscope methods." Powder Technology **203**(2): 206-210.

Israelachvili, J. N. (2011). 14 - Electrostatic Forces between Surfaces in Liquids. Intermolecular and Surface Forces (Third Edition). J. N. Israelachvili. Boston, Academic Press**:** 291-340.

Israelachvili, J. N. (2011). Chapter 13 - Van der Waals Forces between Particles and Surfaces. Intermolecular and Surface Forces (Third Edition). J. N. Israelachvili. Boston, Academic Press**:** 253-289.

Kadla, J. F., S. Kubo, R. A. Venditti, R. D. Gilbert, A. L. Compere and W. Griffith (2002). "Lignin-based carbon fibers for composite fiber applications." Carbon **40**(15): 2913-2920.

Kannangara, M., M. Marinova, L. Fradette and J. Paris (2016). "Effect of mixing hydrodynamics on the particle and filtration properties of precipitated lignin." Chemical Engineering Research and Design **105**: 94-106.

Laine, J., L. Lövgren, P. Stenius and S. Sjöberg (1994). "Potentiometric titration of unbleached kraft cellulose fibre surfaces." Colloids and Surfaces A: Physicochemical and Engineering Aspects **88**(2): 277-287.

Lawoko, M. (2005). Lignin polysaccharide networks in softwood and chemical pulps: Characterisation, structure and reactivity. Doctoral Degree, Royal Institute of Technology.

Lievonen, M., J. J. Valle-Delgado, M.-L. Mattinen, E.-L. Hult, K. Lintinen, M. A. Kostiainen, A. Paananen, G. R. Szilvay, H. Setälä and M. Österberg (2016). "A simple process for lignin nanoparticle preparation." Green Chemistry **18**(5): 1416-1422.

Lindström, T. (1980). "The colloidal behaviour of kraft lignin Part II. Coagulation of kraft lignin sols in the presence of simple and complex metal ions." Colloid and Polymer Science **258**(2): 168-173.

Lora, J. H. and W. G. Glasser (2002). "Recent Industrial Applications of Lignin: A Sustainable Alternative to Nonrenewable Materials." Journal of Polymers and the Environment **10**(1): 39-48.

Mancinelli, R., A. Botti, F. Bruni, M. A. Ricci and A. K. Soper (2007). "Hydration of Sodium, Potassium, and Chloride Ions in Solution and the Concept of Structure Maker/Breaker." The Journal of Physical Chemistry B **111**(48): 13570-13577.

Mattsson, C., S.-I. Andersson, T. Belkheiri, L.-E. Åmand, L. Olausson, L. Vamling and H. Theliander (2016). "Using 2D NMR to characterize the structure of the low and high molecular weight fractions of bio-oil obtained from LignoBoost™ kraft lignin depolymerized in subcritical water." Biomass and Bioenergy **95**(Supplement C): 364-377.

Mattsson, C., M. Hasani, B. Dang, M. Mayzel and H. Theliander (2017). About structural changes of lignin during kraft cooking and the kinetics of delignification. Holzforschung. **71:** 545.

Mähler, J. and I. Persson (2012). "A Study of the Hydration of the Alkali Metal Ions in Aqueous Solution." Inorganic Chemistry **51**(1): 425-438.

Nguyen, T. D. H., M. Maschietti, T. Belkheiri, L.-E. Åmand, H. Theliander, L. Vamling, L. Olausson and S.-I. Andersson (2014). "Catalytic depolymerisation and conversion of Kraft lignin into liquid products using near-critical water." The Journal of Supercritical Fluids **86**: 67-75.

Norgren, M., H. Edlund and L. Wågberg (2002). "Aggregation of Lignin Derivatives under Alkaline Conditions. Kinetics and Aggregate Structure." Langmuir **18**(7): 2859-2865.

Norgren, M., H. Edlund, L. Wågberg, B. Lindström and G. Annergren (2001). "Aggregation of kraft lignin derivatives under conditions relevant to the process, part I: phase behaviour." Colloids and Surfaces A: Physicochemical and Engineering Aspects **194**(1–3): 85-96.

Norgren, M. and B. Lindström (2000). "Dissociation of Phenolic Groups in Kraft Lignin at Elevated Temperatures." Holzforschung **54**(5): 519-527.

Norgren, M. and B. Lindström (2000). "Physico-Chemical Characterization of a Fractionated Kraft Lignin." Holzforschung **54**(5): 528-534.

Norgren, M. and S. Mackin (2009). "Sulfate and Surfactants as Boosters of Kraft Lignin Precipitation." Industrial & Engineering Chemistry Research **48**(10): 5098-5104.

Obiaga, T. I. and M. Wayman (1973). "Molecular weight distribution of lignin during alkaline pulping." Svensk Papperstidning **76**: 699-703.

Olofsson, G. and I. Olofsson (1977). "The enthalpy of ionization of water between 273 and 323 K." The Journal of Chemical Thermodynamics **9**(1): 65-69.

Pakkanen, H. and R. Alén (2012). "Molecular mass distribution of lignin from the alkaline pulping of hardwood, softwood, and wheat straw." Journal of wood chemistry and technology **32**(4): 279-293.

Parsons, D. F., M. Bostrom, P. Lo Nostro and B. W. Ninham (2011). "Hofmeister effects: interplay of hydration, nonelectrostatic potentials, and ion size." Phys Chem Chem Phys **13**(27): 12352-12367.

Petridis, L., R. Schulz and J. C. Smith (2011). "Simulation Analysis of the Temperature Dependence of Lignin Structure and Dynamics." Journal of the American Chemical Society **133**(50): 20277-20287.

Ragnar, M., C. T. Lindgren and N.-O. Nilvebrant (2000). "pKa-Values of Guaiacyl and Syringyl Phenols Related to Lignin." Journal of Wood Chemistry and Technology **20**(3): 277-305.

Reerink, H. and J. T. G. Overbeek (1954). "The rate of coagulation as a measure of the stability of silver iodide sols." Discussions of the Faraday Society **18**: 74-84.

Robert, D. R., M. Bardet, G. Gellerstedt and E. L. Lindfors (1984). "Structural Changes in Lignin During Kraft Cooking Part 3. On the Structure of Dissolved Lignins." Journal of Wood Chemistry and Technology **4**(3): 239-263.

Salis, A. and B. W. Ninham (2014). "Models and mechanisms of Hofmeister effects in electrolyte solutions, and colloid and protein systems revisited." Chemical Society Reviews **43**(21): 7358-7377.

Schwierz, N., D. Horinek and R. R. Netz (2013). "Anionic and Cationic Hofmeister Effects on Hydrophobic and Hydrophilic Surfaces." Langmuir **29**(8): 2602-2614.

Sjöström, E. (1977). "The behaviour of wood polysaccharides during alkaline pulping processes." Tappi **60**(9): 151.

Sundin, J. and N. Hartler (2000). "Precipitation of kraft lignin by metal cations in alkaline solutions." Nordic Pulp & Paper Research Journal **15**(04): 306-312.

Svärd, A., O. Sevastyanova, G. Dobele, V. Jurkjane and E. Brännvall (2016). "COST Action FP1105: Effect of raw materials and pulping conditions on the characteristics of dissolved kraft lignins." Holzforschung **70**(12): 1105-1114.

Teleman, A. (2008). Hemicelluloses and pectins. The Ljungberg Textbook Wood Chemistry. Stockholm, Vasastadens Bokbinderi AB.

Thakur, V. K., M. K. Thakur, P. Raghavan and M. R. Kessler (2014). "Progress in Green Polymer Composites from Lignin for Multifunctional Applications: A Review." ACS Sustainable Chemistry & Engineering **2**(5): 1072-1092.

Uloth, V. C. and J. T. Wearing (1989). "Kraft lignin recovery: acid precipitation versus ultrafiltration. Part I. Laboratory test results." Pulp and Paper Canada **90**: 67-71.

Vainio, U., N. Maximova, B. Hortling, J. Laine, P. Stenius, L. K. Simola, J. Gravitis and R. Serimaa (2004). "Morphology of Dry Lignins and Size and Shape of Dissolved Kraft Lignin Particles by X-ray Scattering." Langmuir **20**(22): 9736-9744.

Wallmo, H., T. Richards and H. Theliander (2009). "An investigation of process parameters during lignin precipitation from kraft black liquors: A step towards an optimised precipitation operation." Nordic Pulp and Paper Research Journal **24**(2): 158-164.

Wallmo, H., H. Theliander, A.-S. Jönsson, O. Wallberg and K. Lindgren (2009). "The influence of hemicelluloses during the precipitation of lignin in kraft black liquor." Nordic Pulp & Paper Research Journal **24**(2): 165-171.

Wei, Z., Y. Yang, R. Yang and C. Wang (2012). "Alkaline lignin extracted from furfural residues for pH-responsive Pickering emulsions and their recyclable polymerization." Green Chemistry **14**(11): 3230-3236.

Wennerström, H. (2017). "Electrostatic interactions in concentrated colloidal dispersions." Physical Chemistry Chemical Physics **19**(35): 23849-23853.

Verwey, E. J. W. (1947). "Theory of the Stability of Lyophobic Colloids." The Journal of Physical and Colloid Chemistry **51**(3): 631-636.

Wigell, A., H. Brelid and H. Theliander (2007). "Degradation/dissolution of softwood hemicellulose during alkaline cooking at different temperatures and alkali concentrations." Nord. Pulp Pap. Res. J. **22**(4): 489-494.

Yan, J. F., F. Pla, R. Kondo, M. Dolk and J. L. McCarthy (1984). "Lignin. 21. Depolymerization by bond cleavage reactions and degelation." Macromolecules **17**(10): 2137-2142.

Zhu, W. and H. Theliander (2015). "Precipitation of lignin from softwood black liquor: an investigation of the equilibrium and molecular properties of lignin." BioResources **10**(1): 1696-1714.

Zhu, W., G. Westman and H. Theliander (2015). "The molecular properties and carbohydrate content of lignins precipitated from black liquor." Holzforschung **69**(2): 143-152.

Zhu, W., G. Westman and H. Theliander (2016). "Lignin separation from kraft black liquor by combined ultrafiltration and precipitation: a study of solubility of lignin with different molecular properties." Nordic Pulp & Paper Research Journal **31**(2): 270-278.

Zinovyev, G., I. Sumerskii, P. Korntner, I. Sulaeva, T. Rosenau and A. Potthast (2017). "Molar mass-dependent profiles of functional groups and carbohydrates in kraft lignin." Journal of Wood Chemistry and Technology **37**(3): 171-183.

Öhman, F. and H. Theliander (2007). "Filtration properties of lignin precipitated from black liquor." Tappi Journal **6**(7): 3-9.

Öhman, F., H. Theliander, P. Tomani and P. Axegard (2013). Method for separating lignin from black liquor, Google Patents.

Öhman, F., H. Wallmo and H. Theliander (2007). "A novel method for washing lignin precipitated from kraft black liquor – Laboratory trials." Nordic Pulp & Paper Research Journal **22**(1): 9-16.